Reliability and Accuracy of a Newly Developed Intraoral Ultrasound Device to Evaluate the Facial Alveolar Bone Height

by

Claudiu Corbea

A thesis submitted in partial fulfillment of requirements for the degree of
Master of Science

Medical Sciences-Orthodontics
University of Alberta

© Claudiu Corbea, 2022

Abstract

Introduction: The purpose of this study was to evaluate the reliability and accuracy of a newly developed intraoral ultrasound (US) device to evaluate the facial alveolar bone height.

Methods: 38 cadaver teeth distributed across 3 human cadavers were prepared by having placed two or more notches on the facial enamel surface. The maxillary and mandibular teeth were imaged with a custom designed intra-oral 20 MHz ultrasound probe. This custom designed US is small and is specifically designed for intra-oral use, as currently available medical US probes are bulky and are unsuited to be used intra-orally. After the US scans were done, the maxilla and mandibles were sectioned from the cadavers and scanned with Micro-CT (μCT) (gold standard). For each sample, the distance from the inferior border of the most apical notch to the tip of the alveolar bone crest on the facial aspect of the teeth was measured from the US and μCT images. ITK-Snap was used to orient and measure the μCT images and RadiANT was used to measure the US images.

Results: The intra examiner and inter examiner reliability for both the μCT and US alveolar bone crest measurements was found to be excellent (intra examiner ICC is 0.998 for μCT and 0.997 for US, inter examiner ICC is 0.996 for μCT and in between 0.947 and 0.950 for US). The accuracy of the US was found to be good compared to μCT (ICC in between 0.885 and 0.894).

Conclusion: Using the ultrasound device to evaluate the facial alveolar bone height has excellent reliability and good accuracy compared to the μCT gold standard.

Preface

This thesis is an original work by Claudiu Corbea.

For this project no University of Alberta Ethics Board approval was required.

No part of this thesis has been previously published.

Acknowledgements

I wish to express my gratitude to my supervisor, Dr. Paul Major for all his support, patience and guidance throughout my 3 years of post-graduate education at the University of Alberta. Dr. Major is an exceptional clinician and teacher, with a wealth of knowledge and he is always ready to share his experience with the residents.

Also, I would like to thank Dr. Lawrence Le for his support on completing this project, Dr. Fabiana Almeida for her easy-going nature and her willingness to always help, Dr. Giseon Heo for guiding me with the statistics part of this thesis and for having a good sense of humour, Dr. Maria Alexiou for helping with the μCT scans of the samples, and to Kim-Cuong T Nguyen (KC) for her help with the ultrasound scans.

This thesis would not have been possible without all your help. Thank you!

TABLE OF CONTENTS

LIST OF TABLES

LIST OF FIGURES

Glossary of Terms

R1 = Rater 1

R2 = Rater 2

T1 = Measurement at time T1

T2 = Measurement at time T2

T3 = Measurement at time T3

US = Ultrasound

CBCT = Cone Beam Computed Tomography

CT = Computed Tomography

μCT = Micro Computed Tomography

PFM = Porcelain fused to metal crow

CHAPTER 1 – INTRODUCTION

The periodontium is a dynamic structure composed of tissues that support and surround the tooth. These tissues include the gingiva, periodontal ligament, cementum, and alveolar bone. Vascular and nerve tissue supplies are also vital to the normal functioning of periodontal tissues. The structure and function of the tissues that make up the periodontium are mutually dependent; their dynamic biological renewal and adaptation processes maintain a harmonious relationship under normal conditions. The knowledge of the architecture and biology of the normal tissue is a prerequisite for understanding diseased tissue (Nanci & Bosshardt, 2006).

The thickness of the alveolar bone defines the limits of orthodontic movement and challenging these boundaries can result in iatrogenic side effects to the supporting and protective periodontium. The most critical orthodontic movements include expansion of the dental arches and anterior retraction/proclination movements. Such mechanics can decentralize the teeth from the supporting bone tissue envelope, resulting in dehiscence, bone fenestrations and gingival recession, depending on the initial morphology of the periodontium, as well as the amount of movement (Fuhrmann, 2002).

Many advances have occurred in technology in the world and dentistry has benefited significantly from them, especially in the field of radiology. New methods of assessment such as cone beam computed tomography (CBCT), magnetic resonance imaging (MRI) and ultrasound have been explored increasingly in the periodontal, oral pathology and orthodontics fields (Evirgen & Kamburoglu, 2016; Nguyen et al., 2018; Shah, Bansal, & Logani, 2014).

There is a great variety of clinical and radiographic methods that can be used to assess periodontal status (Agrawal, Sanikop, & Patil, 2012). Periodontal probing is the most accepted form of assessment of sulcus depth. However, pocket depth evaluation does not offer assessment of the alveolar bone level. For years, 2D intra-oral radiography has been used. This allows the clinician to have some information regarding the alveolar bone level (mesial and distal aspects of the tooth) (Xiang et al., 2010); however, it does not visualize the buccal and lingual aspects surrounding the teeth.

CBCT is presently used in the dental field for hard tissues visualization and, more recently, to examine periodontal loss (Leung, Palomo, Griffith, & Hans, 2010; Sun, Zhang, Shen, Wang, & Fang, 2015; Walter et al., 2020). Its main advantage when compared to 2D intra-oral radiography is that it allows the clinician to have access to a 3D view. The precision of CBCT for small measurements has been described in the literature (Abdelkarim, 2019; Leung, Palomo, Griffith, & Hans, 2010; Loubele et al., 2008; Mol & Balasundaram, 2008; Nguyen et al., 2018; Sun et al., 2015; Swasty et al., 2009; Walter et al., 2020), with an accuracy of 0.4mm for the cemento-enamel junction (CEJ) location and 0.6mm for the alveolar bone height, when it was compared to a digital caliper (Leung, Palomo, Griffith, & Hans, 2010).

Most clinicians do not recommend CBCT as a standard procedure for all patients since the amount of radiation involved is high and so is the financial cost. Due especially to the lifetime cumulative effects of X-ray exposure (Chen, Kachniarz, Gilani, & Shin, 2014), it is not recommended, nor feasible to take CBCT images on a routine basis during active treatment in order to assess how the bony structures respond. This has led some researchers to investigate whether there are alternative methods of bone imaging to assess the alveolar bone structures on a routine basis, and without increasing the patient exposure to radiation (Nguyen et al., 2018). Finding this holy grail of diagnostic bone imaging is not a trivial task and the search is still ongoing.

Thus far, the most promising non-invasive, ionizing radiation-free potential candidate has been US Imaging. In general, medical US imaging works by measuring echoes coming from the tissue interfaces due to impedance contrasts between different tissues. Therefore, it is an alternative to x-rays, and it could be used chairside to measure the alveolar bone in a matter of seconds in real time. So far, some successful attempts have been made to use ultrasound to measure bone in the dental field (Bohner et al., 2019; Chan & Kripfgans, 2020; Palou, McQuade, & Rossmann, 1987; Spranger, 1971; Tsiolis, Needleman, & Griffiths, 2003).

In a recent publication by Chifor et al. (2021), 3D reconstructions of the periodontium were accomplished utilizing a high frequency US imaging prototype on porcine mandibles. The authors concluded that the US had a strong diagnostic potential (precision varied from 0.179 mm and 0.235 mm), however this accuracy has not been demonstrated in a clinical setting in humans to date.

The main challenge has been that many available ultrasound transducers are mainly designed for the imaging of soft tissue, not hard tissue, and are rather bulky, making them unsuitable for intraoral use. For our study, we used a newly developed 20 MHz ultrasound transducer probe that is small enough to be used intraorally.

The primary objective of this study was to determine the reliability and accuracy of the newly developed US for identifying alveolar bone crest height on the facial aspect of maxillary and mandibular human teeth.

In order to determine the reliability and accuracy of the US, the following research questions and hypothesis were investigated:

1. Research Question 1

   How reliable are the measurements done by Rater 1 (R1) for the µCT and US?

   This research question investigates the Intra-Rater reliability of R1 for the µCT and US measurements by using the following null hypothesis and alternate hypothesis:

   H_o1: The µCT and US measurements done by R1 are reliable

   H_a1: The µCT and US measurements done by R1 are not reliable

2. Research Question 2:

   How reliable are the measurements done by Rater 1 (R1) for the US and µCT compared to Rater 2 (R2)?

   This research question investigates the Inter-Rater reliability of R1 compared to R2 for the µCT and US measurements by using the following null hypothesis and alternate hypothesis:

   H_o2: The µCT and US measurements done by R1 are reliable compared to R2

   H_a2: The µCT and US measurements done by R1 are not reliable compared to R2

3. Research Question 3:

   How accurate is the newly developed intraoral US device as a diagnostic tool to evaluate the facial alveolar bone crest?

   This research question investigates the accuracy of the US measurements compared to the μCT gold standard by using the following null hypothesis and alternate hypothesis:

   H_o3: The US device is accurate to determine alveolar bone crest height on the buccal aspect of maxillary and mandibular human teeth

   H_a3: The US device is not accurate to determine alveolar bone crest height on the buccal aspect of maxillary and mandibular human teeth

The secondary objective of this study was to explore if there are regions of the mouth that provide more reliable and/or accurate US measurements.

References

Abdelkarim, A. (2019). Cone-Beam Computed Tomography in Orthodontics. *Dent J (Basel), 7*(3). doi:10.3390/dj7030089

Agrawal, P., Sanikop, S., & Patil, S. (2012). New developments in tools for periodontal diagnosis. *Int Dent J, 62*(2), 57-64. doi:10.1111/j.1875-595X.2011.00099.x

Bohner, L., Habor, D., Tortamano, P., Radermacher, K., Wolfart, S., & Marotti, J. (2019). Assessment of Buccal Bone Surrounding Dental Implants Using a High-Frequency Ultrasound Scanner. *Ultrasound Med Biol, 45*(6), 1427-1434. doi:10.1016/j.ultrasmedbio.2019.02.002

Chan, H. L., & Kripfgans, O. D. (2020). Ultrasonography for diagnosis of peri-implant diseases and conditions: a detailed scanning protocol and case demonstration. *Dentomaxillofac Radiol, 49*(7), 20190445. doi:10.1259/dmfr.20190445

Chen, J. X., Kachniarz, B., Gilani, S., & Shin, J. J. (2014). Risk of malignancy associated with head and neck CT in children: a systematic review. *Otolaryngol Head Neck Surg, 151*(4), 554-566. doi:10.1177/0194599814542588

Chifor R, Li M, Nguyen KT, Arsenescu T, Chifor I, Badea AF, Badea ME, Hotoleanu M, Major PW, Le LH. (2021) Three-dimensional periodontal investigations using a prototype

handheld ultrasound scanner with spatial positioning reading sensor. *Med Ultrason*, 23(3), 297-304. doi: 10.11152/mu-2837. Epub 2021 Mar 3. PMID: 33657191.

Evirgen, S., & Kamburoglu, K. (2016). Review on the applications of ultrasonography in dentomaxillofacial region. *World J Radiol, 8*(1), 50-58. doi:10.4329/wjr.v8.i1.50

Fuhrmann, R. A. W. (2002). Three-dimensional evaluation of periodontalremodeling during orthodontic treatment. *Seminars in Orthodontics, 8*(1), 23-28. doi: https://doi.org/10.1053/sodo.2002.28168

Leung, C. C., Palomo, L., Griffith, R., & Hans, M. G. (2010). Accuracy and reliability of cone-beam computed tomography for measuring alveolar bone height and detecting bony dehiscences and fenestrations. *Am J Orthod Dentofacial Orthop, 137*(4 Suppl), S109-119. doi:10.1016/j.ajodo.2009.07.013

Loubele, M., Van Assche, N., Carpentier, K., Maes, F., Jacobs, R., van Steenberghe, D., & Suetens, P. (2008). Comparative localized linear accuracy of small-field cone-beam CT and multislice CT for alveolar bone measurements. *Oral Surg Oral Med Oral Pathol Oral Radiol Endod, 105*(4), 512-518. doi:10.1016/j.tripleo.2007.05.004

Mol, A., & Balasundaram, A. (2008). In vitro cone beam computed tomography imaging of periodontal bone. *Dentomaxillofac Radiol, 37*(6), 319-324. doi:10.1259/dmfr/26475758

Nanci, A., & Bosshardt, D. D. (2006). Structure of periodontal tissues in health and disease. *Periodontol 2000, 40*, 11-28. doi:10.1111/j.1600-0757.2005.00141.x

Nguyen, K. T., Pacheco-Pereira, C., Kaipatur, N. R., Cheung, J., Major, P. W., & Le, L. H. (2018). Comparison of ultrasound imaging and cone-beam computed tomography for examination of the alveolar bone level: A systematic review. *PLoS One, 13*(10), e0200596. doi:10.1371/journal.pone.0200596

Palou, M. E., McQuade, M. J., & Rossmann, J. A. (1987). The use of ultrasound for the determination of periodontal bone morphology. *J Periodontol, 58*(4), 262-265. doi:10.1902/jop.1987.58.4.262

Shah, N., Bansal, N., & Logani, A. (2014). Recent advances in imaging technologies in dentistry. *World J Radiol, 6*(10), 794-807. doi:10.4329/wjr.v6.i10.794

Spranger, H. (1971). Ultra-sonic diagnosis of marginal periodontal diseases. *Int Dent J, 21*(4), 442-455. Retrieved from https://www.ncbi.nlm.nih.gov/pubmed/5292204

Sun, L., Zhang, L., Shen, G., Wang, B., & Fang, B. (2015). Accuracy of cone-beam computed tomography in detecting alveolar bone dehiscences and fenestrations. *Am J Orthod Dentofacial Orthop, 147*(3), 313-323. doi:10.1016/j.ajodo.2014.10.032

Swasty, D., Lee, J. S., Huang, J. C., Maki, K., Gansky, S. A., Hatcher, D., & Miller, A. J. (2009). Anthropometric analysis of the human mandibular cortical bone as assessed by cone-beam computed tomography. *J Oral Maxillofac Surg, 67*(3), 491-500. doi:10.1016/j.joms.2008.06.089

Tsiolis, F. I., Needleman, I. G., & Griffiths, G. S. (2003). Periodontal ultrasonography. *J Clin Periodontol, 30*(10), 849-854. doi:10.1034/j.1600-051x.2003.00380.x

Walter, C., Schmidt, J. C., Rinne, C. A., Mendes, S., Dula, K., & Sculean, A. (2020). Cone beam computed tomography (CBCT) for diagnosis and treatment planning in periodontology: systematic review update. *Clin Oral Investig, 24*(9), 2943-2958. doi:10.1007/s00784-020-03326-0

Xiang, X., Sowa, M. G., Iacopino, A. M., Maev, R. G., Hewko, M. D., Man, A., & Liu, K. Z. (2010). An update on novel non-invasive approaches for periodontal diagnosis. *J Periodontol, 81*(2), 186-198. doi:10.1902/jop.2009.090419

CHAPTER 2 – LITERATURE REVIEW

2.1 The Periodontium

The periodontium comprises of structures that surround the tooth, and is divided into gingiva, alveolar bone, periodontal ligament and cementum (Figure 2.1). The gingival unit consists of free gingiva, attached gingiva and alveolar mucosa. The attachment unit consists of the alveolar bone, fibers of the periodontal ligament and cementum. These structures hold the tooth in position while absorbing the chewing forces applied to the tooth. Together they promote homeostasis, sealing the environment and thus allowing the host to maintain periodontal health in the face of constant aggression caused by the presence of bacterial plaque or by physical stimuli (Lindhe, Lang, & Karring, 2008; Newman, Takei, Klokkevold, & Carranza, 2012).

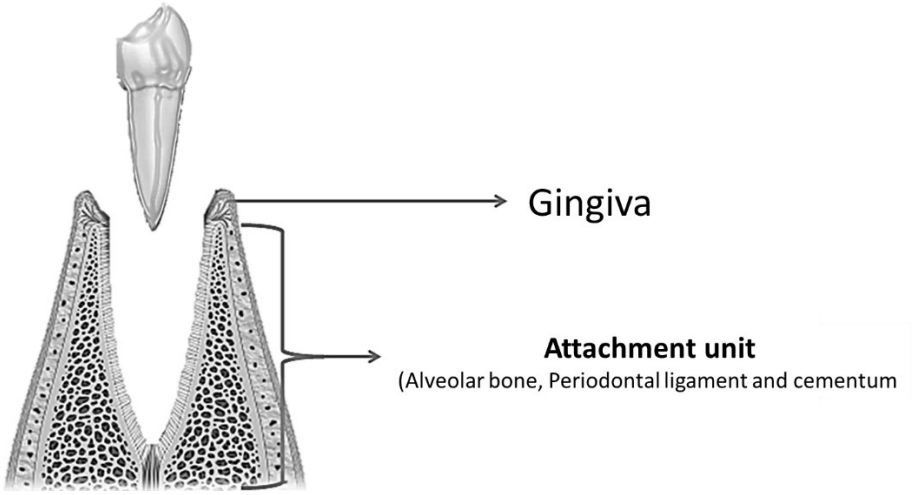

Figure 2.1 - Periodontium structures (Modified from (Jain, 2020))

The gingiva is the part of the masticatory mucosa that covers the alveolar process and surrounds the cervical portion of the teeth. It consists of an epithelial layer and underlying connective tissue called lamina propria. The gingiva assumes its definitive shape and texture in association with tooth eruption. Towards the crown, the pink gingiva ends at the free gingival margin, which has a scalloped contour. The gingiva is continuous in the apical direction with the

alveolar mucosa (lining mucosa), which is loose and red in color; it is usually separated by an easily recognized boundary line called the mucogingival junction or mucogingival line (Figure 2.2).

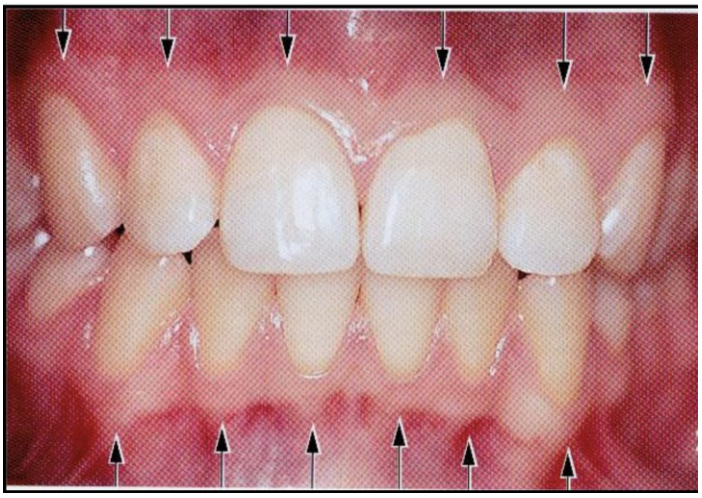

Figure 2.2 - Normal gingiva in a young adult. Arrows demarcate the mucogingival line between the attached gingiva and the darker alveolar mucosa (Figure from (Lindhe et al., 2008)).

The gingival sulcus is of great clinical importance during restorative procedures. It is defined in the studies of Ainamo and Löe (1966) as a gap or shallow space around the tooth, limited by the tooth surface and the layer of epithelium that lines the free margin of the gingiva (histological gingival sulcus) (Ainamo & Loe, 1966). It is a V-shaped depression, and it allows the entry of a periodontal probe with resistance (around 0.5 to 1.5 millimetres of depth in health) (Gargiulo, Wentz, & Orban, 1961). The gingival sulcus is divided into histological gingival sulcus and clinical gingival sulcus situated more apically. The depth of the histological gingival sulcus added to the depth of the junctional epithelium characterizes the clinical gingival area, which measures approximately 1 to 2 millimetres in the buccal and lingual and 2 to 3 millimetres in the proximal regions (Lindhe et al., 2008).

The attached gingiva is the gingiva located firmly on the periosteum below the bone crest. It is attached firmly to the underlying tissues via connective tissue fibers, and is therefore comparatively immobile in relation to the underlying tissues. It is located between the free marginal gingiva and the alveolar mucosa, from which it is separated by the mucogingival line

(Figure 2.3). In the upper arch, there is no defined boundary, and the same occurs on the lingual side in the lower arch, where the attached gingiva is continuous with the mucosa of the floor of the mouth (Lindhe et al., 2008; Newman et al., 2012).

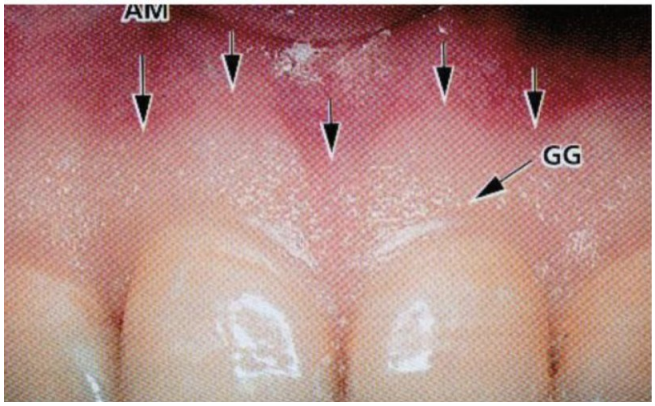

Figure 2.3 - "Orange peel" appearance of attached gingiva due to connective fiber insertions. The attached gingiva is coronally bounded by the Gingival Groove (GG). Alveolar mucosa (AM) (Figure from (Lindhe et al., 2008))

The width of the keratinized mucosa on the buccal surface varies from 1 to 9 millimetres in the different parts of the mouth and is firmly embedded in the underlying alveolar bone and cementum. It can be determined by measuring the distance from the gingival groove to the mucogingival junction (Shirmohammadi, Faramarzie, & Lafzi, 2008).

The periodontal ligament is an important component of the attachment unit, formed by loose connective tissue, richly vascularized and cellular, which surrounds the roots of the teeth and joins the root cementum to the lamina dura or to the alveolar bone. Coronally, the periodontal ligament is continuous with the lamina propria of the gingiva and is separated from it by bundles of collagen fibers that connect the crest of the alveolar bone to the root. The periodontal ligament space is narrow at the level of the middle third of the root, having an average width of 0.25 millimetres (Lindhe et al., 2008). The periodontal ligament plays an important role in transmitting and resisting occlusal loads to the bone (shock absorption and neutralization), in addition to its formative, nutritional and sensory functions (Newman et al., 2012). The periodontal ligament is vital to maintain the physiologic mobility of the tooth, and is largely determined by its width, height and quality (Newman et al., 2012).

The alveolar process is defined as the bony structures of the maxilla and mandible that form and support the dental sockets. The walls of the alveoli are lined with compact bone (cribriform plate). Cancellous bone occupies most of the interdental septa and only a small extent on the buccal and lingual bone plates. The spongy bone contains bony trabeculae, whose architecture and size are determined, in part, by the forces that the teeth are exposed to during function. In conjunction with root cementum and periodontal ligament, the alveolar bone constitutes the apparatus of insertion of the tooth, the main function of which is to distribute and absorb the forces generated by chewing and other dental contacts (Lindhe et al., 2008; Newman et al., 2012).

Bone contour varies in thickness from one region to another. In the area of incisors and premolars, the cortical bone plate of the facial surface is considerably thinner than on the lingual side. In the molar region, bone is thicker on the buccal surface than on the lingual. In addition, the alveolar process normally adapts to the prominence of the roots, merged with vertical depressions that taper towards the margin. On the buccal side, bone coverage is sometimes absent in the coronal portion of the root, forming a dehiscence. If the defect is in the middle portion of the root, the root is covered only by the periodontal ligament and the overlying gingiva (Ainamo & Loe, 1966; Gargiulo et al., 1961; Nanci & Bosshardt, 2006).

Root cementum is a highly specialized, mineralized tissue that covers, by apposition of layers, the root dentin. It also provides attachment to collagen fibers and the periodontal ligament. Structurally, it resembles bone, but it differs from it in several functional aspects such as the absence of innervation, blood supply, and lymphatic drainage. Its nutrition is directly dependent on the blood vessels of the periodontal ligament and any vascular compromise of this can lead to cementum degeneration. Cementum's ability to slowly and consistently deposit over time in humans allows it to compensate for the extrusion of the teeth and to protect the root dentin from direct contact with connective tissue. In addition to working as a root surface repairer, it also functions as a means of inserting Sharpey's fibers in order to maintain and control the width of the periodontal ligament space. The factors that trigger the activity of cementum remodeling are the healing stimulus after periodontal therapy, the orthodontic movement and primary trauma injury (Foster, 2017).

2.2 Periodontal Loss

Gingival inflammation is almost always present in all forms of periodontal disease due to bacterial plaque and irritating factors that favor the accumulation of these microbial deposits frequently present in the oral environment. Periodontitis is the most common form of periodontal disease and results from the extension of the inflammatory process initiated in the gingiva to the supporting tissues. Periodontal health depends on a balance between the internal and external environment. The internal environment is organically controlled, as per the tissue metabolism, while occlusion is an important component of the external environment. For the periodontium to remain healthy regarding its metabolism, it is necessary for mechanical stimuli from the occlusal forces of functional activity to be present. Consequently, when such functional stimuli are insufficient, there may be a degeneration of the periodontium, and changes such as decreased width of the periodontal ligament, increased thickness of the cementum and reduced bone height may occur (Newman et al., 2012).

Gingival recession can be seen when the marginal gingiva migrates towards the apex of the tooth, exposing the CEJ in the oral environment, a region where there are nerve endings, which, due to known direct causes and predisposing factors, are exposed to the oral environment (Bin Bahar, Alkhalidy, Kaklamanos, & Athanasiou, 2020). The etiology can be due to calculus, tooth brushing, high frenal attachment, position of the tooth, tooth movement by orthodontic forces, improperly designed dentures, primary occlusal trauma, smoking, restorations and some chemical use (Pradeep, Rajababu, Satyanarayana, & Sagar, 2012). One of the most common examples of chronic trauma is incorrect daily tooth brushing. This habit may cause injury to delicate gingival tissues for several years (normally associated with the presence of cervical abrasion).

In periodontal disease, there is the presence of edema and swelling of the gingival tissues caused by the accumulation of exudate and inflammatory infiltrate. This destruction caused by the progression of the disease, causes the gingiva to migrate apically, due to the loss of bone support and the inflammatory process of the bone crest (Pradeep et al., 2012).

Another cause is primary occlusal trauma, characterized by diffuse pain associated with a slight increase in tooth mobility, which, if not stopped within a few weeks, will cause uniform

enlargement of the periodontal ligament and thickening of the lamina dura or cortical alveolar bone of the tooth. The periodontal fibers become thicker and longer in order to meet the increased functional demand and to be able to absorb the most intense occlusal forces. Consequently, the thickness of the cortical alveolar bone also increases so that these fibers, now longer, can be inserted. This repetition of function that the fibers undergo, especially those inserted in the most cervical part of the alveolar bone crest, can lead to the rupture of some collagen bundles, causing stress to the periodontal ligament cells and the release of a greater amount of chemical mediators responsible for bone resorption. This process can result in bone loss from the periodontal surface of the alveolar bone crest (Persson et al., 1998).

Regarding orthodontic treatment and periodontal loss, when lateral movements are present, it can cause gingival recession, because the tooth may be being moved to an area of extremely thin bone, inducing bone crest dehiscence in this region. Tooth movement should be induced only within the limits of the trabecular alveolar bone; however, in some movements the external bone crest region is also involved, producing defects in the cortical alveolar bone (Steiner, Pearson, & Ainamo, 1981; Wennstrom, Lindhe, Sinclair, & Thilander, 1987). Ideally, the tooth involved in the movement would be fully enveloped, so that any iatrogenesis can be prevented (Johal et al., 2013). In order to avoid dehiscence and recession, only light and well-distributed forces should be used on tooth groups – and never on a single tooth. When group movement is not possible, bodily movement should be performed so that the periosteal bone replacement is deposited on the outermost part of the bone that is undergoing deflections (Castro Rodríguez & Grados Pomarino, 2017).

It is very important that great care is taken when preserving the periodontium, because the dental surface where the gingival recession has occurred no longer has the periosteum as a bone support for the gingiva, and the site is impregnated with lipopolysaccharides produced by bacteria in the oral environment, and, due to its high toxicity, it will not allow the cementoblasts to recolonize and the reattachment of periodontal fibers to occur. When this happens, the patient should be referred to a periodontist, who will surgically replace the lost gingiva through a gingival graft procedure with long junctional epithelium (F. J. Hughes, 2013).

2.2.1 Periodontium and Orthodontics

Orthodontic treatment in adults should be seen as a multidisciplinary treatment, ranging in complexity, due to the presence of several factors. Therefore, the interrelationship of medical-dental specialties is quite interesting and important for success in the treatment in adult patients. In addition to Orthodontics, several specialties, such as Periodontics and Prosthodontics as well as General Dentistry should collaborate in the formulation of a treatment plan that includes treatment of periodontal disease, tooth repositioning and subsequent missing teeth rehabilitation (Pye & Pye, 2017).

Orthodontic treatment, as part of periodontal rehabilitation, may have benefits such as the improvement in the individual's access to dental hygiene. Properly aligned teeth can contribute to the maintenance or improvement of oral health (Alfuriji et al., 2014). However, with the increase in the number of adult patients seeking orthodontic treatment, the importance of periodontal health has also increased. Non-axial loads conjugated with dental plaque can act as accelerating cofactors in the destruction of the periodontium. Therefore, orthodontic tooth movement should aim at redirecting occlusal forces so that they act along the axis of the teeth, distributing the loads more harmoniously (Gorbunkova, Pagni, Brizhak, Farronato, & Rasperini, 2016; Li, Zhan, Bao, Yi, & Li, 2021).

During the clinical examination, prior to orthodontic diagnosis and treatment planning, the patient's periodontal condition should be evaluated (gingival inflammation, edema, gingival recession, tooth mobility and periodontal pockets) (Gyawali & Bhattarai, 2017). Tooth movement in patients with reduced but healthy periodontium does not result in additional bone loss (Czochrowska & Rosa, 2014; Reichert, Hagner, Jepsen, & Jäger, 2011). However, it is known that for any type of orthodontic movement to be performed, it is essential that the patient presents a healthy periodontium, as it is imperative that, during orthodontic correction, periodontal tissue damage is not caused. Although periodontal disease is not an absolute contraindication for orthodontic treatment (Sim et al., 2017), tooth movement in patients with active periodontal disease can lead to greater loss of attachment and is therefore contraindicated (Czochrowska & Rosa, 2014).

In fact, most orthodontic treatment plans are designed with the intent that this biologic bony envelope is not violated during treatment. However, in clinical practice, the resulting treatment outcome is not always the same as the theoretical intended treatment goal; bony dehiscence and periodontal complications do occur and are some of the undesired side effects of orthodontic treatment (Gorbunkova et al., 2016; Reichert et al., 2011; Sim et al., 2017; Steiner et al., 1981).

The pre-treatment diagnostic data include patient history and examination, intra and extra oral photos, models, the evaluation of the severity of tooth crowding on the dental arch and the inclination of the teeth relative to the basal alveolar bone. Most importantly, a crucial pre-diagnostic tool is a lateral cephalometric radiograph, and it has been the diagnostic standard of care in orthodontics. Traditionally, the cephalometric radiograph was used to determine the inclination and the position of the incisors relative to the bony base and consequently, the risk of bony dehiscence. In more recent years, some practitioners have transitioned to using the more detailed three-dimensional (3D) CBCT compared to the traditional two-dimensional (2D) cephalometric radiograph (Gracco, Lombardo, Mancuso, Gravina, & Siciliani, 2009).

2.3 Periodontal Assessment

Periodontal assessment is usually made based on the visual examination of the gingiva (observing the clinical appearance in relation to staining, consistency, thickness, texture and presence/absence of bleeding) and clinical examination with the help of a periogram (with a periodontal probe to assess the depth of the gingival sulcus). Radiographic examination is also necessary to classify the periodontitis as to the stage and grade according to the current Classification of Periodontal Diseases (Papapanou et al., 2018).

For many years, 2D radiographs were the only way to perform periodontal assessment other than clinically. Prior to the introduction of computed tomography, the buccal and lingual bone plates could not be properly visualized, hidden on conventional radiographs due to image superimpositions and clinically made up by the gingival overlay (Mol & Balasundaram, 2008).

Radiology has been evolving continuously since the discovery of the X-ray in 1895 (Tubiana, 1996). Due to the technological revolution of the last few decades, it has achieved

advances that were previously unimaginable. CBCT allows dentistry to glimpse what conventional radiographs have never shown: the thickness and level of the bone plates that cover the teeth buccally and lingually. Due to their high definition and sensitivity, images from helical computed tomography and CBCT can reveal sites with periodontal bone dehiscence and fenestrations (R. Fuhrmann, Bucker, & Diedrich, 1997; R. A. Fuhrmann, Bucker, & Diedrich, 1995; Loubele et al., 2008; Mol & Balasundaram, 2008). Prior to the advent of computed tomography, efforts to define the impact of tooth movement on the buccal and lingual bone plates focused on animal studies (Steiner et al., 1981; Wennstrom et al., 1987) and studies with conventional radiographs (Mulie & Hoeve, 1976). Currently, CBCT studies on the morphology of buccal and lingual bone plates are increasing (Gracco et al., 2009; Swasty et al., 2009; Yamada et al., 2007); as well as assessments of the repercussions of tooth movement on the alveolar bone during orthodontic treatment (Garib, Henriques, Janson, de Freitas, & Fernandes, 2006; Leung, Palomo, Griffith, & Hans, 2010; Rungcharassaeng, Caruso, Kan, Kim, & Taylor, 2007; Sarikaya, Haydar, Ciger, & Ariyurek, 2002). These findings may alter usual planning, pointing out the limits of therapeutic possibilities in Orthodontics.

2.3.1 Cone Beam Computed Tomography (CBCT)

The CBCT device has a conical beam of radiation and a 2D detector, which rotate up to 360° in the region of interest. During the rotation, numerous records, with information necessary for the creation of the 3D image, are sent to the computer. There, the image is reconstructed by means of a software. Axial, coronal and sagittal cuts can be easily made through the assembly created virtually during the reconstruction (Abdelkarim, 2019). The total 3D volumetric dataset of the scanned area has a cylindrical shape that can vary according to the type of equipment, and is composed of the voxel unit, that is, the smallest unit of the image in the slice thickness. A voxel size can vary from 0.08 mm to 0.5 mm, depending on the image resolution and the field of view size applied. In large field of views, image quality ends up decreasing due to the image resolution applied and the amount of scattering radiation. In CBCT, the voxel is called isometric: both height and width have equal dimensions which means it provides information on the real size of the object (Pauwels R et al., 2015).

The voxel size of a 3D image is equivalent to the pixel resolution in 2D images (Spin-Neto et al., 2013). The voxel size determines the resolution image (Scarfe et al., 2006). The smaller the voxel size, the greater the resolution and sharpness of images (Ballrick et al., 2008). However, not necessarily small voxel sizes are the most used in studies. Depending on the structure that is analyzed, the intermediate or large voxel size can present a good diagnostic accuracy (Liedke et al., 2009; Maret et al., 2012; Vizzotto et al.,2013). Liedke et al. (2009) evaluated the detection of external root resorption images by CBCT utilizing different voxel sizes. They observed that the 0.3mm voxel was associated with good diagnosis accuracy, with less radiation exposure.

It is of common knowledge that practitioners must minimize any harm to their patients and should adhere to ALARA principle (as low as reasonably achievable) (Lurie & Kantor, 2020) since all x-ray radiation has a cumulative dosage effect over a lifetime. Although CBCT overcomes some limitations of conventional 2D radiographs, it delivers a higher radiation dose to the patients. As a comparative, the typical effective dose resulting from a panoramic radiograph varies between 0.014 mSv to 0.024 mSv, from a cephalometric radiograph that value is approximately 0.002-0.005 mSv, for an interproximal examination (four views) using image receptors (stimulated phosphor plate) the effective dose is about 0.005 mSv, whereas the dose in a CBCT is about 50 μSv (small/ medium-sized scanning) and 0.1 mSv for large volumes (Shatskiy, 2021).

Children and adolescents have increased cell and tissue sensitivity to radiation than adults and are therefore radiosensitive and susceptible to the ionizing effects of radiation (Applegate & Cost, 2013; Applegate & Thomas, 2011; Kleinerman, 2006). However, any quantity of ionizing radiation, regardless of how small, can cause a detrimental effect to all age groups, given the biological effect produced by the deposition of energy in the exposed tissues and/or organs. Radiation is also considered a carcinogen and the safety practices are built on the linear non-threshold, which assumes that even very minimal doses of radiation can lead to cancer (Hall & Giaccia, 2006). Therefore, the fundamental principles of radiation protection, that includes justification, optimization and dose limitation should always be followed when considering radiation exposure for orthodontic purposes.

2.3.2 Micro-CT (μCT)

The progress of computing was fundamental to the great development of tomographic exams. The union of the computer with the x-rays is considered one of the most important innovations of the second half of the 20th century (Hessenbruch, 2002). In the early 1970s, researchers developed several techniques for digital reconstruction of tomographic images that enabled a new era in radiological diagnosis (Lee & Crean, 2013). The use of CT in other areas such as materials engineering and nanotechnology required the formation of high-resolution images at a micrometer scale. Soon, a group of researchers engaged themselves in the development of tomographic equipment capable of reconstructing three-dimensional images in microstructural dimensions (Stock, 1999).

Derived from CT, micro computed tomography (micro-CT or μCT) is capable of producing high resolution images of very small objects. In the years that followed, it became evident that μCT would revolutionize areas of bone biology and biomechanics (Boerckel et al., 2014). This technique makes the reconstruction of three-dimensional images possible, which are formed by the digital union of hundreds of cross-sections of the evaluated material (Baird & Taylor, 2017). From then on, in Dentistry, this imaging test began to be used in the evaluation of biological samples, mainly in bone and dental assessments. Thus, there was a large growth in the number of publications that used μCT in the evaluation of the most diverse types of materials (Schambach et al., 2010). Currently, several μCT systems are available on the market and the technological innovations continue to increase resolution and applicability (Boerckel et al., 2014).

All structural indices normally determined from two-dimensional histological sections could be obtained in a non-destructive manner, as this technique does not cause damage to the material (Du Plessis & Boshoff, 2019). The reconstruction from a large number of slices in each of the three orthogonal directions allowed a detailed description of structural variation within a small specimen and greatly facilitated the study of structural anisotropy. Therefore, μCT overcomes many limitations of current approaches to the study of bone architecture at the microscopic level (Feldkamp et al., 1989). Another advantage of μCT is the possibility of manipulating the images using specific software.

Early diagnosis of minor changes in alveolar bone, resulting from pathological processes such as periodontitis, periapical lesions, root resorption, or due to regenerative treatment, requires accurate and sensitive diagnostic methods. With the advent of μCT it is possible to evaluate dynamic changes in the thickness of the periodontal ligament and in the alveolar bone clearly and precisely (Ferrare et al., 2013).

The physical principle for the formation of the microtomographic image is based on the properties of x-ray attenuation materials (Machado et al., 2014), which depends on the composition and density of the evaluated material (Duplessis; Boshoff, 2019). μCT has been applied in several areas of knowledge, such as: characterization of materials (Hanke et al., 2016), archeology (Zanolli et al., 2017), geology (Jacques et al., 2014), tissue engineering (Boerckel et al., 2014), dentistry (Dalstra et al., 2015; Catunda et al., 2021; Park et al., 2007; Steiner, Synek, & Pahr, 2020; Wilensky et al., 2005) and orthopedics (Roberto-Rodrigues et al., 2015).

The μCT equipment is made up of a few main components: the micro-focal x-ray emitter, the collimator, the sample holder and the x-rays. The latter consists of a scintillation detector and a coupled charge device (CCD) (Boerckel et al., 2014). Initially, in ex-vivo evaluations of rigid samples such as bone and tooth, the fragment is fixed firmly to a support inside the micro-tomograph. The μCT equipment is quite compact and does not require large physical structures for installation and can be commercially acquired by research centers and universities (Figure 2.4).

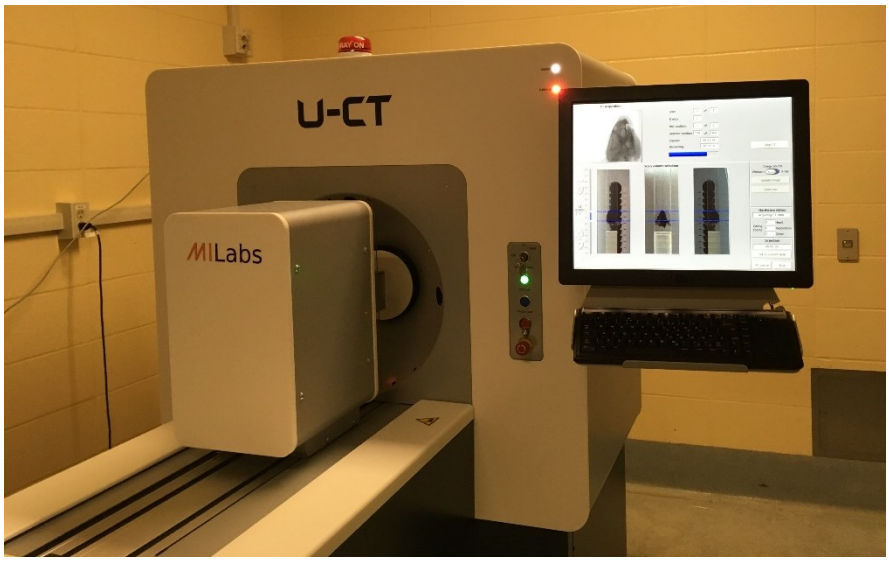

Figure 2.4 - μCT device at the University of Alberta demonstrating the compactness of the equipment (picture was generously donated by Dr. Raisa Catunda)

X-rays are generated by the micro-focal emitter of radiation, collimated and, in sequence, reach the sample, where part of these rays are attenuated according to the characteristics of the sample composition. The remainder of the radiation passes through and reaches the scintillation detector (Clark & Badea, 2014). Upon reaching the scintillation detector, the radiation is transformed into visible light (photons), which are identified by the CCD. When light photons fall on the CCD, they generate an electronic signal, which is scanned and sent to the computer, where the data is processed (Holdsworth & Thornton, 2002; Li et al., 2008). Each pixel of an image obtained in the scan corresponds to the average absorption of photons by the detector (Figure 2.5). In the 3D image reconstruction process, the pixel is transformed into a voxel, a three-dimensional unit capable of representing the depth in the microtomographic image (Lopes et al., 2012).

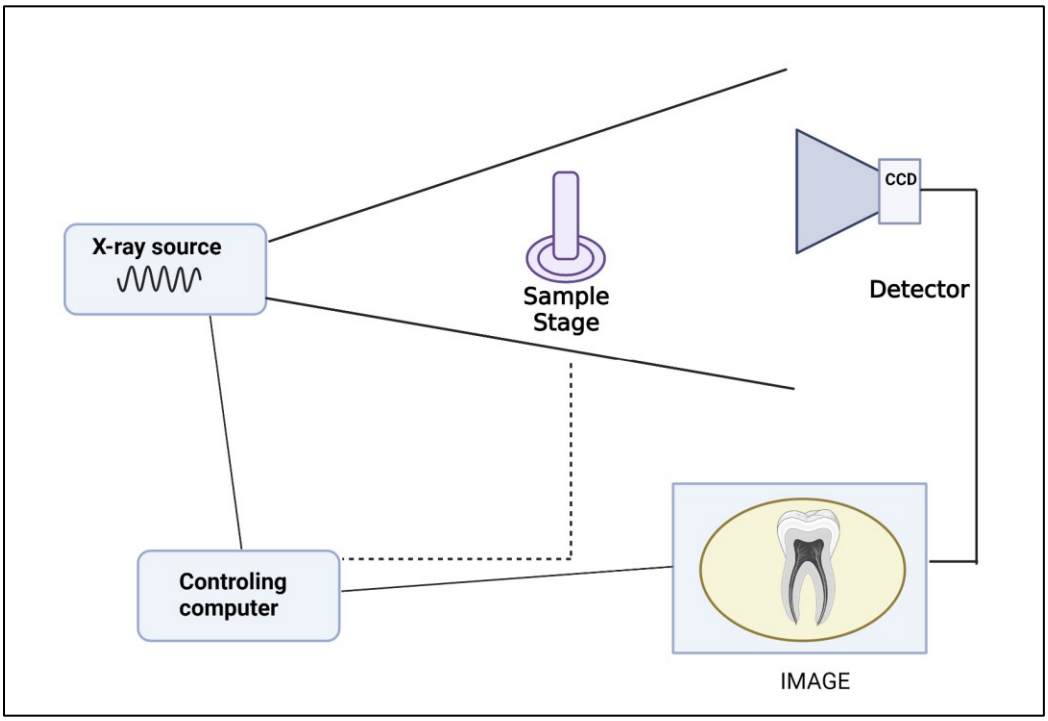

Figure 2.5 - Schematic of a µCT equipment.

The sample is placed on the sample stage and the radiographic projections are obtained by the scintillation detector, which is connected to a charge-coupled device (CCD). The CCD transforms visible light into a digital signal. During scanning, the controlling computer sets the intensity of x-ray emission and the rotation of the sample, allowing the acquisition of hundreds

of projections at various angles of incidence. The above image was created using the Biorender software and adapted from Holdsworth & Thornton (2002).

Microtomographic scanning produces 3D images at microscopic resolution by reconstructing hundreds of two-dimensional images, obtained from multiple angles around the sample (Clark & Badea, 2014). In this way, μCT generates large amounts of gigabytes of data, which are stored on the computer hardware. To visualize the samples, two-dimensional models and reconstruction of three-dimensional models are generated and the images are loaded into specialized analysis software, preferably on a high-performance computer (Baird & Taylor, 2017). The software links the three-dimensional and the two-dimensional projections, based on a pre-established algorithm.

μCT is a technique that has been widely used in dental research (Catunda et al., 2021; Park et al., 2007; Steiner, Synek, & Pahr, 2020; Wilensky et al., 2005; Hutchinson et al., 2017; Particelli et al., 2012). The use of microtomography in dental studies include the assessment of the mineral concentration of enamel and dentin, identification of demineralization sites, measurement of cavities, quantification of dentin removed in different restorative treatments, evaluation of root canal morphology and identification of microleakage in dental sealants (Neves et al., 2014; Chalas et al., 2017). As a comparison, the standard CT ones normally have a reconstructed voxel resolution down to 30 μm, whereas the high-resolution μCT can have a reconstructed voxel resolution even lower (down to 10 μm), the ones called “ultra-high resolution” can go down to 4 μm, and finally the named “extra-ultra-high resolution” with reconstructed voxel resolution down to 2.4 μm (MiLabs, 2022).

The accuracy of μCT in dental samples was demonstrated in a study which compared the results obtained by the microtomographic examination with other already established measurement techniques (direct measurement of the tooth with a caliper, measurement of the tooth in photographic images and measurement of the tooth by three-dimensional image obtained by a surface scanner). The μCT was a reliable and accurate method for performing linear measurements on teeth (Kim et al., 2007).

Therefore, μCT allows the 3D reconstruction of the internal structures of samples and can generate accurate quantitative and qualitative data. In this way, it allows extensive analysis of tissue morphometry when compared to histological evaluation and electron microscopy (which

are limited to a few transversal sections) which are also considered gold standard for tissue analysis (Bouxsein et al., 2022).

However, for *in vivo* studies, it is limited to the imaging and longitudinal analysis of small animals, Therefore, most research utilizing μCT has been accomplished with *ex vivo* and not *in vivo* specimens. In addition to the increased radiation dose, μCT allows only the analysis of samples of reduced size, which ends up restricting even the *ex vivo* niche of analysis (Marciano et al., 2012).

2.3.3 Ultrasound

Ultrasonography or ultrasound (US) is an image modality that takes advantage of the echo/reflections produced by ultrasound signals coming from internal structures of the human body that allows the clinician to visualize them in real time (Mahesh, 2013). US devices in general use a varied frequency, depending on the type of transducer, from 2 to 40 MHz, emitting through a piezoelectric crystal source that is in contact with the skin and is receiving the generated echoes, which are interpreted through computer graphics (Coatney, 2001). The probe also functions as a transmitter/receiver. The higher the frequency, the higher the resolution obtained, and the more precision we have in visualizing the surface structures. However, the higher the frequency, the less is the penetrating depth. According to the density and composition of the tissue interfaces, the attenuation and phase change of the emitted signals varies. This change is what allows the translation into a gray scale, which will form the computer image of the internal organs (Aldrich, 2007).

When the ultrasonic beam passes through or interacts with tissues of different acoustic impedances, it is lowered by a combination of the absorption, reflection, refraction and scattering. The sound waves that are reflected (echo) back to the transducer cause a change in the thickness of the piezoelectric crystal, which, in turn, produces an electrical signal that is amplified, processed, and finally displayed as an image on the monitor. Current techniques permit for the echoes to be processed fast enough to allow the perception of motion: real-time image (Shah, Bansal, & Logani, 2014).

US is currently one of the most popular diagnostic imaging methods in general medicine as it is versatile, ubiquitous and relatively simple to apply. In the last two decades of the

twentieth century, technological development has transformed this method into a powerful instrument of directed medical research, requiring constant training and a participatory conduct of the examiner (Shah et al., 2014).

According to Jones and Frost (1984) the image obtained in an ultrasonography depends on the type of device used (Jones & Frost, 1984). For example, the frequency is represented by cycles of pressure changes (1 s Hertz). In high-frequency ultrasound (HFUS), the wavelengths are shorter, so they can be absorbed more easily (meaning they aren't as penetrating). This implies that it can be applied to investigate superficial structures, spreading its application to fields such as dermatology and dentistry (Aldrich, 2007; Nguyen et al., 2018). Another important feature is the propagation speed, which basically characterizes the speed that the US circulates across a medium (1540 m/s in soft tissues). Unlike frequency, which depends solely on the sound source, the propagation speed depends on the attributes of the medium (such as density and rigidity) in which the wave propagates (Reda et al., 2021).

When utilizing an US, the angle of incidence is also particularly important. If the US beam hits the border obliquely, it can be in part reflected, making the clinical evaluation of the image generated more complicated. Therefore, when part of the beam is deflected, refraction occurs, and it depends on the speed of the US at the sides of the interface. According to Snell's law, the calculation of the amount of beam deflection can be performed and it correlates to the angle of refraction and speed of the US beam passing through that interface (Reda et al., 2021).

There are different types of images that the ultrasound forms, depending on the intensity of the echo produced by the tissues. The tissues are determined according to the degree of reflection they produce, (that is, how their echogenicity is), and are displayed using a grayscale. Depending on the direction of the transducer, the image will be in different slices. If the transducer is horizontal, the cuts will show up as: soft tissue and bone, then muscles as it deepens (Evirgen & Kamburoglu, 2016). Regarding the type of image formed, there are the following classifications:

- Hypoechoic - images of lower intensity than those of the adjacent tissues.
- Hyperechoic - images of greater intensity than the adjacent tissues.
- Isoechoic - images of similar intensity to the adjacent tissues.

- Anechoic - the absence of echo in the tissues.
- Hypoechogenic - moderate echo of low intensity, represented by gray levels.

According to Schön, Düker and Schmelzeisen (2002), the main advantages of using US are:

- It is a non-invasive or minimally invasive method.
- Presents anatomy in sectional or two-dimensional images and most recently even three-dimensional, with the help of computer reconstruction.
- It has no significant harmful effects within the specifications of diagnostic use in the health field.
- It does not use ionizing radiation.
- It enables the non-invasive study of body hemodynamics through the Doppler effect.
- It allows the acquisition of dynamics images, in real time, enabling studies of the movement of body structures.

Some of the disadvantages are:

- Technique-wise it is operator dependent (experience counts), a specialist in radiology is required for real time analysis
- Difficulty in interpretation given the low resolution of the images (Schon, Duker, & Schmelzeisen, 2002).

Some of the current clinical US applications in dentistry are: detection of stones in the ducts of the salivary glands (sialolithiasis), swellings in the neck region, determination of the relationship between the vascularity of the masses and vascular structures of glandular inflammation when the use of sialography is contraindicated. In the dental field, the exploration has been more so on soft tissues, since it allows the clinician to measure height, width and depth of any changes.

Some systematic reviews have tried to gather reliable information on previous publications involving US intra-orally in Dentistry (Marotti et al., 2013; Nguyen et al., 2018; Reda et al., 2021). In the one by Nguyen et al. (2018), they compared the accuracy of US vs

CBCT to measure alveolar bone level (distance from CEJ to alveolar bone crest). In the four studies included in their systematic review (all *ex vivo*, either porcine or human cadavers), they found that the mean difference between US and CBCT varied from 0.07 mm to 0.68 mm (1.6% - 8.8%). Therefore, the contemporary application techniques of US are essential in the technological evolution, since they represent a potential diagnostic tool and are an especially important area for investigation in Dentistry with the aim to lessen the harm and radiation side effects. The use of US in Dentistry can represent a high potential for a radiation-free alternative, in specific contexts, to the previous highly utilized assessment methods.

2.3.4 Ultrasound in the Alveolar Bone Complex

US seems to be a promising device for imaging the hard and soft tissue structures in the oral cavity (Marotti et al., 2013; Palou, McQuade, & Rossmann, 1987; Salmon & Le Denmat, 2012). Some of the uses in the alveolar bone complex to date have been to map enamel-dentin/cementum junctions in human teeth (D. A. Hughes et al., 2009), alveolar bone crest location (Tsiolis, Needleman, & Griffiths, 2003), alveolar crest height (Spranger, 1971), determination of periodontal bone morphology in periodontal disease patients (Palou et al., 1987) and peri-implantitis patients (Chan & Kripfgans, 2020), assessment of bone around dental implants (Bohner et al., 2019), early caries diagnosis (Kim, Shin, Kong, Hwang, & Hyun, 2019) and buccal crestal bone level and dimension (Chan et al., 2017). The CEJ, which is an anatomical landmark, has a significant clinical importance in the oral health evaluation, given that several periodontal measurements depend on it (Preshaw, Kupp, Hefti, & Mariotti, 1999).

From the very first study by Spranger (1971) to the most up to date one by Chan & Kripfgans (2020), the image quality has improved significantly. The high-resolution US clearly allows the clinician to have access to the cross-sectional morphological images of the hard and soft tissues, the alveolar crest level, the location of CEJ, and the thickness the of alveolar crest. In this way, accuracy of diagnosis and assessment can be improved, and periodontal risks for the patients can be decreased (Reda et al., 2021).

Other prospective uses, as mentioned previously, with HFUS (40 MHz) are that radiolucent areas where the alveolar cortex is thinned or even nonexistent can be detected, or children (as their alveolar bone is of a thinner depth) who have developing/retained teeth can

have a safer mean of diagnosis (Cotti, Campisi, Garau, & Puddu, 2002; Nguyen et al., 2018). In treating a patient orthodontically, several factors need to be considered. Some of these factors are crowding, the position of the lower incisors and the growth pattern. Contemporary orthodontics also include facial and smile esthetics in this list (Proffit, 2013). Over time, imaging has been elucidating the accepted range for dental compensation or decompensation in each individual patient. Additionally, the knowledge of the morphology of the buccal bone plate helps orthodontists to discern between patients who could and who should not undergo expansion mechanics, for example. Knowing the anatomical details of patients and understanding the side effects of tooth movement means recognizing our limits and practicing orthodontics more safely (Abdelkarim, 2019).

References

Abdelkarim, A. (2019). Cone-Beam Computed Tomography in Orthodontics. *Dent J (Basel), 7*(3). doi:10.3390/dj7030089

Ainamo, J., & Loe, H. (1966). Anatomical characteristics of gingiva. A clinical and microscopic study of the free and attached gingiva. *J Periodontol, 37*(1), 5-13. doi:10.1902/jop.1966.37.1.5

Aldrich, J. E. (2007). Basic physics of ultrasound imaging. *Crit Care Med, 35*(5 Suppl), S131-137. doi:10.1097/01.CCM.0000260624.99430.22

Alfuriji, S., Alhazmi, N., Alhamlan, N., Al-Ehaideb, A., Alruwaithi, M., Alkatheeri, N., & Geevarghese, A. (2014). The effect of orthodontic therapy on periodontal health: a review of the literature. *Int J Dent, 2014*, 585048. doi:10.1155/2014/585048

Applegate, K. E., & Cost, N. G. (2013). Image Gently: a campaign to reduce children's and adolescents' risk for cancer during adulthood. *J Adolesc Health, 52*(5 Suppl), S93-97. doi:10.1016/j.jadohealth.2013.03.006

Applegate, K. E., & Thomas, K. (2011). Pediatric CT--the challenge of dose records. *Pediatr Radiol, 41 Suppl 2*, 523-527. doi:10.1007/s00247-011-2161-9

Baird, E., Taylor, G. (2017). X-ray micro computed-tomography. *Current Biology*, 27(8), 289-291. doi: 10.1016/j.cub.2017.01.066.

Ballrick, J.W., Palomo, J.M., Ruch, E., Amberman, B.D., Hans, M.G. (2008). Image distortion and spatial resolution of a commercially available cone-beam computed tomography machine. Am *J Orthod Dentofacial Orthop*, 134(4), 573-82. doi: 10.1016/j.ajodo.2007.11.025

Bin Bahar, B. S. K., Alkhalidy, S. R., Kaklamanos, E. G., & Athanasiou, A. E. (2020). Do orthodontic patients develop more gingival recession in anterior teeth compared to untreated individuals? A systematic review of controlled studies. *Int Orthod, 18*(1), 1-9. doi:10.1016/j.ortho.2019.08.025

Boerckel, J. D., Mason, D. E., Mcdermott, A. M., Alsberg, E. (2014). Microcomputed tomography: approaches and applications in bioengineering. *StemCell Research & Therapy*, 5(6),144. doi: 10.1186/scrt534.

Bohner, L., Habor, D., Tortamano, P., Radermacher, K., Wolfart, S., & Marotti, J. (2019). Assessment of Buccal Bone Surrounding Dental Implants Using a High-Frequency Ultrasound Scanner. *Ultrasound Med Biol, 45*(6), 1427-1434. doi:10.1016/j.ultrasmedbio.2019.02.002

Bouxsein, M.L., Boyd, S.K., Christiansen, B.A., Guldberg, R.E., Jepsen, K.J., Müller, R. (2010). Guidelines for assessment of bone microstructure in rodentsusing micro-computed tomography. *J Bone Miner Res*, 25,1468–1486. Doi: 10.1002/jbmr.141

Castro Rodríguez, Y., & Grados Pomarino, S. (2017). Orthodontic dental movement and its association with the presence of gingival recession. *Revista Odontológica Mexicana, 21*(1), e8-e11. doi:https://doi.org/10.1016/j.rodmex.2017.02.005

Catunda, R. Q., Ho, K. K.-Y., Patel, S., & Febbraio, M. (2021). A 2-plane micro-computed tomographic alveolar bone measurement approach in mice. *Imaging Sci Dent*, 51(4), 389-398. doi: 10.5624/isd.20210058

Chałas, R., Szlązak, K., Wójcik-Chęcińska, I., Jaroszewicz, J., Molak, R. (2017). Observations of mineralised tissues of teeth in X-ray micro-computed tomography. *Folia Morphologica*, 76(2), 143-148. doi: 10.5603/FM.a2016.0070

Chan, H. L., & Kripfgans, O. D. (2020). Ultrasonography for diagnosis of peri-implant diseases and conditions: a detailed scanning protocol and case demonstration. *Dentomaxillofac Radiol, 49*(7), 20190445. doi:10.1259/dmfr.20190445

Chan, H. L., Sinjab, K., Chung, M. P., Chiang, Y. C., Wang, H. L., Giannobile, W. V., & Kripfgans, O. D. (2017). Non-invasive evaluation of facial crestal bone with ultrasonography. *PLoS One, 12*(2), e0171237. doi:10.1371/journal.pone.0171237

Clark, D. P., Badea, C. T. (2014). Micro-CT of rodents: state-of-the-art and future perspectives. *Physica medica*, 30(6), 619-634. doi: 10.1016%2Fj.ejmp.2014.05.011

Coatney, R. W. (2001). Ultrasound imaging: principles and applications in rodent research. *ILAR J, 42*(3), 233-247. doi:10.1093/ilar.42.3.233

Cotti, E., Campisi, G., Garau, V., & Puddu, G. (2002). A new technique for the study of periapical bone lesions: ultrasound real time imaging. *Int Endod J, 35*(2), 148-152. doi:10.1046/j.1365-2591.2002.00458.x

Czochrowska, E., & Rosa, M. (2014). The Orthodontic / Periodontal Interface. *Seminars in Orthodontics, 21*. doi:10.1053/j.sodo.2014.12.001

Dalstra, M., Cattaneo, P. M., Laursen, M. G., Beckmann, F., Melsen, B. (2015). Multi-level synchrotron radiation-based microtomography of the dental alveolus and its consequences for orthodontics. *Journal of Biomechanics*, 48 (5), 801-806. doi: 10.1016/j.jbiomech.2014.12.014

Du Plessis, A., Boshoff, W. P. (2019). A review of X-ray computed tomography of concrete and asphalt construction materials. *Construction and Building Materials*, 199, 637-651. doi.org/10.1016/j.conbuildmat.2018.12.049.

Evirgen, S., & Kamburoglu, K. (2016). Review on the applications of ultrasonography in dentomaxillofacial region. *World J Radiol, 8*(1), 50-58. doi:10.4329/wjr.v8.i1.50

Feldkamp, L.A., Goldstein, S.A., Parfitt, A.M., Jesion, G. (1989). The direct examination of three-dimensional bone architecture in vitro by computed tomography. Journal of Bone Mineral Research, 4,3-11. doi: 10.1002/jbmr.5650040103

Ferrare, N, Leite, A.F., Caracas, H.C.P.M., Azevedo, R.B., Melo, N.S., Figueiredo, P.T.S. (2013). Cone-beam computed tomography and microtomography for alveolar bone measurements. Surgical and Radiologic Anatomy, 35, 495-502. doi: 10.1007/s00276-013-1080-x

Foster, B. L. (2017). On the discovery of cementum. *J Periodontal Res, 52*(4), 666-685. doi:10.1111/jre.12444

Fuhrmann, R. A., Bucker, A., & Diedrich, P. R. (1995). Assessment of alveolar bone loss with high resolution computed tomography. *J Periodontal Res, 30*(4), 258-263. doi:10.1111/j.1600-0765.1995.tb02131.x

Fuhrmann, R., Bucker, A., & Diedrich, P. (1997). Radiological assessment of artificial bone defects in the floor of the maxillary sinus. *Dentomaxillofac Radiol, 26*(2), 112-116. doi:10.1038/sj.dmfr.4600223

Gargiulo, A. W., Wentz, F. M., & Orban, B. (1961). Dimensions and Relations of the Dentogingival Junction in Humans. *The Journal of Periodontology, 32*(3), 261-267. doi:https://doi.org/10.1902/jop.1961.32.3.261

Garib, D. G., Henriques, J. F., Janson, G., de Freitas, M. R., & Fernandes, A. Y. (2006). Periodontal effects of rapid maxillary expansion with tooth-tissue-borne and tooth-borne expanders: a computed tomography evaluation. *Am J Orthod Dentofacial Orthop, 129*(6), 749-758. doi:10.1016/j.ajodo.2006.02.021

Gonzalez, S. M. (2013). *Interpretation Basics of Cone Beam Computed Tomography*. Ames, Iowa: Wiley-Blackwell.

Gorbunkova, A., Pagni, G., Brizhak, A., Farronato, G., & Rasperini, G. (2016). Impact of Orthodontic Treatment on Periodontal Tissues: A Narrative Review of Multidisciplinary Literature. *Int J Dent, 2016*, 4723589. doi:10.1155/2016/4723589

Gracco, A., Lombardo, L., Mancuso, G., Gravina, V., & Siciliani, G. (2009). Upper incisor position and bony support in untreated patients as seen on CBCT. *Angle Orthod, 79*(4), 692-702. doi:10.2319/081908-437.1

Gyawali, R., & Bhattarai, B. (2017). Orthodontic Management in Aggressive Periodontitis. *Int Sch Res Notices, 2017*, 8098154. doi:10.1155/2017/8098154

Hall, E. J., & Giaccia, A. J. (2006). *Radiobiology for the radiologist*(6th ed., pp. ix, 546 p.). Retrieved from https://ovidsp.ovid.com/ovidweb.cgi?T=JS&PAGE=booktext&NEWS=N&DF=bookdb&AN=01382670/6th_Edition&XPATH=/PG(0)

Hanke, R., Fuchs, T., Salamon, M., & Zabler, S. (2016). 3 - X-ray microtomography for materials characterization. In G. Hübschen, I. Altpeter, R. Tschuncky, & H.-G. Herrmann (Eds.), Materials Characterization Using Nondestructive Evaluation (NDE) Methods (pp. 45-79): Woodhead Publishing.

Holdsworth, D. W., Thornton, M. M. (2002). Micro-CT in small animal and specimen imaging. *Trends in Biotechnology*, 20 (8), 34-39. doi: 10.1016/S0167- 7799(02)02004-8

Hughes, D. A., Girkin, J. M., Poland, S., Longbottom, C., Button, T. W., Elgoyhen, J., Hughes, H., Meggs, C., Cochran, S. (2009). Investigation of dental samples using a 35MHz focussed ultrasound piezocomposite transducer. *Ultrasonics, 49*(2), 212-218. doi:10.1016/j.ultras.2008.08.007

Hughes, F. J. (2013). *Clinical problem solving in periodontology & implantology* (1st ed.). Edinburgh ; New York: Churchill Livingstone Elsevier.

Hutchinson, J.C., Shelmerdine, S.C., Simcock, I.C., Sebire, N.J., Arthurs, O.J. (2017). Early clinical applications for imaging at microscopic detail: microfocus computed tomography (micro-CT). *Br J Radiol*, 90(1075), 20170113. doi: 10.1259/bjr.20170113.

Jacques, P. D., Nummer, A. R., Heck, R. J., Machado, R. (2014). The use of microtomography in structural geology: A new methodology to analyse fault faces. *Journal of Structural Geology*, 66, 347-355. doi: 10.1016/j.jsg.2014.06.004

Jain, S. (2020). What is the periodontium. In. Prestige Dental Care Raipur.

Johal, A., Katsaros, C., Kiliaridis, S., Leitao, P., Rosa, M., Sculean, A., . . . Zachrisson, B. (2013). State of the science on controversial topics: orthodontic therapy and gingival recession (a report of the Angle Society of Europe 2013 meeting). *Prog Orthod, 14*, 16. doi:10.1186/2196-1042-14-16

Jones, J. K., & Frost, D. E. (1984). Ultrasound as a diagnostic aid in maxillofacial surgery. Report of a case. *Oral Surg Oral Med Oral Pathol, 57*(6), 589-594. doi:10.1016/0030-4220(84)90277-9

Kim, I., Paik, K.S., Lee, S.P. (2007). Quantitative evaluation of the accuracy of micro- computed tomography in tooth measurement. *Clinical Anatomy*, 20(1), 27- 34. doi: 10.1002/ca.20265

Kim, J., Shin, T. J., Kong, H. J., Hwang, J. Y., & Hyun, H. K. (2019). High-Frequency Ultrasound Imaging for Examination of Early Dental Caries. *J Dent Res, 98*(3), 363-367. doi:10.1177/0022034518811642

Kleinerman, R. A. (2006). Cancer risks following diagnostic and therapeutic radiation exposure in children. *Pediatr Radiol, 36 Suppl 2*, 121-125. doi:10.1007/s00247-006-0191-5

Lee, S., Crean, M. (2013). The story of radiology contents. Vienna, Austria (101p): European Society of Radiology.

Leung, C. C., Palomo, L., Griffith, R., & Hans, M. G. (2010). Accuracy and reliability of cone-beam computed tomography for measuring alveolar bone height and detecting bony dehiscences and fenestrations. *Am J Orthod Dentofacial Orthop, 137*(4 Suppl), S109-119. doi:10.1016/j.ajodo.2009.07.013

Li, H., Zhang, H., Tang, Z., Hu, G. (2008) Micro-computed tomography for small animal imaging: Technological details. *Progress in Natural Science*, 18(5), 513- 521. doi: 10.1016/j.pnsc.2008.01.002.

Li, Y., Zhan, Q., Bao, M., Yi, J., & Li, Y. (2021). Biomechanical and biological responses of periodontium in orthodontic tooth movement: up-date in a new decade. *Int J Oral Sci, 13*(1), 20. doi:10.1038/s41368-021-00125-5

Liedke G.S., da Silveira H.E., da Silveira H.L., Dutra V., de Figueiredo J.A. (2009). Influence of voxel size in the diagnostic ability of cone beam tomography to evaluate simulated external root resorption. *J Endod*, 35(2), 233-5. doi: 10.1016/j.joen.2008.11.005

Lindhe, J., Lang, N. P., & Karring, T. (2008). *Clinical periodontology and implant dentistry* (5th ed.). Oxford ; Ames, Iowa: Blackwell Munksgaard.

Lopes, A. P.; Fiori A. P.; Reis Neto, J. M.; Marchese, C.; Vasconcellos, E. M. G. et al. (2002). Three-dimensional analysis of rocks through X-ray computerized microtomography Integrated to petrography. *Geociencias*, 31(1), 129-142. Retrieved from http://www.ppegeo.igc.usp.br/index.php/GEOSP/article/view/7248.

Loubele, M., Van Assche, N., Carpentier, K., Maes, F., Jacobs, R., van Steenberghe, D., & Suetens, P. (2008). Comparative localized linear accuracy of small-field cone-beam CT and multislice CT for alveolar bone measurements. *Oral Surg Oral Med Oral Pathol Oral Radiol Endod, 105*(4), 512-518. doi:10.1016/j.tripleo.2007.05.004

Lurie, A. G., & Kantor, M. L. (2020). Contemporary radiation protection in dentistry: Recommendations of National Council on Radiation Protection and Measurements Report No. 177. *J Am Dent Assoc, 151*(10), 716-719 e713. doi:10.1016/j.adaj.2020.05.007

Machado, A. C., Lima, I., Lopes, R. T. (2014). Effect of 3D computed microtomography resolution on reservoir rocks. *Radiation Physics and Chemistry*, 95, 405-407. doi: 10.1016/j.radphyschem.2012.12.029.

Mahesh, M. (2013). The Essential Physics of Medical Imaging, Third Edition. *Med Phys, 40*(7). doi:10.1118/1.4811156

Marciano, M.A., Duarte, M.A.H., Ordinola-Zapata, R., Del Carpio-Perochena, A., Cavenago, B.C., Villas-Bôas, M.H., Minotti, P.G., Bramante, C.M., Moraes, I.G. (2012). Applications of micro-computed tomography in endodontic research. In: Méndez-Vilas A, editor. Current microscopy contributions to advances in science and technology. Badajoz, Spain (p782-788): Formatex research center.

Maret, D., Telmon, N., Peters, O.A., Lepage, B., Treil, J., Inglese, J.M., et al. (2012). Effect of voxel size on the accuracy of 3D reconstructions with cone beam CT. *Dentomaxillofac Radiol*, 41(8), 649-55. doi: 10.1259/dmf/81804525

Marotti, J., Heger, S., Tinschert, J., Tortamano, P., Chuembou, F., Radermacher, K., & Wolfart, S. (2013). Recent advances of ultrasound imaging in dentistry--a review of the literature. *Oral Surg Oral Med Oral Pathol Oral Radiol, 115*(6), 819-832. doi:10.1016/j.oooo.2013.03.012

MiLabs (2022). Adaptive diagnostic CT. Retrieved August 16, 2022, from https://www.milabs.com/u-ct/

Mol, A., & Balasundaram, A. (2008). In vitro cone beam computed tomography imaging of periodontal bone. *Dentomaxillofac Radiol, 37*(6), 319-324. doi:10.1259/dmfr/26475758

Mulie, R. M., & Hoeve, A. T. (1976). The limitations of tooth movement within the symphysis, studied with laminagraphy and standardized occlusal films. *J Clin Orthod, 10*(12), 882-893, 886-889. Retrieved from https://www.ncbi.nlm.nih.gov/pubmed/1074868

Nanci, A., & Bosshardt, D. D. (2006). Structure of periodontal tissues in health and disease. *Periodontol 2000, 40*, 11-28. doi:10.1111/j.1600-0757.2005.00141.x

Neves, A. A., Jaecques, S., Van Ende, A., Cardoso, M. V., Coutinho, E. et al. (2014). 3D-microleakage assessment of adhesive interfaces: exploratory findings by uct. *Dental Materials*, 30(8), 799-807. doi: 10.1016/j.dental.2014.05.003

Olejniczak, A. J., Grine, F. E. (2006). Assessment of the accuracy of dental enamel thickness measurements using microfocal X-ray computed tomography. *The Anatomical Record*, 288 (3), 263-275. doi: 10.1002/ar.a.20307

Newman, M. G., Takei, H. H., Klokkevold, P. R., & Carranza, F. A. (2012). *Carranza's clinical periodontology*(11th ed., pp. 1 online resource (xlv, 824 p.)). Retrieved from https://search.ebscohost.com/login.aspx?direct=true&scope=site&db=nlebk&db=nlabk&AN=448414

Nguyen, K. T., Pacheco-Pereira, C., Kaipatur, N. R., Cheung, J., Major, P. W., & Le, L. H. (2018). Comparison of ultrasound imaging and cone-beam computed tomography for

examination of the alveolar bone level: A systematic review. *PLoS One, 13*(10), e0200596. doi:10.1371/journal.pone.0200596

Palou, M. E., McQuade, M. J., & Rossmann, J. A. (1987). The use of ultrasound for the determination of periodontal bone morphology. *J Periodontol, 58*(4), 262-265. doi:10.1902/jop.1987.58.4.262

Papapanou, P. N., Sanz, M., Buduneli, N., Dietrich, T., Feres, M., Fine, D. H., . . . Tonetti, M. S. (2018). Periodontitis: Consensus report of workgroup 2 of the 2017 World Workshop on the Classification of Periodontal and Peri-Implant Diseases and Conditions. *J Periodontol, 89 Suppl 1*, S173-S182. doi:10.1002/JPER.17-0721

Park, C. H., Abramson, Z. R., Taba, M., Jr., Jin, Q., Chang, J., Kreider, J. M., . . . Giannobile, W. V. (2007). Three-dimensional micro-computed tomographic imaging of alveolar bone in experimental bone loss or repair. *J Periodontol*, 78(2), 273-281. doi:10.1902/jop.2007.060252

Particelli, F., Mecozzi, L., Beraudi, A., Montesi, M., Baruffaldi, F., Viceconti, M. (2012). A comparison between micro-CT and histology for the evaluation of cortical bone: effect of polymethylmethacrylate embedding on structural parameters. *J Microsc*, 245(3),302-10. doi: 10.1111/j.1365-2818.2011.03573

Pauwels R, Araki K, Siewerdsen JH, Thongvigitmanee SS. Technical aspects of dental CBCT: state of the art. Dentomaxillofac Radiol. 2015;44(1):20140224. doi: 10.1259/dmfr.20140224. PMID: 25263643; PMCID: PMC4277439.

Persson, R. E., Hollender, L. G., Laurell, L., & Persson, G. R. (1998). Horizontal alveolar bone loss and vertical bone defects in an adult patient population. J Periodontol, 69(3), 348-356. doi:10.1902/jop.1998.69.3.348

Preshaw, P. M., Kupp, L., Hefti, A. F., & Mariotti, A. (1999). Measurement of clinical attachment levels using a constant-force periodontal probe modified to detect the cemento-enamel junction. *J Clin Periodontol, 26*(7), 434-440. doi:10.1034/j.1600-051x.1999.260704.x

Pye, G., & Pye, A. (2017). Orthodontic and periodontal multidisciplinary care. *Dental Update, 44*(6), 558-562. doi:10.12968/denu.2017.44.6.558

Reda, R., Zanza, A., Cicconetti, A., Bhandi, S., Miccoli, G., Gambarini, G., & Di Nardo, D. (2021). Ultrasound Imaging in Dentistry: A Literature Overview. *J Imaging, 7*(11). doi:10.3390/jimaging7110238

Reichert, C., Hagner, M., Jepsen, S., & Jäger, A. (2011). Interfaces between orthodontic and periodontal treatment: their current status. *J Orofac Orthop, 72*(3), 165-186. doi:10.1007/s00056-011-0023-6

Roberto-Rodrigues, M., Fernandes, R. M., Senos, R., Scoralick, A. C., Bastos, A. A. et al. (2015). Novel rat model of nonunion fracture with vascular deficit. *Injury*, 46(4), 649-654. doi: 10.1016/j.injury.2015.01.033

Rungcharassaeng, K., Caruso, J. M., Kan, J. Y., Kim, J., & Taylor, G. (2007). Factors affecting buccal bone changes of maxillary posterior teeth after rapid maxillary expansion. *Am J Orthod Dentofacial Orthop, 132*(4), 428 e421-428. doi:10.1016/j.ajodo.2007.02.052

Salmon, B., & Le Denmat, D. (2012). Intraoral ultrasonography: development of a specific high-frequency probe and clinical pilot study. *Clin Oral Investig, 16*(2), 643-649. doi:10.1007/s00784-011-0533-z

Sarikaya, S., Haydar, B., Ciger, S., & Ariyurek, M. (2002). Changes in alveolar bone thickness due to retraction of anterior teeth. *Am J Orthod Dentofacial Orthop, 122*(1), 15-26. doi:10.1067/mod.2002.119804

Scarfe WC, Farman AG, Sukovic P. (2006). Clinical applications of cone-beam computed tomography in dental practice. *J Can Dent Assoc*, 72(1), 75-80. PMID: 16480609

Schambach, S. J., Bag, S., Groden, C., Schiling, L., Brockmann, M. A. (2009). Vascular imaging in small rodents using micro-CT. *Methods*, 50(1), 26-35. doi: 10.1016/j.ymeth.2009.09.003

Schon, R., Duker, J., & Schmelzeisen, R. (2002). Ultrasonographic imaging of head and neck pathology. *Atlas Oral Maxillofac Surg Clin North Am, 10*(2), 213-241. doi:10.1016/s1061-3315(02)00009-4

Shah, N., Bansal, N., & Logani, A. (2014). Recent advances in imaging technologies in dentistry. *World J Radiol, 6*(10), 794-807. doi:10.4329/wjr.v6.i10.794

Shatskiy, I . (2021) Effective doses and radiation risks from common dental radiographic, panoramic and cbct examinations. Radiation Protection Dosimetry, 195 (3-4), 296–305. D oi: 10.1093/rpd/ncab069

Shirmohammadi, A., Faramarzie, M., & Lafzi, A. (2008). A clinical evaluation of anatomic features of gingiva in dental students in tabriz, iran. *J Dent Res Dent Clin Dent Prospects, 2*(3), 90-94. doi:10.5681/joddd.2008.019

Sim, H. Y., Kim, H. S., Jung, D. U., Lee, H., Lee, J. W., Han, K., & Yun, K. I. (2017). Association between orthodontic treatment and periodontal diseases: Results from a national survey. *Angle Orthod, 87*(5), 651-657. doi:10.2319/030317-162.1

Spin-Neto R, Gotfredsen E, Wenzel A. (2013). Impact of voxel size variation on CBCT based diagnostic outcome in dentistry: a systematic review. *J Digit Imaging*, 26(4), 813-20. doi: 10.1007/s10278-012-9562-7

Spranger, H. (1971). Ultra-sonic diagnosis of marginal periodontal diseases. *Int Dent J, 21*(4), 442-455. Retrieved from https://www.ncbi.nlm.nih.gov/pubmed/5292204

Steiner, G. G., Pearson, J. K., & Ainamo, J. (1981). Changes of the marginal periodontium as a result of labial tooth movement in monkeys. *J Periodontol, 52*(6), 314-320. doi:10.1902/jop.1981.52.6.314

Steiner, L., Synek, A., & Pahr, D. H. (2020). Comparison of different uct-based morphology assessment tools using human trabecular bone. *Bone Rep*, 12, 100261. doi:10.1016/j.bonr.2020.100261

Stock, S. R. (1999). X-ray microtomography of materials. *International Materials Reviews*, 44 (4), 141-164. doi: 10.1179/095066099101528261

Swain, M.V., Xue, J. (2009). State of the art of Micro-CT applications in dental research. *Int J Oral Sci*, 1(4), 177-88. doi: 10.4248/IJOS09031.

Swasty, D., Lee, J. S., Huang, J. C., Maki, K., Gansky, S. A., Hatcher, D., & Miller, A. J. (2009). Anthropometric analysis of the human mandibular cortical bone as assessed by cone-beam computed tomography. *J Oral Maxillofac Surg, 67*(3), 491-500. doi:10.1016/j.joms.2008.06.089

Tsiolis, F. I., Needleman, I. G., & Griffiths, G. S. (2003). Periodontal ultrasonography. *J Clin Periodontol, 30*(10), 849-854. doi:10.1034/j.1600-051x.2003.00380.x

Tubiana, M. (1996). [Wilhelm Conrad Rontgen and the discovery of X-rays]. *Bull Acad Natl Med, 180*(1), 97-108. Retrieved from https://www.ncbi.nlm.nih.gov/pubmed/8696882

Vizzotto, M.B., Silveira, P.F., Arus, N.A., Montagner, F., Gomes, B.P., da Silveira, H.E. (2013). CBCT for the assessment of second mesiobuccal (MB2) canals in maxillary molar teeth: effect of voxel size and presence of root filling. *Int Endod J*, 46(9),870-6. doi: 10.1111/iej.12075

Wennstrom, J. L., Lindhe, J., Sinclair, F., & Thilander, B. (1987). Some periodontal tissue reactions to orthodontic tooth movement in monkeys. *J Clin Periodontol, 14*(3), 121-129. doi:10.1111/j.1600-051x.1987.tb00954.x

Wilensky, A., Gabet, Y., Yumoto, H., Houri-Haddad, Y., & Shapira, L. (2005). Three-dimensional quantification of alveolar bone loss in Porphyromonas gingivalis-infected mice using micro-computed tomography. *J Periodontol*, 76(8), 1282-1286. doi:10.1902/jop.2005.76.8.1282

Yamada, C., Kitai, N., Kakimoto, N., Murakami, S., Furukawa, S., & Takada, K. (2007). Spatial relationships between the mandibular central incisor and associated alveolar bone in adults with mandibular prognathism. *Angle Orthod, 77*(5), 766-772. doi:10.2319/072906-309

Zanolli, C., Schillinger B., Beaudet, A., Kullmer, O., Macchiarelli, R. et al. (2017). Exploring hominin and non-hominin primate dental fossil remains with neutron microtomography. *Physics Procedia*, 88, 109-115. doi: 10.1016/j.phpro.2017.06.014

CHAPTER 3 – METHODOLOGY

3.1 Study Design and Sample Distribution

For this study, human cadaver teeth supported by the corresponding alveolar bone and soft tissues were used. Cadaver maxillae and cadaver mandibles from 3 human cadavers were used for imaging and data collection. The 1st cadaver had 16 teeth available, the 2nd cadaver had 21 teeth and the 3rd cadaver had 21 teeth for a total number of 58 teeth distributed over the three cadavers. The three cadaver heads were provided by the Department of Anatomy at the University of Alberta in a fresh state rather than preserved cadavers, as the preservation process could change the soft tissue US imaging, and ultimately, affect the alveolar bone crest identification. The US images were obtained with the maxillae and mandibles still in the craniofacial complex with the lips cut away for improved access. The cadavers were adult individuals, with the age of 60, 68 and 72 years old. All three cadavers had advanced tooth attrition, deep enamel fractures, extensive restorations, crowns, recession with cervical carious lesions and periodontal bone loss. In general, the teeth available along with the supporting periodontium were not in a pristine healthy condition prior to the individuals' death.

Before image acquisition, the cadaver teeth were prepared by placing small round notches in the enamel on the facial surface by using a small bur with approximately 1mm diameter at the tip, in a high-speed handpiece. All viable samples (individual cadaver teeth) had at least two notches placed vertically, at non-calibrated distances and were oriented roughly along the long axis of the clinical crown of each tooth (Figure 3.1). The reason for placing the notches was to help better orient the teeth visually and to serve as a reference point while doing the measurements and comparing the data among the two imaging modalities.

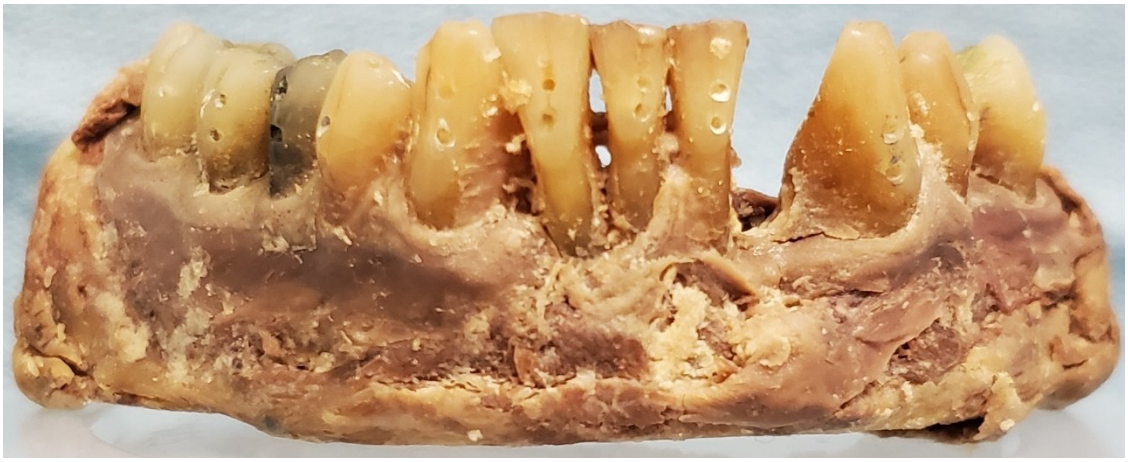

Figure 3.1 - Notches placed along the long axis of the clinical crown

The samples inclusion criteria among the total 58 cadaver teeth are as follows:

- Two vertically aligned notches are present on the tooth that could be fully seen by using both imaging modalities. Visualizing both notches ensures that there is minimal angulation (mesio-distal tip) distortion that could negatively affect the measurements.
- For some teeth that have large clinical crows (molars), notches were placed in the enamel in the centre of the crown, but also toward the mesial or distal line angles. For those teeth, separate measurements were made and considered on both µCT and US: in the centre of the crown, mesial or distal depending on the presence of reference notches.
- No major defects present along the cemento-enamel junction that could produce artefacts on the US images.
- The alveolar bone crest and the reference notch had to be visible on both µCT and US images.
- No large metal restorations present that could produce scatter radiation in the µCT images and prevent an accurate measurement.

Only the teeth that met all the above criteria were included in this study and those teeth are referred to as samples. The teeth that did not meet all the sample inclusion criteria were not used for any measurements and were discarded from this study. The exclusion list is presented in Table 3.1.

Cadaver 1 (tooth number)	**Reason for exclusion**
15	Metal restoration - µCT fuzzy
14	Metal restoration - µCT fuzzy
13	Defect at the CEJ - errors on US
11	Defect at the CEJ - errors on US
26 Mid notches	No US files available, only for Mesial notches
33	Big cavity at the CEJ
41	Big cavity at the CEJ
Cadaver 2 (tooth number)	**Reason for exclusion**
16	Metal crown
15	Porcelain fused to metal crown
14	Porcelain fused to metal crown
21	Fracture on facial, facial not fully visible in µCT
23	Porcelain fused to metal crown
24	Porcelain fused to metal crown
25	Porcelain fused to metal crown
26	Metal crown
44	Porcelain fused to metal crown
45	Metal restoration - µCT fuzzy
Cadaver 3 (tooth number)	**Reason for exclusion**
15	Porcelain fused to metal crown
27	Bone not visible on US - too much bone loss
31	Bone not visible on US - too much bone loss
41	Bone not visible on US - too much bone loss
42	Bone not visible on US - too much bone loss
43	Bone not visible on US - too much bone loss
45	Metal restoration - µCT fuzzy
47 Mid notches	Bone not visible on US

Table 3.1 - Sample exclusion list

3.2 Ultrasound Imaging

For the Ultrasound imaging (US), a special 20 MHz handheld transducer that is small enough for use on teeth was developed (Nguyen et al., 2021). Readily available medical US devices are too bulky and unsuitable for intra-oral use. For each tooth, the US measurement was made with the transducer handheld by the operator and relatively perpendicular to the buccal surface of the tooth. Also, for each measurement, acoustic coupling was ensured by using ultrasonic gel (Aquasonic 100, Parker Laboratories, USA) and gel pad (Aquaflex, Parker Laboratories, USA), that would act as a medium in transmitting the US waves without the waves crossing through the air. The use of a properly fitting gel is important because US waves reflection and refraction are substantially less when crossing from a gel into the tissues rather than crossing from the air into the tissues. The US operator was Kim-Cuong T Nguyen (KC), and she has 10 years of experience working with US.

3.2.1 US Image Analysis

The raw US digital data from each tooth measurement was initially saved as an .AVI video file format as it was output directly from the US transducer software. The AVI files were then converted to DICOM files which is the standard for digital imaging analysis. In the conversion process, all individual video frames in an AVI file were converted to a DICOM file with scrollable slices without any visual alternations or distortions, with one frame in the AVI file corresponding to one slice in the DICOM file.

For each DICOM file associated with any tooth, there were 245 or 246 slices that could theoretically be used to measure the distance from the inferior border of the pre-cut notch in the enamel, to the tip of the crestal bone. Only one single slice for each sample tooth was selected for measurement that was considered to visually have the best tooth orientation in relation to the pre-cut orientation notches, with the notches and alveolar bone crest fully visible. Therefore, random selection of a slice among the 245 or 246 slices that were theoretically possible was not considered to be the best selection method.

For each US file chosen slice corresponding to any viable sample, the distance from the inferior border of the most apical notch on the buccal aspect of the tooth to the alveolar bone

crest was measured in RadiANT DICOM viewer software (Windows PC Version 2021.2.2, www.radiantviewer.com) and the result was saved in millimetres (Figure 3.2).

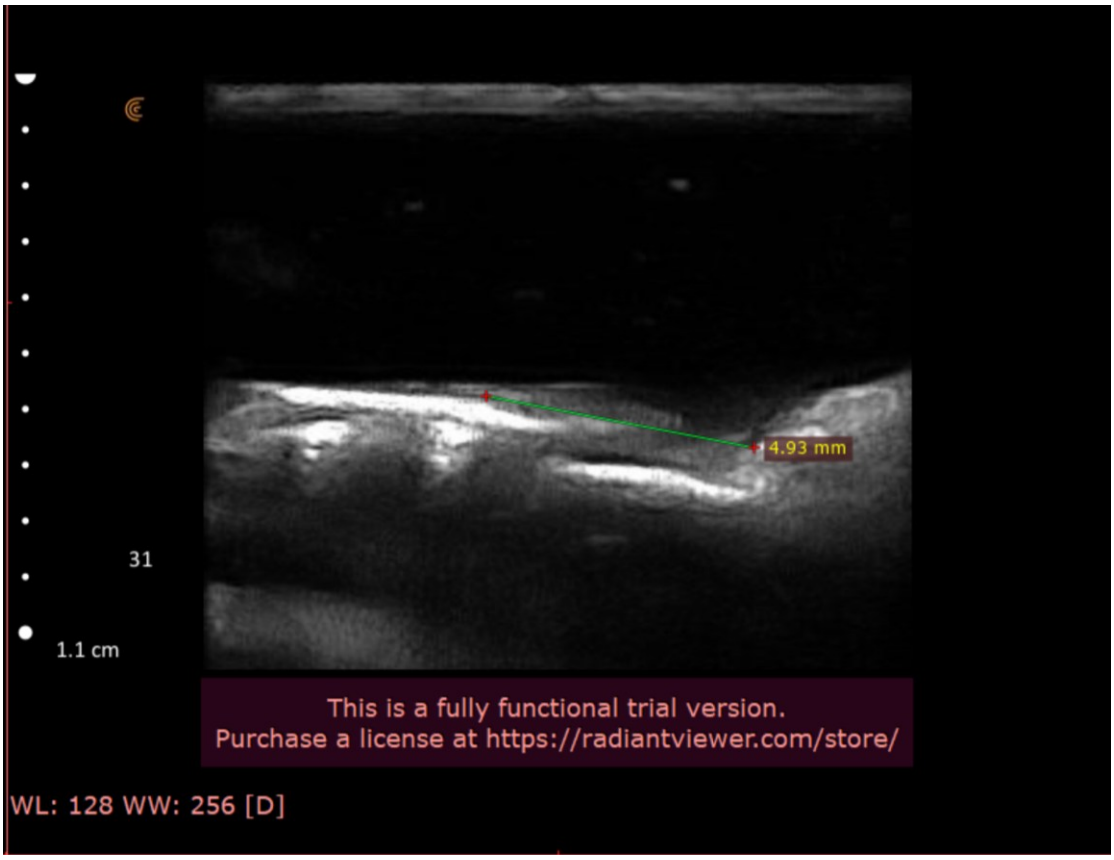

Figure 3.2 - The distance in millimetres from the inferior border of the most apical notch on the facial aspect of the tooth to the alveolar bone crest.

3.3 Micro Computed Tomography Imaging (µCT)

After the US scans were done, the maxillae and mandibles were sectioned from the cadavers' head and then kept in the refrigerator until the µCT scan was performed. All teeth samples supported by their corresponding maxillae and mandibles were scanned by a µCT system, model number U-SPECT-II/CT manufactured by MiLabs, Utrecht, Netherlands. The parameters applied for the scan of the cadavers were: voltage 55kV, current 0.19mA, exposure time 75ms, in 960 steps of 0.3 degrees/step. The scans were reconstructed at a voxel size of 0.03mm and the µCT digital scan data was saved as DICOM files for digital analysis and

measurement. For this project, with its very high resolution, μCT was selected as the gold standard imaging technique.

3.3.1 μCT Image Analysis

For each sample, the μCT data was imported into ITK-SNAP software (Windows PC version 3.8, www.itksnap.org) in DICOM format. Before any measurements could be made, each individual sample had to be rotated and oriented to minimize any angulation errors in such a way that the visual anatomical representation of each tooth in the μCT software resembles the same tooth measured with the US. The sample rotation and orientation were done by using the Registration function in the ITK-SNAP software and the following criteria were used (Figure 3.3):

- The landmarks used in the orientation process for each sample were the pre-drilled notches.
- In the μCT sagittal orientation, the crown of each sample tooth was aligned with the axial axis intersecting the facial of the crown at 90 degrees. In addition, two vertically aligned notches had to be visible in the enamel to minimize angulation errors.
- In the μCT coronal (frontal) orientation, the root of each sample was aligned parallel to the coronal axis. By following the general direction of the root canal, angulation errors due to root tipping were minimized.
- In the μCT axial (transverse) orientation, the crown was oriented until the reference notch is fully visible with the CT sagittal axis intersecting the facial of the crown at 90 degrees with no angulation.

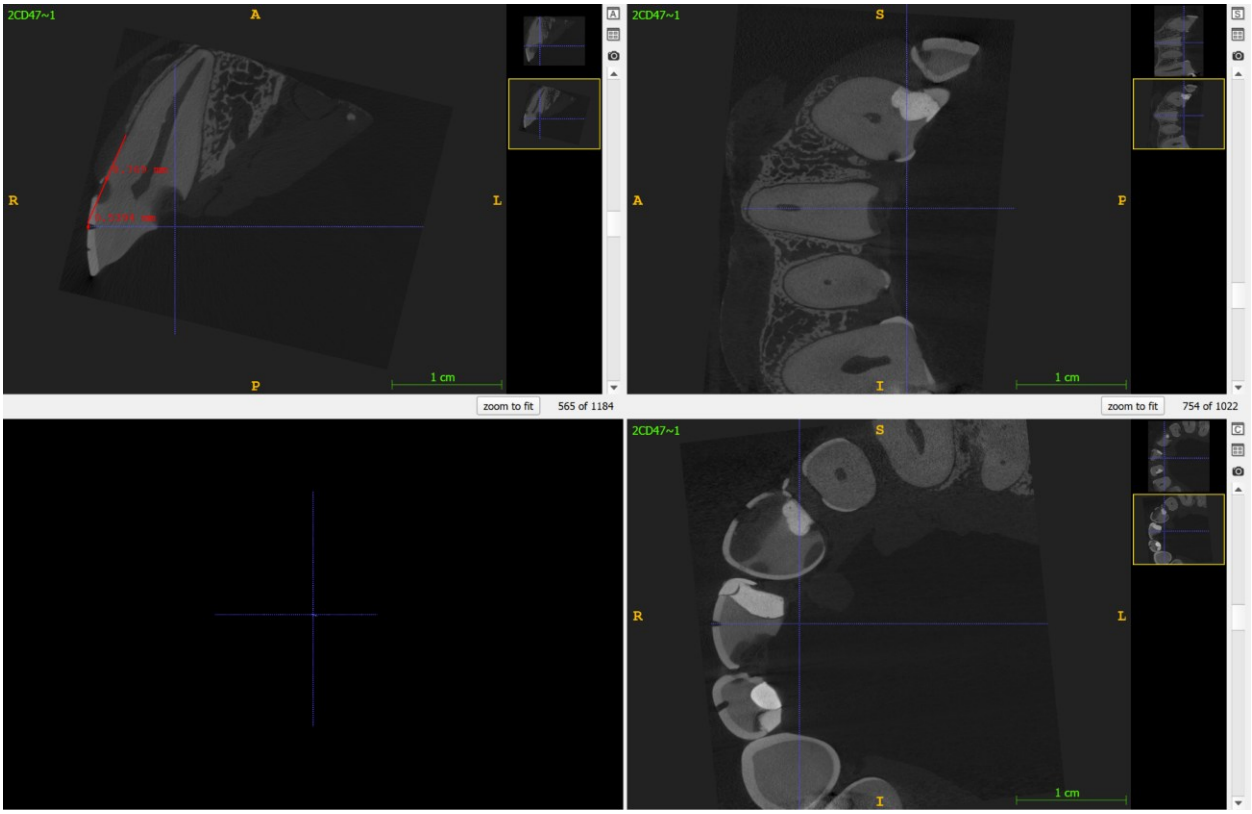

Figure 3.3 - Sample oriented in ITK-SNAP that is ready for measurement

After each sample was rotated and oriented, by using the "Image Annotation Mode" available in ITK-SNAP, the distance from the inferior border of the reference notch to the tip of the crestal bone was measured and recorded in millimetres (Figure 8). This distance from the tip of the alveolar bone crest to the inferior border of the reference notch as anatomical landmarks is the same distance that is measured on all the samples by means of µCT and US imaging. The diameter of the notch was also recorded in millimetres along with the distance from the mesial and distal edges of the reference notch to the tip of the crestal bone. For the measurements from the mesial and distal edges of the reference notch, since the notch is circular, measuring from the sides of the notch compared to the inferior border, will add the radius of the notch to the overall measurement to the crestal bone. All measurements done in this study used the inferior border of a given notch as a reference point. Also, all measurements must be calibrated to the inferior border of the notch in case the inferior border was not directly visible (when measuring towards the mesial or distal edge of a notch). Therefore, the true calibrated distance that was recorded between the crest of the alveolar bone to the inferior border of the reference notch when

measured towards the mesial and distal edges of the notch, was calculated by subtracting the radius of the notch from the measured distance. For the remainder of this study, when mentioning the measurements from the tip of the crestal bone to the inferior border of the reference notch measured from the mesial and distal edges of the notch, it will be assumed that the measurement will have been calibrated to the inferior border of the notch and that the mesial and distal notch to bone measurement already has the radius of the notch subtracted (Figure 3.4).

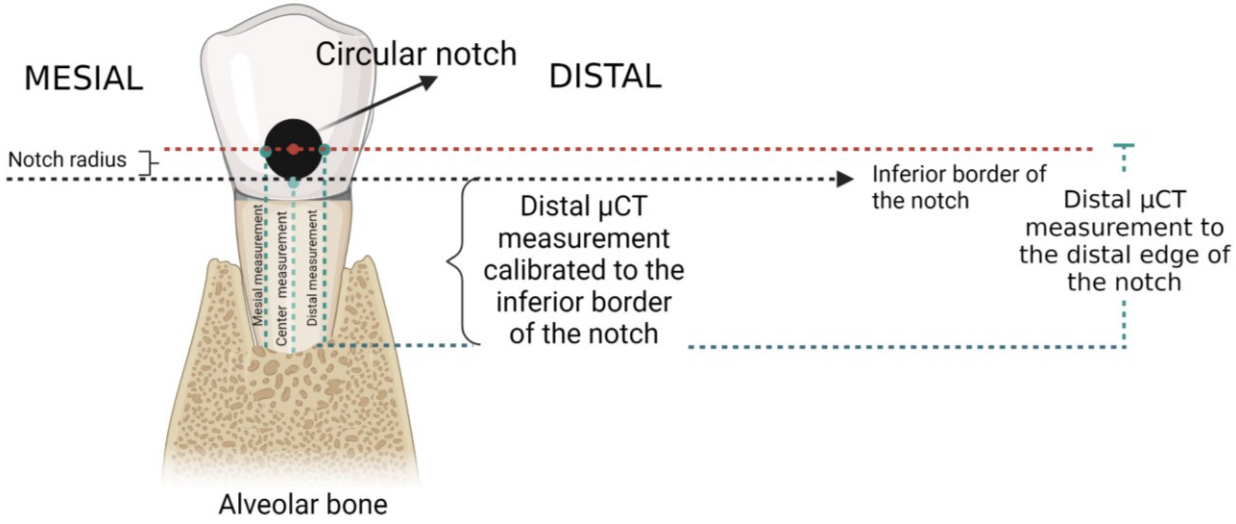

Figure 3.4 - Diagram of µCT measurements. The above image was created using the Biorender software.

For µCT images, the distance from the tip of the bone to the reference notch in the tooth was represented by the average of three measurements:

1. From the tip of the bone to the inferior border of the notch in the centre of the notch.
2. From the tip of the bone to the inferior border on of the notch, 0.45-0.5 mm towards the mesial edge of the notch.
3. From the tip of the bone to the inferior border on of the notch, also 0.45-0.5 mm since the notches are circular, towards the distal edge of the notch.

These three uCT measurements, calibrated to the inferior border of the notch, span mesio-distally just under 1 mm which is the diameter of the notch. In this study, the µCT samples measured in this way and averaged will be referred as µCT. This uCT measurement was necessary due to the way the US transducer records data as a transverse slice with a variable

thickness of a few millimetres that is ultimately averaged and superimposed in a two-dimensional sagittal image (Nguyen et al., 2021). The intent was to replicate as much as possible the US volumetric averaging / superimposition in the way the µCT data was measured by using the notches present in the samples as reference landmarks, with each notch having a diameter of almost 1 mm.

3.4 Raters for US and µCT

For this study, two raters were involved in measuring the samples by using the two imaging modalities. Rater 1 (R1) is a 3rd year Orthodontics Graduate Resident and Rater 2 (R2) is an Oral and Maxillofacial Radiologist with 5 years of experience working with Ultrasound.

Before any final measurements and image analysis were performed, R1 had a few sessions with Kim-Cuong T Nguyen (KC) who has 10 years of experience with US images for R1 to become familiar with the landmarks on the US images. After R1 became familiar with the US images, as the evaluators, R1 and R2 went through a calibration process which consisted of presenting the anatomical landmarks of 5 different samples in both US and µCT in the selected images (alveolar bone tip and notches), the software to be used and the distances to be measured. The calibration process was considered as complete after both raters came to the same consensus regarding the landmarks on the 5 presented samples.

R1 measured all the US and µCT samples in this study three times over the course of four months while R2 measured all the US and µCT samples once. The measurements done by R1 were labelled as follows: T1 for the first complete set of US and µCT measurements, T2 for the second complete set of measurements and T3 for the third complete set of measurements.

3.5 Statistical Analysis Methodology

For the statistical analysis, we are comparing quantitative measurements that are organized into groups and the goal is to describe how strongly the units in the same group resemble each other. Therefore, the Intraclass Correlation Coefficient (ICC) analysis were performed which is a measure of reliability for continuous variables. The Intraclass Correlation Coefficient (ICC) statistical analysis was performed with the following characteristics: single measure, absolute agreement under two-way mixed model. For the magnitude of the ICC, Koo et

al. (2016) suggests the following guidelines: values less than 0.5 are indicative of poor reliability, values in between 0.5-0.75 are indicative of moderate reliability, values in between 0.75 to 0.90 are indicative of good reliability and values over 0.9 are indicative of excellent reliability.

The Intra-Rater reliability can be described as the level of stability presented when the same rater is performing a repeated measurement in the same conditions. The Inter-Rater reliability can be described as the level of stability presented when different raters are performing a repeated measurement in the same conditions (Koo et. al., 2016). The accuracy is defined as "how close or how far off a given set of measurements are to their true value". (Menditto et al., 2007). In other words, how close is the US measured value for each sample to the true value which is represented by the gold standard μCT.

For the statistical analysis, IBM SPSS software (Windows PC version 28.0.1.1, www.ibm.com/analytics/spss-statistics-software) and Excel software (Windows PC part of Microsoft Office 365, www.microsoft.com/microsoft-365) were used. Standard deviation was used to gauge the variation in millimetres, descriptive statistics (mean, standard deviation, 95% confidence interval) and graphs (45-degree scatter plots, estimated marginal means) were presented to further explain and support the ICC findings.

References

Koo, T.K., Li, M.Y. A Guideline of Selecting and Reporting Intraclass Correlation Coefficients for Reliability Research (2016). J Chiropr Med, 15 (2), 155-63. doi: 10.1016/j.jcm.2016.02.012

Menditto, A., Patriarca, M., Magnusson, B. Understanding the meaning of accuracy, trueness and precision (2007). Accred Qual Assur 12, 45–47. doi: 10.1007/s00769-006-0191-z

Nguyen, K. T., Le, B. M., Li, M., Almeida, F. T., Major, P. W., Kaipatur, N. R., . . . Le, L. H. (2021). Localization of cementoenamel junction in intraoral ultrasonographs with machine learning. J Dent, 112, 103752. doi:10.1016/j.jdent.2021.103752

CHAPTER 4 – RESULTS

4.1 INTRA-Rater Reliability

4.1.1 µCT INTRA-Rater Reliability Statistical Analysis

Table 4.1 shows the Intraclass Correlation Coefficient and the 95% confidence interval (CI) of µCT Rater 1 measurements at Time 1, 2 and 3. The Intraclass Correlation of 0.998 (0.997, 0.999) indicates the µCT reliability of Rater 1 at Time 1, 2 and 3 is excellent.

Intraclass Correlation	95% Confidence Interval	
	Lower Bound	Upper Bound
0.998	0.997	0.999

Table 4.1 - ICC Intra-Rater µCT, R1_T1 vs R1_T2 vs R1_T3

Figure 4.1 shows a positive relationship between Rater 1 µCT measurements at Time 1 and 2.

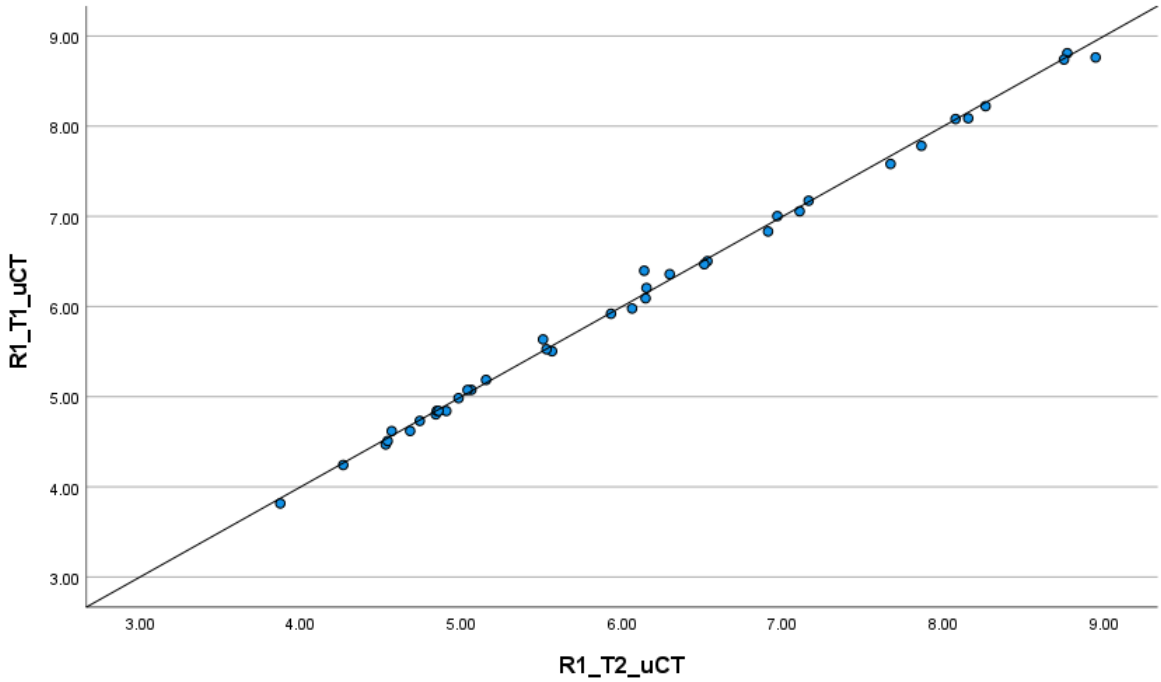

Figure 4.1 - 45º Scatter Plot Intra-Rater µCT Average Notch, R1, T1 vs T2

Figure 4.2 shows a positive relationship between Rater 1 measurements of the µCT by using the average measurements at the notch at Time 1 and 3.

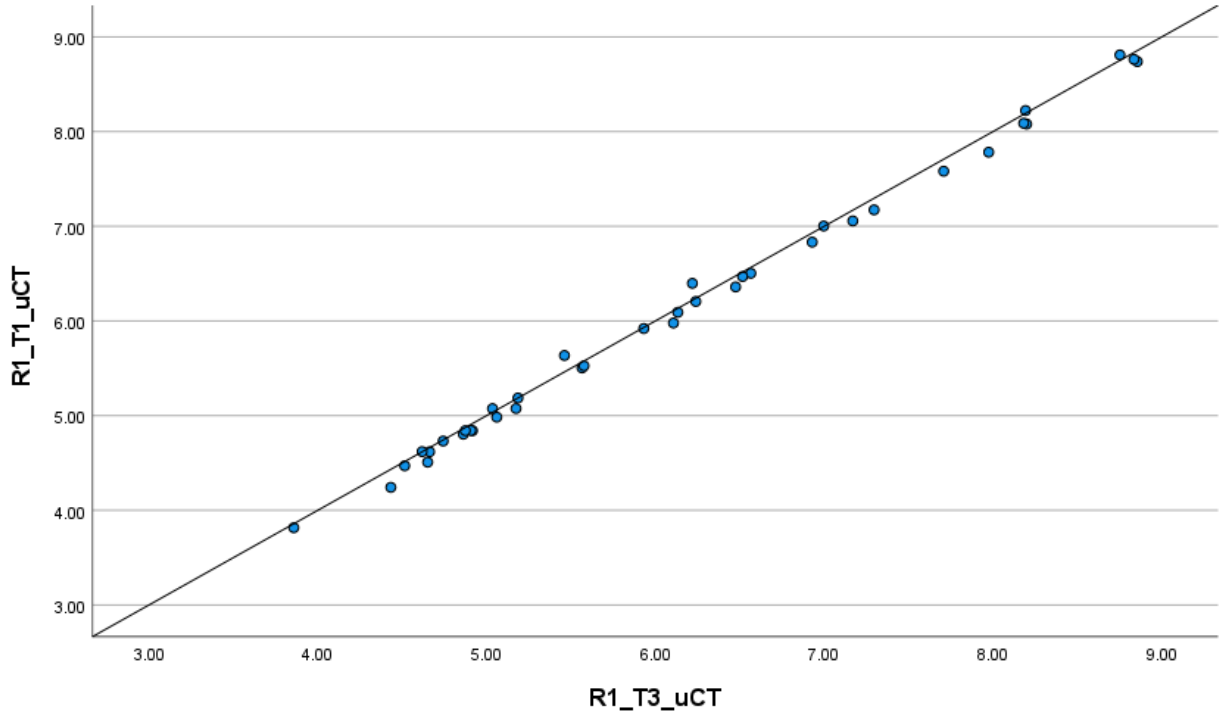

Figure 4.2 - 45º Scatter Plot Intra-Rater µCT Average Notch, R1, T1 vs T3

Figure 4.3 shows positive relationship between Rater 1 measurements of the µCT by using the average measurements at the notch at Time 2 and 3.

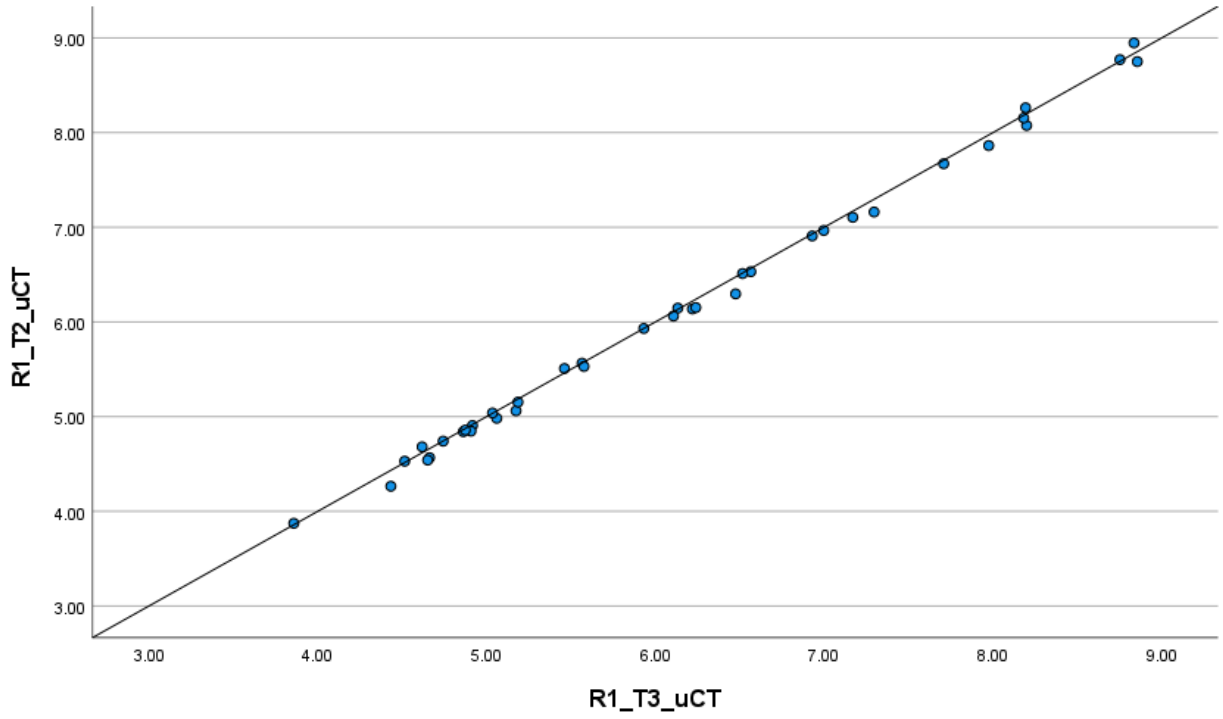

Figure 4.3 - 45º Scatter Plot Intra-Rater µCT, R1, T2 vs T3

Table 4.2 shows the Standard Deviation in millimetres for the µCT **Intra-Rater measurements.** The standard deviation value for the 38 samples, measured by Rater 1 at time T1, T2 and T3, varies between 0.006 mm at the lowest value to 0.133 mm at the highest value with an average value of 0.05 mm for all the samples.

Sample Number	Cadaver Number	R1_T1 µCT	R1_T2 µCT	R1_T3 µCT	Standard Deviation µCT R1_T1, R1_T2, R1_T3
1	1	8.810	8.771	8.753	**0.029**
2	1	8.740	8.750	8.856	**0.064**
3	1	8.080	8.076	8.200	**0.070**
4	1	8.223	8.263	8.194	**0.035**
5	1	7.057	7.106	7.170	**0.057**
6	1	6.504	6.532	6.566	**0.031**
7	1	6.092	6.147	6.134	**0.029**

8	1	6.398	6.138	6.220	**0.133**
9	1	5.921	5.932	5.932	**0.007**
10	1	8.764	8.948	8.836	**0.093**
11	2	5.505	5.565	5.566	**0.035**
12	2	8.088	8.155	8.183	**0.048**
13	2	7.783	7.863	7.975	**0.097**
14	2	5.076	5.063	5.175	**0.061**
15	2	7.582	7.671	7.709	**0.065**
16	2	4.243	4.265	4.434	**0.104**
17	2	4.471	4.530	4.516	**0.031**
18	2	4.842	4.907	4.917	**0.041**
19	2	4.804	4.842	4.863	**0.030**
20	2	4.844	4.848	4.908	**0.036**
21	2	4.619	4.567	4.663	**0.048**
22	3	6.833	6.909	6.930	**0.051**
23	3	3.817	3.874	3.859	**0.030**
24	3	4.985	4.983	5.061	**0.045**
25	3	5.527	5.531	5.578	**0.028**
26	3	4.509	4.542	4.652	**0.075**
27	3	4.842	4.858	4.875	**0.016**
28	3	6.360	6.297	6.476	**0.091**
29	3	7.174	7.162	7.296	**0.074**
30	3	6.470	6.512	6.517	**0.026**
31	3	7.003	6.967	6.998	**0.020**
32	3	5.979	6.063	6.108	**0.066**
33	3	5.187	5.154	5.187	**0.019**
34	3	6.206	6.153	6.240	**0.044**
35	3	5.075	5.039	5.036	**0.022**
36	3	5.636	5.509	5.462	**0.090**
37	3	4.620	4.682	4.619	**0.036**
38	3	4.732	4.742	4.743	**0.006**
Average in mm					**0.050**

Table 4.2 - Standard Deviation in millimetres for the µCT Intra-Rater measurements

4.1.2 US INTRA-Rater Reliability statistical analysis

Table 4.3 shows the Intraclass Correlation Coefficient and the 95% confidence interval (CI) of Rater 1 measurements of the US at Time 1, 2 and 3. The Intraclass Correlation of 0.997 (0.995, 0.999) indicates the reliability of Rater 1 at Time 1, 2 and 3 is excellent.

Intraclass Correlation	95% Confidence Interval	
	Lower Bound	Upper Bound
0.997	0.995	0.999

Table 4.3 - ICC Intra-Rater US, R1_T1 vs R1_T2 vs R1_T3

Figure 4.4 shows positive relationship between Rater 1 measurements of the US at the centre of the notch at Time 1 and Time 2.

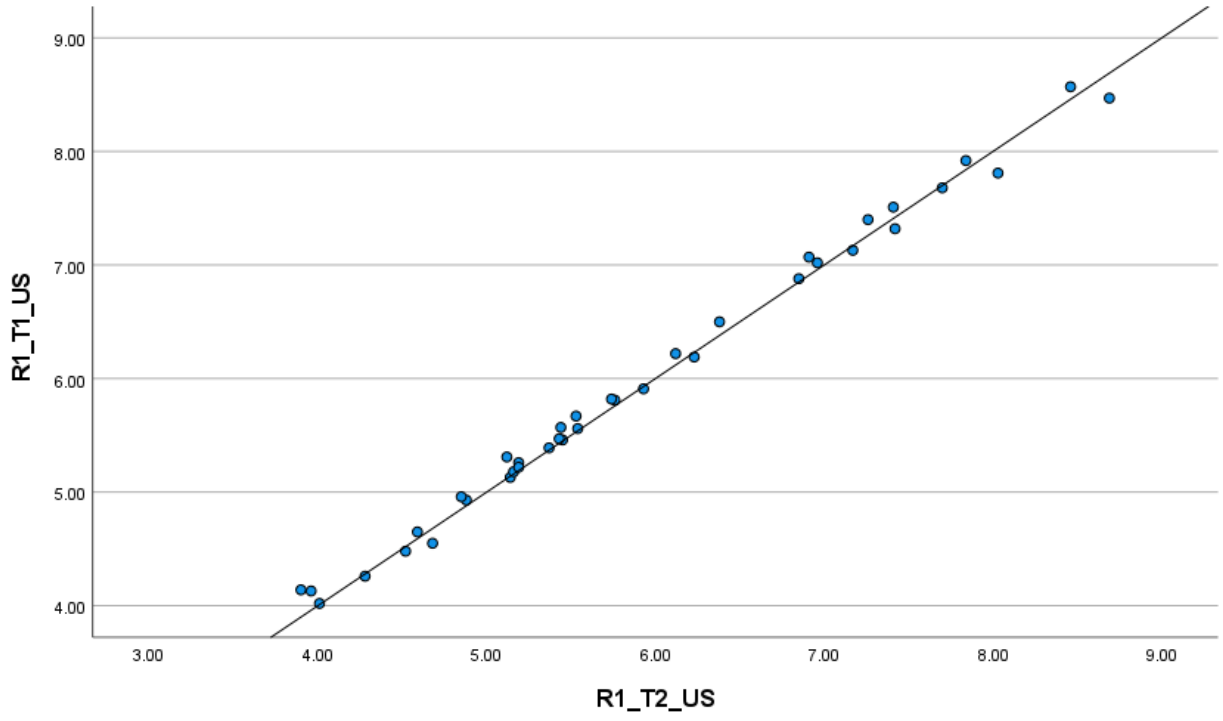

Figure 4.4 - 45º Scatter Plot Intra-Rater US, R1, T1 vs T2

Figure 4.5 shows positive relationship between Rater 1 measurements of the US at the centre of the notch at Time 1 and Time 3.

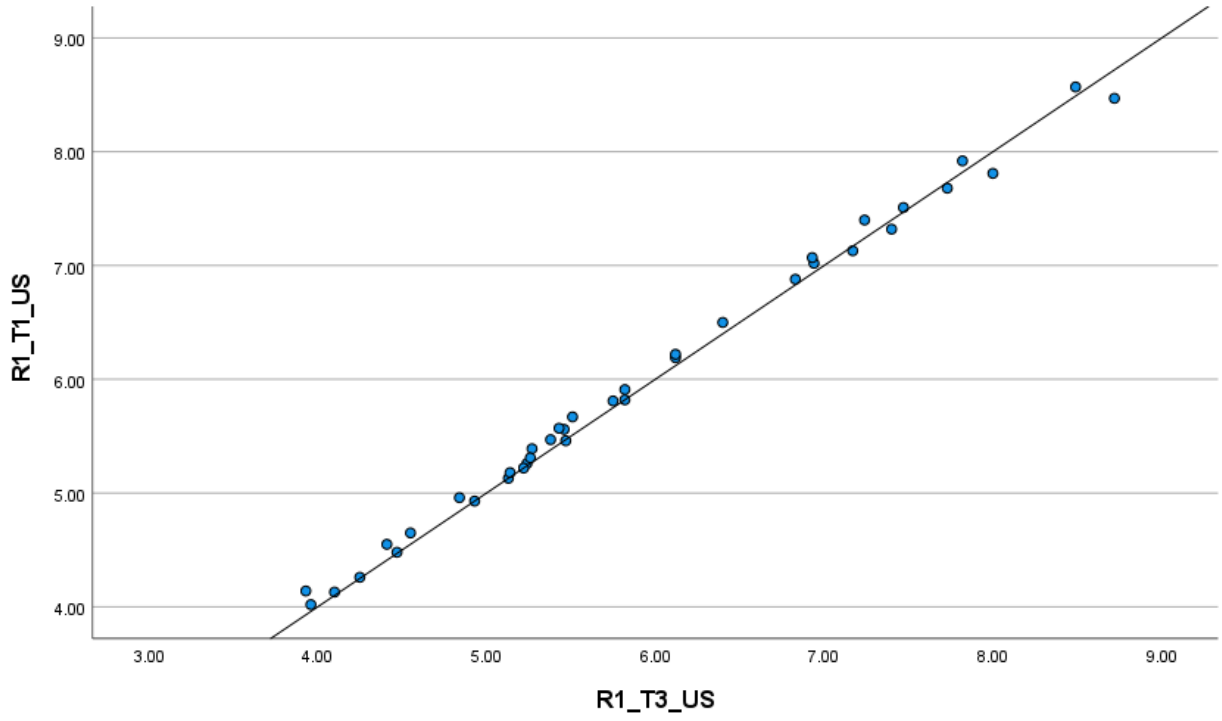

Figure 4.5 - 45º Scatter Plot Intra-Rater US, R1, T1 vs T3

Figure 4.6 shows positive relationship between Rater 1 measurements of the US at the centre of the notch at Time 2 and Time 3.

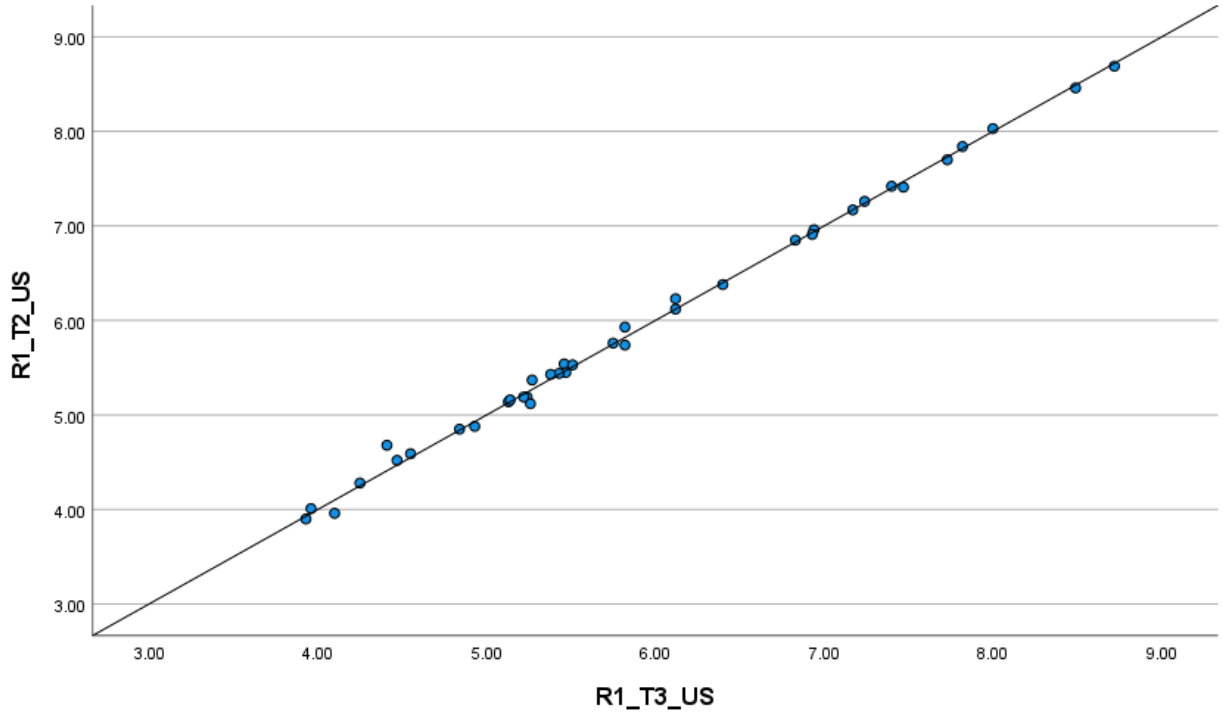

Figure 4.6 - 45º Scatter Plot Intra-Rater US, R1, T2 vs T3

Table 4.4 shows the Standard Deviation in millimetres for the **US Intra-Rater measurements**. The standard deviation value for the 38 samples, measured by Rater 1 at time T1, T2 and T3, varies between 0.006 mm at the lowest value to 0.137 mm at the highest value with an average value of 0.057mm for all the samples.

Sample Number	Cadaver Number	R1_T1 US	R1_T2 US	R1_T3 US	Standard Deviation US R1_T1, R1_T2, R1_T3
1	1	7.92	7.84	7.82	**0.053**
2	1	8.47	8.69	8.72	**0.137**
3	1	7.4	7.26	7.24	**0.087**
4	1	7.81	8.03	8	**0.119**
5	1	7.13	7.17	7.17	**0.023**
6	1	5.81	5.76	5.75	**0.032**
7	1	5.91	5.93	5.82	**0.059**
8	1	6.19	6.23	6.12	**0.056**
9	1	5.56	5.54	5.46	**0.053**
10	1	8.57	8.46	8.49	**0.057**

11	2	5.39	5.37	5.27	**0.064**
12	2	7.68	7.7	7.73	**0.025**
13	2	7.32	7.42	7.4	**0.053**
14	2	4.65	4.59	4.55	**0.050**
15	2	7.02	6.96	6.94	**0.042**
16	2	4.02	4.01	3.96	**0.032**
17	2	4.26	4.28	4.25	**0.015**
18	2	4.93	4.88	4.93	**0.029**
19	2	5.13	5.14	5.13	**0.006**
20	2	5.46	5.45	5.47	**0.010**
21	2	4.48	4.52	4.47	**0.026**
22	3	7.07	6.91	6.93	**0.087**
23	3	4.13	3.96	4.1	**0.091**
24	3	5.26	5.19	5.24	**0.036**
25	3	4.96	4.85	4.84	**0.067**
26	3	5.57	5.44	5.43	**0.078**
27	3	4.55	4.68	4.41	**0.135**
28	3	5.47	5.43	5.38	**0.045**
29	3	7.51	7.41	7.47	**0.050**
30	3	6.22	6.12	6.12	**0.058**
31	3	5.67	5.53	5.51	**0.087**
32	3	5.82	5.74	5.82	**0.046**
33	3	5.31	5.12	5.26	**0.098**
34	3	6.88	6.85	6.83	**0.025**
35	3	5.18	5.16	5.14	**0.020**
36	3	4.14	3.9	3.93	**0.131**
37	3	6.5	6.38	6.4	**0.064**
38	3	5.22	5.19	5.22	**0.017**
Average in mm					**0.057**

Table 4.4 - Standard Deviation in millimetres for the US Intra-Rater measurements

4.2 INTER-Rater Reliability

4.2.1 µCT INTER-Rater Reliability statistical analysis

Table 4.5 shows the Intraclass Correlation Coefficient and the 95% confidence interval (CI) for the µCT measurements for Rater 1 at Time 1 compared to the µCT measurements of Rater 2. The Intraclass Correlation of 0.996 (0.993, 0.998) indicates the reliability between Rater 1 at Time 1 and Rater 2 is excellent.

Intraclass Correlation	95% Confidence Interval	
	Lower Bound	Upper Bound
0.996	0.993	0.998

Table 4.5 - ICC Inter-Rater µCT R1_T1 vs R2

Figure 4.7 shows positive relationship between the µCT measurements for Rater 1 at Time 1 and the µCT measurements of Rater 2.

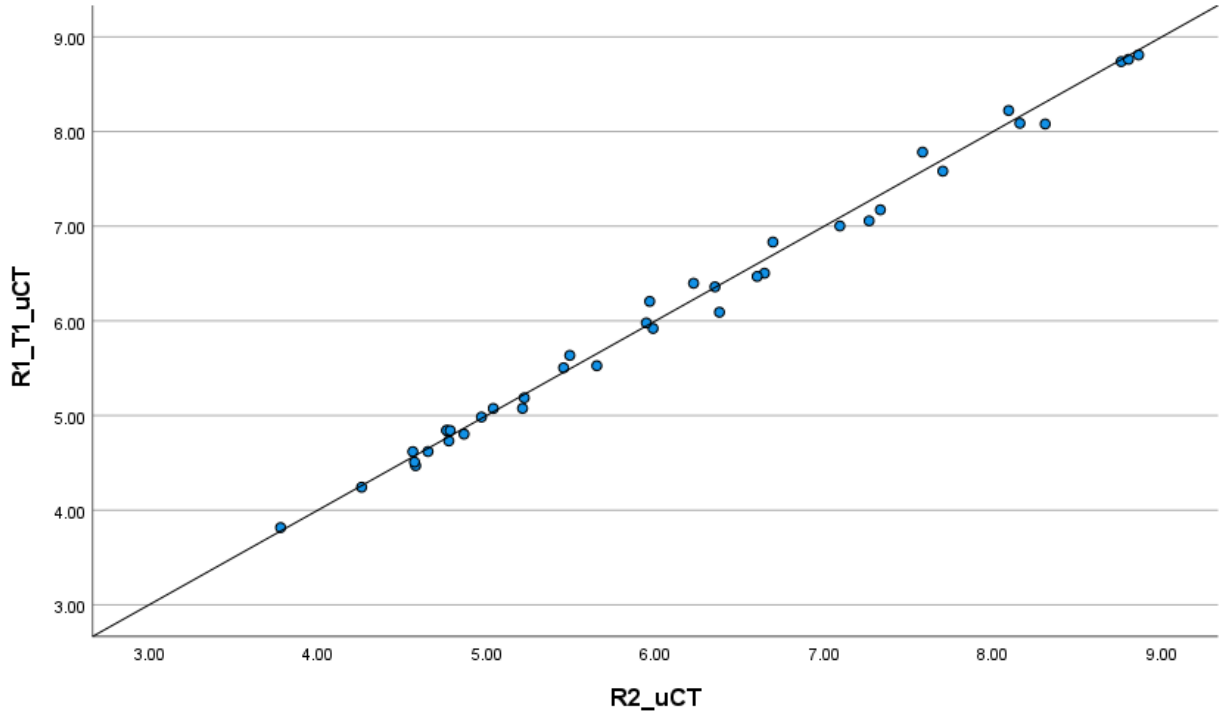

Figure 4.7 - 45º Scatter Plot Inter-Rater µCT R1_T1 vs R2

Table 4.6 shows the Intraclass Correlation Coefficient and the 95% confidence interval (CI) for the µCT measurements for Rater 1 at Time 2 compared to the µCT measurements for Rater 2. The Intraclass Correlation of 0.996 (0.993, 0.998) indicates the reliability between Rater 1 at Time 2 and Rater 2 is excellent.

Intraclass Correlation	95% Confidence Interval	
	Lower Bound	Upper Bound
0.996	0.993	0.998

Table 4.6 - ICC Inter-Rater µCT R1_T2 vs R2

Figure 4.8 shows positive relationship between µCT measurements for Rater 1 at Time 2 and the µCT measurements of Rater 2.

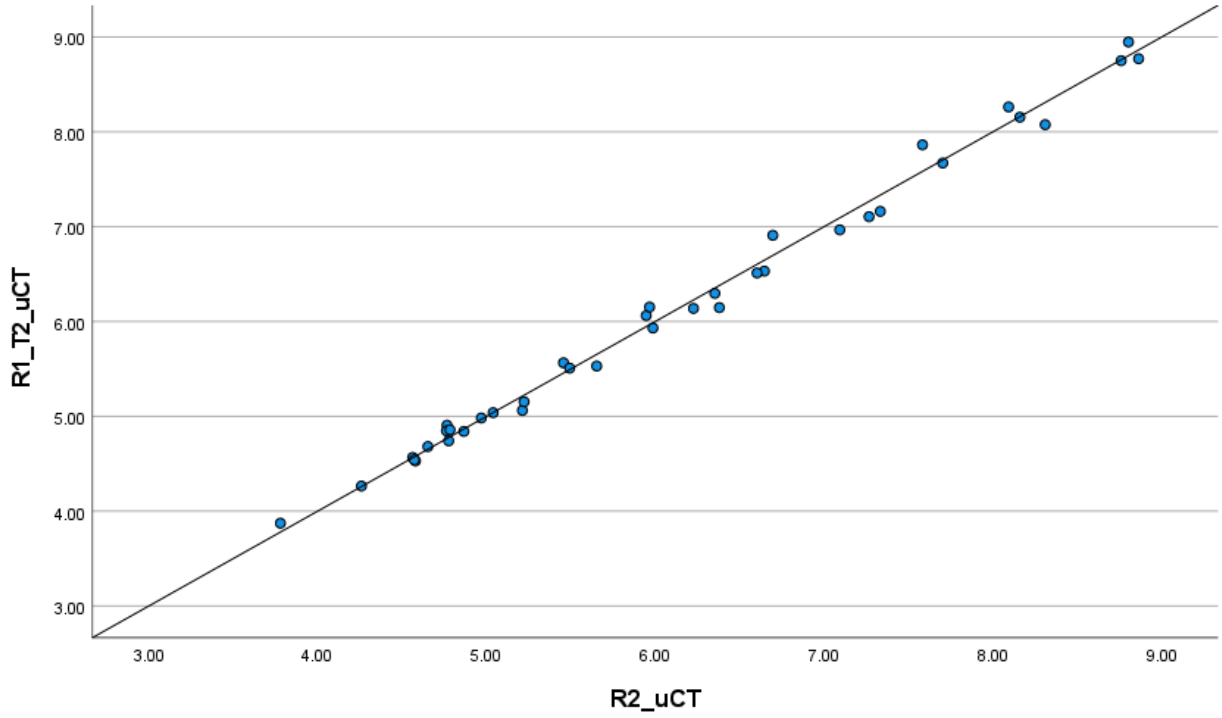

Figure 4.8 - 45º Scatter Plot Inter-Rater µCT, R1_T2 vs R2

Table 4.7 shows the Intraclass Correlation Coefficient and the 95% confidence interval (CI) for the µCT measurements for Rater 1 at Time 3 compared to the µCT measurements of Rater 2. The Intraclass Correlation of 0.996 (0.992, 0.998) indicates the reliability between Rater 1 at Time 3 and Rater 2 is excellent.

Intraclass Correlation	95% Confidence Interval	
	Lower Bound	Upper Bound
0.996	0.992	0.998

Table 4.7 - ICC Inter-Rater µCT, R1_T3 vs R2

Figure 4.9 shows positive relationship between Rater 1 measurements of the µCT by using the average measurements at the notch at Time 3 and the measurements of Rater 2.

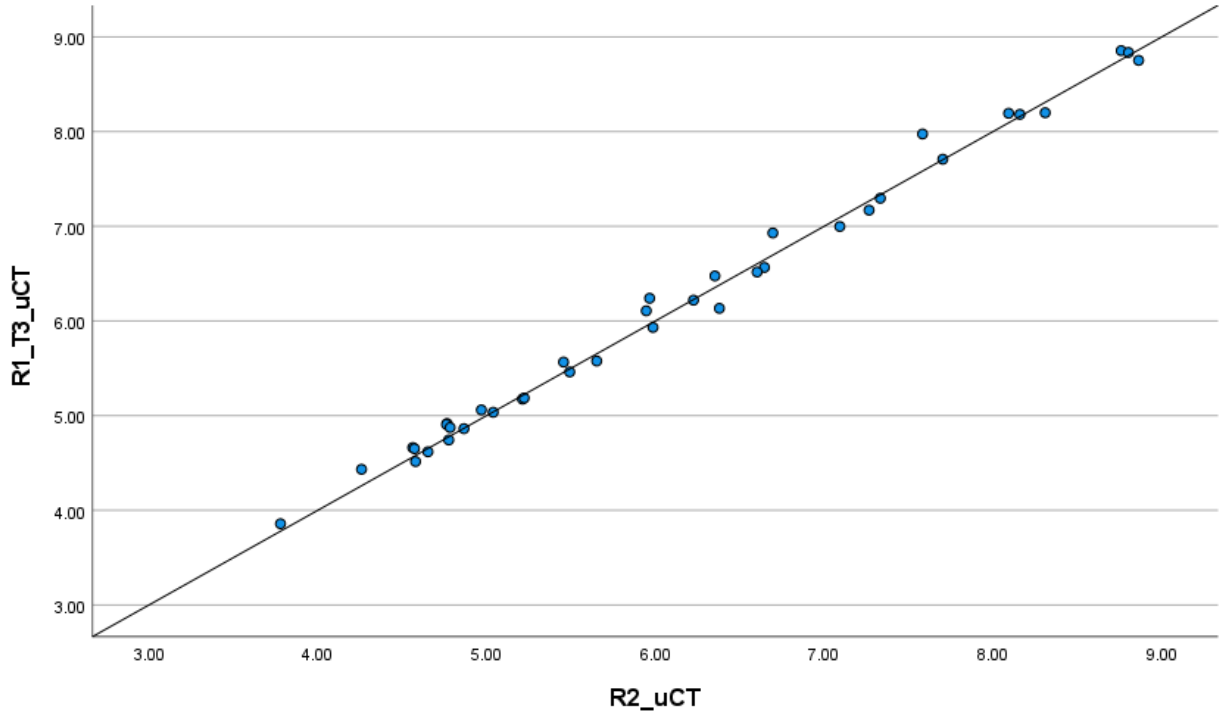

Figure 4.9 - 45º Scatter Plot Inter-Rater µCT, R1_T3 vs R2

Table 4.8 shows the Standard Deviation in millimetres for the µCT **Inter-Rater measurements.** The standard deviation value for the 38 samples, measured by Rater 1 at time T1, T2 and T3 compared to R2, has an average value of 0.069 mm for Time 1, 0.068 mm for Time 2 and 0.069 mm for Time 3.

Sample	Cadaver	R1_T1 µCT	R1_T2 µCT	R1_T3 µCT	R2 µCT	Standard Deviation µCT: R1_T1, R2	Standard Deviation µCT: R1_T2, R2	Standard Deviation µCT: R1_T3, R2
1	1	8.810	8.771	8.753	8.863	**0.037**	**0.065**	**0.078**
2	1	8.740	8.750	8.856	8.760	**0.014**	**0.007**	**0.068**
3	1	8.080	8.076	8.200	8.310	**0.162**	**0.166**	**0.078**
4	1	8.223	8.263	8.194	8.093	**0.092**	**0.120**	**0.071**
5	1	7.057	7.106	7.170	7.267	**0.148**	**0.114**	**0.068**
6	1	6.504	6.532	6.566	6.647	**0.101**	**0.081**	**0.057**
7	1	6.092	6.147	6.134	6.380	**0.204**	**0.165**	**0.174**
8	1	6.398	6.138	6.220	6.227	**0.121**	**0.062**	**0.005**
9	1	5.921	5.932	5.932	5.987	**0.047**	**0.039**	**0.039**
10	1	8.764	8.948	8.836	8.803	**0.028**	**0.102**	**0.023**
11	2	5.505	5.565	5.566	5.457	**0.034**	**0.076**	**0.077**
12	2	8.088	8.155	8.183	8.160	**0.051**	**0.004**	**0.016**
13	2	7.783	7.863	7.975	7.583	**0.141**	**0.198**	**0.277**
14	2	5.076	5.063	5.175	5.213	**0.097**	**0.107**	**0.027**
15	2	7.582	7.671	7.709	7.703	**0.086**	**0.023**	**0.004**
16	2	4.243	4.265	4.434	4.260	**0.012**	**0.004**	**0.123**
17	2	4.471	4.530	4.516	4.580	**0.077**	**0.035**	**0.045**
18	2	4.842	4.907	4.917	4.767	**0.053**	**0.099**	**0.106**
19	2	4.804	4.842	4.863	4.867	**0.044**	**0.018**	**0.003**
20	2	4.844	4.848	4.908	4.763	**0.057**	**0.060**	**0.103**
21	2	4.619	4.567	4.663	4.563	**0.039**	**0.002**	**0.070**
22	3	6.833	6.909	6.930	6.697	**0.096**	**0.150**	**0.165**
23	3	3.817	3.874	3.859	3.780	**0.026**	**0.066**	**0.056**
24	3	4.985	4.983	5.061	4.970	**0.010**	**0.009**	**0.064**
25	3	5.527	5.531	5.578	5.653	**0.090**	**0.087**	**0.054**
26	3	4.509	4.542	4.652	4.573	**0.045**	**0.022**	**0.056**
27	3	4.842	4.858	4.875	4.785	**0.041**	**0.052**	**0.064**
28	3	6.360	6.297	6.476	6.353	**0.005**	**0.040**	**0.087**
29	3	7.174	7.162	7.296	7.333	**0.113**	**0.121**	**0.026**
30	3	6.470	6.512	6.517	6.603	**0.095**	**0.065**	**0.061**
31	3	7.003	6.967	6.998	7.093	**0.064**	**0.090**	**0.067**
32	3	5.979	6.063	6.108	5.947	**0.023**	**0.082**	**0.114**
33	3	5.187	5.154	5.187	5.223	**0.026**	**0.049**	**0.026**
34	3	6.206	6.153	6.240	5.967	**0.169**	**0.132**	**0.193**
35	3	5.075	5.039	5.036	5.040	**0.025**	**0.001**	**0.003**
36	3	5.636	5.509	5.462	5.493	**0.101**	**0.011**	**0.022**
37	3	4.620	4.682	4.619	4.653	**0.023**	**0.020**	**0.024**
38	3	4.732	4.742	4.743	4.777	**0.031**	**0.025**	**0.023**
Average in mm						**0.069**	**0.068**	**0.069**

Table 4.8 - Standard Deviation in millimetres for the µCT Inter-Rater measurements

Figure 4.10 shows the estimated marginal means of the measurements for the µCT, for Rater 1 at time T1, T2, T3 and Rater 2. The line graphs of Rater 1 at time T1, T2, T3 and Rater 2 are following a similar pattern along the sample numbers.

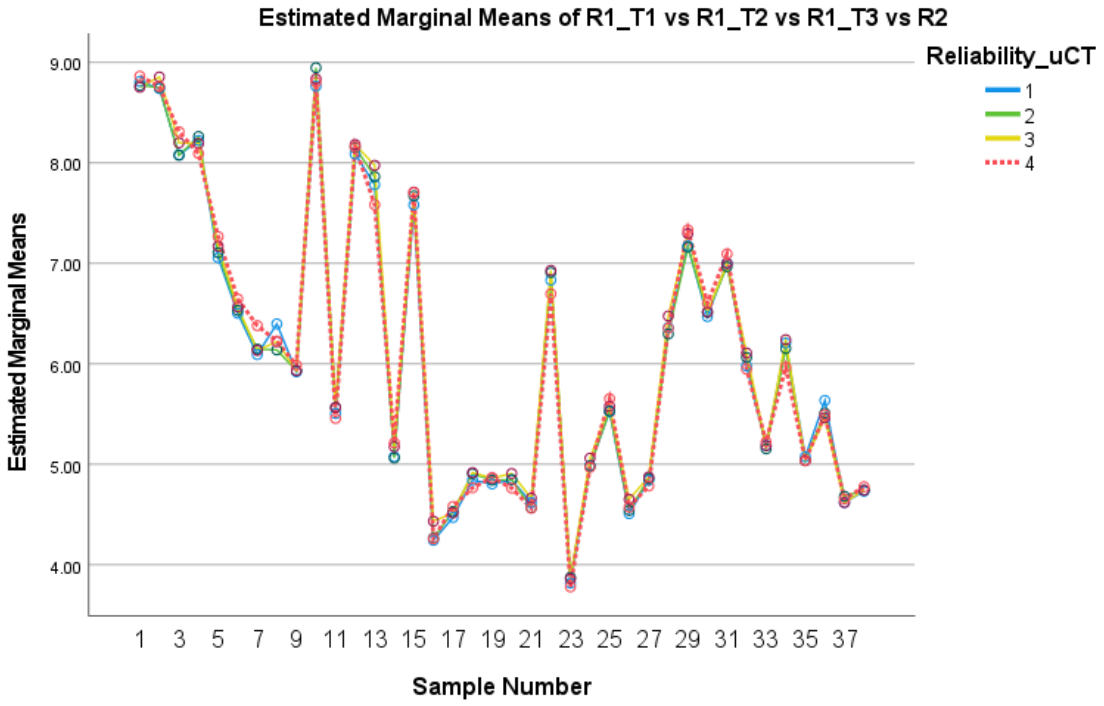

Figure 4.10 - Estimated Marginal means µCT R1_T1 (blue), R1_T2 (green), R1_T3 (yellow), R2 (red)

4.2.2 US INTER-Rater Reliability statistical analysis

Table 4.9 shows the Intraclass Correlation Coefficient and the 95% confidence interval (CI) of Rater 1 measurements of the US at Time 1 compared to the measurements of Rater 2. The Intraclass Correlation of 0.950 (0.906, 0.974) indicates the reliability between Rater 1 at Time 1 and Rater 2 is excellent.

Intraclass Correlation	95% Confidence Interval	
	Lower Bound	Upper Bound
0.950	0.906	0.974

Table 4.9 - ICC Inter-Rater US, R1_T1 vs R2

Figure 4.11 shows positive relationship between Rater 1 measurements of the US at Time 1 and the measurements of Rater 2. Except one data point, all data points are very close to the straight line.

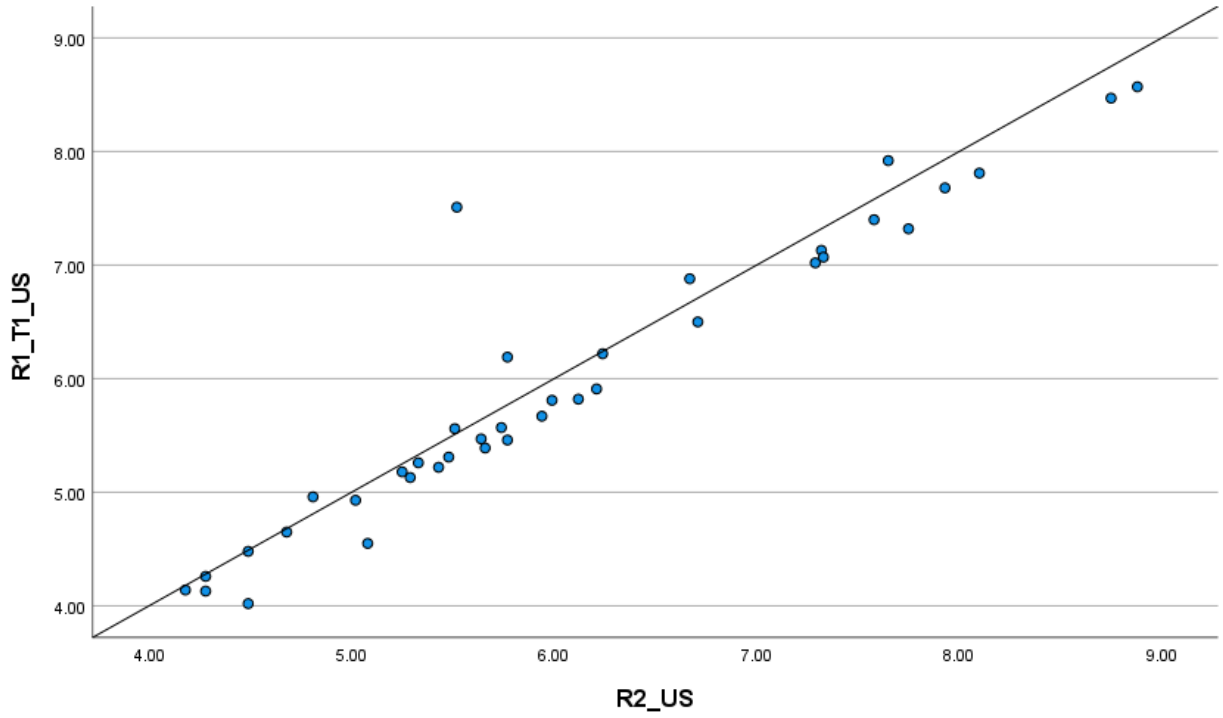

Figure 4.11 - 45º Scatter Plot Inter-Rater US, R1_T1 vs R2

Table 4.10 shows the Intraclass Correlation Coefficient and the 95% confidence interval (CI) of Rater 1 measurements of the US at Time 2 compared to the measurements of Rater 2. The Intraclass Correlation of 0.950 (0.902, 0.974) indicates the reliability between Rater 1 at Time 2 and Rater 2 is excellent.

Intraclass Correlation	95% Confidence Interval	
	Lower Bound	Upper Bound
0.950	0.902	0.974

Table 4.10 - ICC Inter-Rater US, R1_T2 vs R2

Figure 4.12 shows positive relationship between Rater 1 measurements of the US at Time 2 and the measurements of Rater 2. Except one data point, all data points are very close to the straight line.

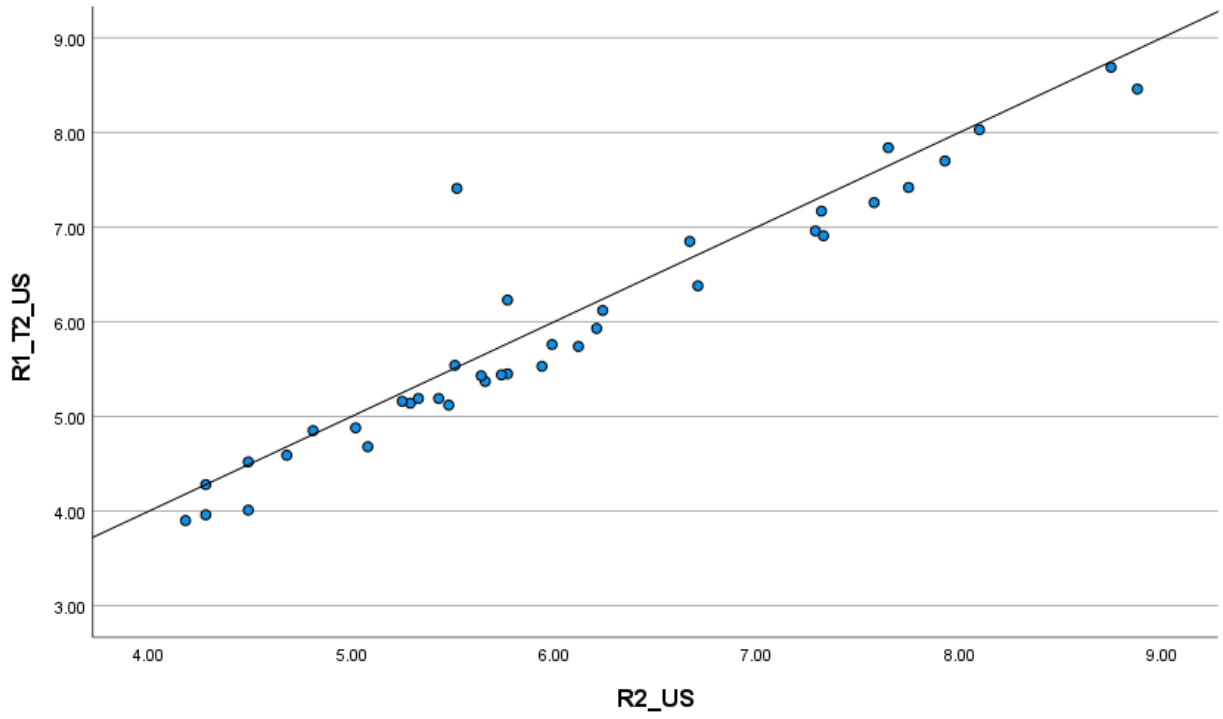

Figure 4.12 - 45º Scatter Plot Inter-Rater US, R1_T2 vs R2

Table 4.11 shows the Intraclass Correlation Coefficient and the 95% confidence interval (CI) of Rater 1 measurements of the US at Time 3 compared to the measurements of Rater 2. The Intraclass Correlation of 0.947 (0.896, 0.973) indicates the reliability between Rater 1 at Time 3 and Rater 2 is excellent.

Intraclass Correlation	95% Confidence Interval	
	Lower Bound	Upper Bound
0.947	0.896	0.973

Table 4.11 - ICC Inter-Rater US, R1_T3 vs R2

Figure 4.13 shows positive relationship between Rater 1 measurements of the US at Time 3 and the measurements of Rater 2. Except one data point, all data points are very close to the straight line.

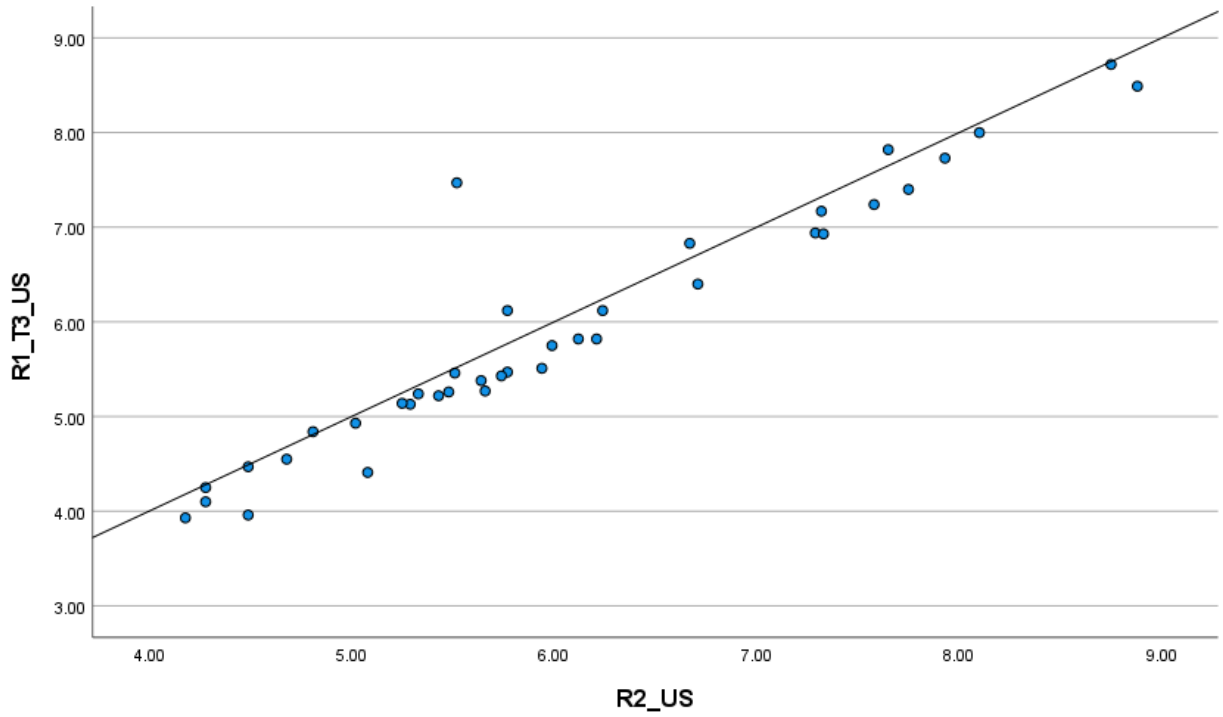

Figure 4.13 - 45º Scatter Plot Inter-Rater US, R1_T3 vs R2

Figure 4.14 shows the estimated marginal means of the measurements of the US for Rater 1 at time T1, T2, T3 and Rater 2. The line graphs of Rater 1 at time T1, T2, T3 and Rater 2 are following are following a similar pattern along the sample numbers.

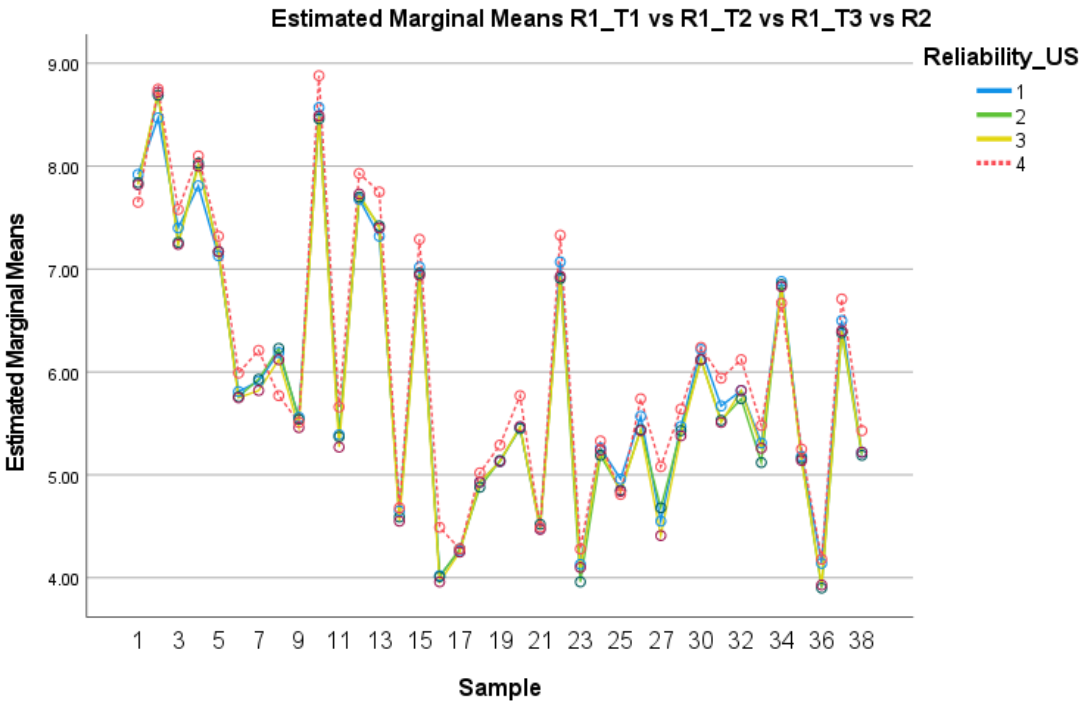

Figure 4.14 - Estimated Marginal means Ultrasound R1_T1 (blue), R1_T2 (green), R1_T3 (yellow), R2 (red)

Table 4.12 shows the Standard Deviation in millimetres for the **US Inter-Rater measurements.** The standard deviation value for the 38 samples, measured by Rater 1 at time T1, T2 and T3 compared to R2, has an average value of 0.182 mm for Time 1, 0.199 mm for Time 2 and 0.2 mm for Time 3.

Sample	Cadaver	R1_T1 US	R1_T2 US	R1_T3 US	R2 US	Standard Deviation US R1_T1, R2	Standard Deviation US R1_T2, R2	Standard Deviation US R1_T3, R2
1	1	7.92	7.84	7.82	7.65	**0.191**	**0.134**	**0.120**
2	1	8.47	8.69	8.72	8.75	**0.198**	**0.042**	**0.021**
3	1	7.4	7.26	7.24	7.58	**0.127**	**0.226**	**0.240**
4	1	7.81	8.03	8	8.1	**0.205**	**0.049**	**0.071**
5	1	7.13	7.17	7.17	7.32	**0.134**	**0.106**	**0.106**
6	1	5.81	5.76	5.75	5.99	**0.127**	**0.163**	**0.170**
7	1	5.91	5.93	5.82	6.21	**0.212**	**0.198**	**0.276**

8	1	6.19	6.23	6.12	5.77	**0.297**	**0.325**	**0.247**
9	1	5.56	5.54	5.46	5.51	**0.035**	**0.021**	**0.035**
10	1	8.57	8.46	8.49	8.88	**0.219**	**0.297**	**0.276**
11	2	5.39	5.37	5.27	5.66	**0.191**	**0.205**	**0.276**
12	2	7.68	7.7	7.73	7.93	**0.177**	**0.163**	**0.141**
13	2	7.32	7.42	7.4	7.75	**0.304**	**0.233**	**0.247**
14	2	4.65	4.59	4.55	4.68	**0.021**	**0.064**	**0.092**
15	2	7.02	6.96	6.94	7.29	**0.191**	**0.233**	**0.247**
16	2	4.02	4.01	3.96	4.49	**0.332**	**0.339**	**0.375**
17	2	4.26	4.28	4.25	4.28	**0.014**	**0.000**	**0.021**
18	2	4.93	4.88	4.93	5.02	**0.064**	**0.099**	**0.064**
19	2	5.13	5.14	5.13	5.29	**0.113**	**0.106**	**0.113**
20	2	5.46	5.45	5.47	5.77	**0.219**	**0.226**	**0.212**
21	2	4.48	4.52	4.47	4.49	**0.007**	**0.021**	**0.014**
22	3	7.07	6.91	6.93	7.33	**0.184**	**0.297**	**0.283**
23	3	4.13	3.96	4.1	4.28	**0.106**	**0.226**	**0.127**
24	3	5.26	5.19	5.24	5.33	**0.049**	**0.099**	**0.064**
25	3	4.96	4.85	4.84	4.81	**0.106**	**0.028**	**0.021**
26	3	5.57	5.44	5.43	5.74	**0.120**	**0.212**	**0.219**
27	3	4.55	4.68	4.41	5.08	**0.375**	**0.283**	**0.474**
28	3	5.47	5.43	5.38	5.64	**0.120**	**0.148**	**0.184**
29	3	7.51	7.41	7.47	5.52	**1.407**	**1.336**	**1.379**
30	3	6.22	6.12	6.12	6.24	**0.014**	**0.085**	**0.085**
31	3	5.67	5.53	5.51	5.94	**0.191**	**0.290**	**0.304**
32	3	5.82	5.74	5.82	6.12	**0.212**	**0.269**	**0.212**
33	3	5.31	5.12	5.26	5.48	**0.120**	**0.255**	**0.156**
34	3	6.88	6.85	6.83	6.67	**0.148**	**0.127**	**0.113**
35	3	5.18	5.16	5.14	5.25	**0.049**	**0.064**	**0.078**
36	3	4.14	3.9	3.93	4.18	**0.028**	**0.198**	**0.177**
37	3	6.5	6.38	6.4	6.71	**0.148**	**0.233**	**0.219**
38	3	5.22	5.19	5.22	5.43	**0.148**	**0.170**	**0.148**
Average in mm						**0.182**	**0.199**	**0.200**

Table 4.12 - Standard Deviation in millimetres for the US Inter-Rater measurements.

Table 4.13 shows the Standard Deviation in millimetres for the US inter-rater reliability measurements, grouped by regions of the mouth: upper anterior (from canine to canine), lower anterior, upper premolars, lower premolars, upper molars and lower molars respectively. From the data, it appears that the lower molar region has the highest reliability with the lowest SD at 0.094 – 0.166 mm, followed by the lower anterior region with an SD range of 0.142 – 0.169 mm, upper anterior with an SD 0.162 – 0.171 mm, upper molars with SD 0.139 – 0.222 mm, lower premolars with an SD 0.184 – 0.210 mm and the upper premolars having the lowest reliability

with an SD range of 0.438 – 0.460 mm. However, since only the upper and lower anterior regions have enough samples in all the groups for a meaningful statistical difference, the data available is not conclusive in order to compare the US reliability by regions of the mouth.

Sample	Cadaver	Tooth Number	Standard Deviation R1_T1, R2	Standard Deviation R1_T2, R2	Standard Deviation R1_T3, R2
11	2	13	0.191	0.205	0.276
22	3	13	0.184	0.297	0.283
13	2	11	0.304	0.233	0.247
24	3	11	0.049	0.099	0.064
2	1	21	0.198	0.042	0.021
25	3	21	0.106	0.028	0.021
1	1	12	0.191	0.134	0.120
12	2	12	0.177	0.163	0.141
23	3	12	0.106	0.226	0.127
3	1	22	0.127	0.226	0.240
14	2	22	0.021	0.064	0.092
26	3	22	0.120	0.212	0.219
4	1	23	0.205	0.049	0.071
27	3	23	0.375	0.283	0.474
Average SD Upper Anterior			**0.168**	**0.162**	**0.171**
16	2	33	0.332	0.339	0.375
33	3	33	0.120	0.255	0.156
21	2	43	0.007	0.021	0.014
9	1	31	0.035	0.021	0.035
18	2	31	0.064	0.099	0.064
19	2	41	0.113	0.106	0.113
8	1	32	0.297	0.325	0.247
17	2	32	0.014	0.000	0.021
10	1	42	0.219	0.297	0.276
20	2	42	0.219	0.226	0.212
Average SD Lower Anterior			**0.142**	**0.169**	**0.151**
5	1	24	0.134	0.106	0.106
28	3	24	0.120	0.148	0.184
6	1	25	0.127	0.163	0.170
29	3	25	1.407	1.336	1.379
Average SD Upper Premolars			**0.447**	**0.438**	**0.460**
15	2	34	0.191	0.233	0.247
32	3	34	0.212	0.269	0.212

34	3	44	0.148	0.127	0.113
Average SD Lower Premolars			**0.184**	**0.210**	**0.191**
7	1	26 Mesial	0.212	0.198	0.276
30	3	37 Distal	0.014	0.085	0.085
31	3	37 Mesial	0.191	0.290	0.304
Average SD Upper Molars			**0.139**	**0.191**	**0.222**
35	3	46 Mid	0.049	0.064	0.078
36	3	46 Distal	0.028	0.198	0.177
37	3	47 Mesial	0.148	0.233	0.219
38	3	47 Distal	0.148	0.170	0.148
Average SD Lower Molars			**0.094**	**0.166**	**0.156**

Table 4.13 - Standard Deviation in millimetres for the US inter-rater reliability measurements, grouped by regions of the mouth

4.3 Accuracy Statistical Analysis

Table 4.14 shows the Intraclass Correlation Coefficient and the 95% confidence interval (CI) of Rater 1 measurements of US and µCT, at Time 2. The Intraclass Correlation of 0.894 (0.804, 0.944) indicates the accuracy of US compared to µCT is good.

Intraclass Correlation	95% Confidence Interval	
	Lower Bound	Upper Bound
0.894	0.804	0.944

Table 4.14 - ICC R1_T2_US vs R1_T2_µCT

Figure 4.15 shows positive relationship between Rater 1 measurements of US and µCT, at Time 2.

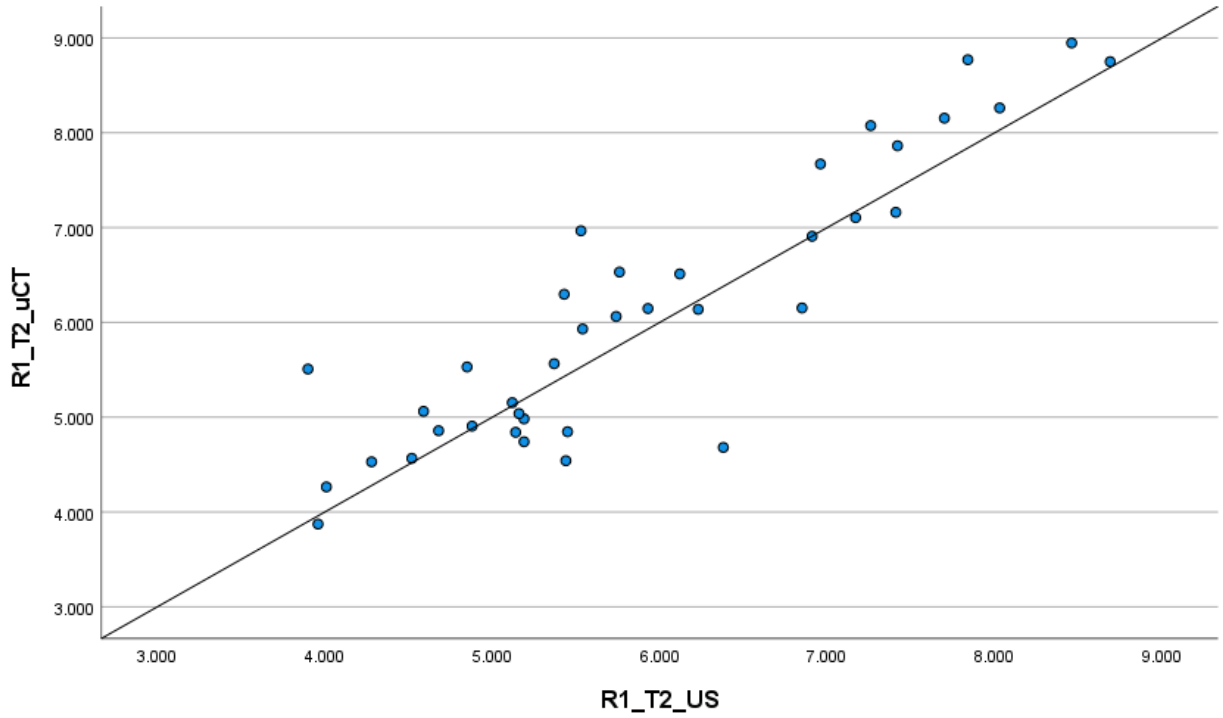

Figure 4.15 - 45º Scatter Plot R1_T2_µCT vs R1_T2_US

Table 4.15 shows the Standard Deviation in millimetres for the Accuracy measurements. The standard deviation value for the 38 samples, measured by Rater 1 at Time 2 by US and µCT, varies between 0.001 mm at the lowest value to 1.201 mm at the highest value, with an average value of 0.330 mm.

Sample	Cadaver	R1_T2 US	R1_T2 µCT	Standard Deviation R1_T2, US vs µCT
1	1	7.84	8.771	**0.658**
2	1	8.69	8.750	**0.043**
3	1	7.26	8.076	**0.577**
4	1	8.03	8.263	**0.164**
5	1	7.17	7.106	**0.045**
6	1	5.76	6.532	**0.546**
7	1	5.93	6.147	**0.153**

8	1	6.23	6.138	**0.065**
9	1	5.54	5.932	**0.277**
10	1	8.46	8.948	**0.345**
11	2	5.37	5.565	**0.138**
12	2	7.7	8.155	**0.321**
13	2	7.42	7.863	**0.314**
14	2	4.59	5.063	**0.334**
15	2	6.96	7.671	**0.503**
16	2	4.01	4.265	**0.181**
17	2	4.28	4.530	**0.177**
18	2	4.88	4.907	**0.019**
19	2	5.14	4.842	**0.211**
20	2	5.45	4.848	**0.426**
21	2	4.52	4.567	**0.033**
22	3	6.91	6.909	**0.001**
23	3	3.96	3.874	**0.061**
24	3	5.19	4.983	**0.146**
25	3	4.85	5.531	**0.481**
26	3	5.44	4.542	**0.635**
27	3	4.68	4.858	**0.126**
28	3	5.43	6.297	**0.613**
29	3	7.41	7.162	**0.176**
30	3	6.12	6.512	**0.277**
31	3	5.53	6.967	**1.016**
32	3	5.74	6.063	**0.228**
33	3	5.12	5.154	**0.024**
34	3	6.85	6.153	**0.493**
35	3	5.16	5.039	**0.086**
36	3	3.9	5.509	**1.138**
37	3	6.38	4.682	**1.201**
38	3	5.19	4.742	**0.317**
Average in mm				**0.330**

Table 4.15 - Standard Deviation in millimetres for the accuracy measurements for Rater 1 at Time 2

Table 4.16 shows the Standard Deviation in millimetres for the accuracy measurements, grouped by regions of the mouth: upper anterior (from canine to canine), lower anterior, upper premolars, lower premolars, upper molars and lower molars respectively. From the data, it appears that the lower anterior region has the highest accuracy with the lowest SD at 0.176 –

0.251 mm, followed by the upper anterior region with an SD range of 0.286 – 0.348 mm, lower premolars with an SD range of 0.304 – 0.408 mm, upper premolars with an SD 0.345 – 0.572 mm, upper molars with SD 0.398 – 0.518 mm and the lower molars having the lowest accuracy with an SD range of 0.685 – 0.748 mm. Although only the upper and lower anterior regions have enough samples for a more meaningful statistical significance, the general trend that could be observed in that data available is that the US is more accurate in the anterior regions of the mouth, followed by the premolar regions with the molar regions having the least accuracy. However, since only the upper and lower anterior regions have enough samples in all the groups for a meaningful statistical significance, the available data is not conclusive in order to compare the US accuracy by regions of the mouth.

Sample	Cadaver	Tooth Number	Standard Deviation R1_T1, US vs µCT	Standard Deviation R1_T2, US vs µCT	Standard Deviation R1_T3, US vs µCT	Standard Deviation R2, US vs µCT
11	2	13	0.081	0.138	0.209	0.144
22	3	13	0.168	0.001	0.000	0.448
13	2	11	0.327	0.314	0.407	0.118
24	3	11	0.195	0.146	0.127	0.255
2	1	21	0.191	0.043	0.096	0.007
25	3	21	0.401	0.481	0.522	0.596
1	1	12	0.630	0.658	0.659	0.858
12	2	12	0.289	0.321	0.320	0.163
23	3	12	0.222	0.061	0.171	0.354
3	1	22	0.481	0.577	0.679	0.516
14	2	22	0.301	0.334	0.442	0.377
26	3	22	0.750	0.635	0.550	0.825
4	1	23	0.292	0.164	0.137	0.005
27	3	23	0.206	0.126	0.329	0.209
Average SD Upper Anterior			**0.324**	**0.286**	**0.332**	**0.348**
16	2	33	0.158	0.181	0.335	0.163
33	3	33	0.087	0.024	0.052	0.181
21	2	43	0.098	0.033	0.136	0.052
9	1	31	0.255	0.277	0.334	0.337
18	2	31	0.063	0.019	0.009	0.179
19	2	41	0.230	0.211	0.189	0.299
8	1	32	0.147	0.065	0.071	0.323
17	2	32	0.149	0.177	0.188	0.212

10	1	42	0.137	0.345	0.245	0.054
20	2	42	0.436	0.426	0.397	0.712
Average SD Lower Anterior			**0.176**	**0.176**	**0.196**	**0.251**
5	1	24	0.052	0.045	0.000	0.038
28	3	24	0.629	0.613	0.775	0.504
6	1	25	0.491	0.546	0.577	0.464
29	3	25	0.238	0.176	0.123	1.282
Average SD Upper Premolars			**0.352**	**0.345**	**0.369**	**0.572**
15	2	34	0.397	0.503	0.544	0.292
32	3	34	0.112	0.228	0.204	0.123
34	3	44	0.476	0.493	0.417	0.497
Average SD Lower Premolars			**0.329**	**0.408**	**0.388**	**0.304**
7	1	26 Mesial	0.129	0.153	0.222	0.120
30	3	37 Distal	0.177	0.277	0.281	0.257
31	3	37 Mesial	0.943	1.016	1.052	0.816
Average SD Upper Molars			**0.416**	**0.482**	**0.518**	**0.398**
35	3	46 Mid	0.074	0.086	0.074	0.148
36	3	46 Distal	1.058	1.138	1.083	0.929
37	3	47 Mesial	1.329	1.201	1.259	1.454
38	3	47 Distal	0.345	0.317	0.337	0.462
Average SD Lower Molars			**0.702**	**0.685**	**0.688**	**0.748**

Table 4.16 - Standard Deviation in millimetres for the accuracy measurements, grouped by regions of the mouth

4.4 Statistical Analysis Summary

Table 4.17 is an aggregate of the results for the Intraclass Correlation Coefficient (ICC) and the 95% Confidence Interval for the Intra-Rater reliability statistical analysis for Rater 1. All Intraclass Correlation Coefficients for Rater 1 when measuring the samples with µCT and US are excellent with a value well over 0.9.

Imaging Modality	ICC Intra-Rater	95% Confidence Interval	
		Lower Bound	Upper Bound
µCT R1_T1 vs R1_T2 vs R1_T3	**0.998**	0.997	0.999
US R1_T1 vs R1_T2 vs R1_T3	**0.997**	0.995	0.999

Table 4.17 - Aggregate of the Intra-Rater Intraclass Correlation Coefficient and the 95% Confidence Interval for Rater 1

Table 4.18 is an aggregate of the average Standard Deviation for the Intra-Rater reliability statistical analysis, for all the measurements performed by Rater 1, for all 38 samples, grouped by imaging modality: µCT and Ultrasound. All Standard Deviation averages for Rater 1 are below 0.1 mm.

Average Standard Deviation µCT R1_T1, R1_T2, R1_T3	**0.050** mm
Average Standard Deviation US R1_T1, R1_T2, R1_T3	**0.057** mm

Table 4.18 - Average of the Standard Deviation for Rater 1 measurements

Table 4.19 is an aggregate of all the results for the Intraclass Correlation Coefficient (ICC) and the 95% Confidence Interval for the Intra-Rater reliability statistical analysis for Rater 1 compared to Rater 2. All Intraclass Correlation Coefficients for Rater 1 compared to Rater 2 when measuring the samples with the µCT and Ultrasound are excellent with a value well over 0.9.

Imaging Modality	ICC Inter-Rater Reliability	95% Confidence Interval	
		Lower Bound	Upper Bound
µCT R1_T1 vs R2	**0.996**	0.993	0.998
µCT R1_T2 vs R2	**0.996**	0.993	0.998
µCT R1_T3 vs R2	**0.996**	0.992	0.998
US R1_T1 vs R2	**0.950**	0.906	0.974
US R1_T2 vs R2	**0.950**	0.902	0.974
US R1_T3 vs R2	**0.947**	0.896	0.973

Table 4.19 - Aggregate of the Intra-Rater Intraclass Correlation Coefficient and the 95% Confidence Interval for Rater 1 compared to Rater 2

Table 4.20 is an aggregate of the average Standard Deviation for the Inter-Rater reliability statistical analysis, for all the measurements performed by Rater 1 compared to Rater 2, for all 38 samples, grouped by imaging modality: µCT and US. All Standard Deviation averages for Rater 1 compared to Rater 2 are below 0.1 mm for µCT and below 0.2 mm for US.

Average Standard Deviation µCT R1_T1, R2	**0.069** mm
Average Standard Deviation µCT R1_T2, R2	**0.068** mm
Average Standard Deviation µCT R1_T3, R2	**0.069** mm
Average Standard Deviation US R1_T1, R2	**0.182** mm
Average Standard Deviation US R1_T2, R2	**0.199** mm
Average Standard Deviation US R1_T3, R2	**0.200** mm

Table 4.20 - Average of the Standard Deviation for Rater 1 measurements compared to Rater 2

Table 4.21 is an aggregate of the results for the Intraclass Correlation Coefficient (ICC) and the 95% Confidence Interval for the Accuracy statistical analysis for Rater 1 at Time 1, 2 and 3. All Intraclass Correlation Coefficients when comparing the US measurements to µCT are good with a value in between 0.885 and 0.894.

Imaging Modality	ICC Accuracy	95% Confidence Interval	
		Lower Bound	Upper Bound
R1_T1_US vs R1_T1_µCT	**0.893**	0.805	0.943
R1_T2_US vs R1_T2_µCT	**0.894**	0.804	0.944
R1_T3_US vs R1_T3_µCT	**0.885**	0.780	0.940

Table 4.21 - Aggregate of the Intra-Rater Intraclass Correlation Coefficient and the 95% Confidence Interval for the Accuracy measurements

Table 4.22 shows an aggregate of the average Standard Deviation (SD) for all 38 samples, in millimetres for the accuracy measurements for Rater 1 at Time 1, 2 and 3 and for Rater 2. When comparing the accuracy of the US to the µCT, the average standard deviation is 0.335 mm for Rater 1 at Time 1, 0.33 mm for Rater 1 at Time 2, 0.357 mm for Rater 1 at Time 3 and 0.389 mm for Rater 2.

Average SD R1_T1, US vs µCT	**0.335**
Average SD R1_T2, US vs µCT	**0.330**
Average SD R1_T3, US vs µCT	**0.357**
Average SD R2, US vs µCT	**0.389**

Table 4.22 - Aggregate of the average Standard Deviation (SD) for all the accuracy measurements

CHAPTER 5 –DISCUSSION

The alveolar bone assessments through images play a key role in the evaluation of general periodontal conditions and are a fundamental adjunct to the diagnostic process. It allows the clinician to assess the amount of bone present, the condition of the alveolar ridges, bone loss in the furcation region, thickness of the periodontal ligament space, local irritating factors that may increase the risk of periodontal loss (such as calculus, under-contoured or overextended restorations, mismatched prostheses), root length, morphology and crown-root relationship, lack of point of contact, pathological considerations (carious lesions, periapical lesions, resorptions root) and anatomical considerations (position of a periodontal deformity in relation to the maxillary sinus, missing teeth, supernumerary teeth, impaction and/or dental inclination (White & Pharoah, 2009). Two-dimensional radiographs such as periapical and bitewings have been used to image alveolar bone, however, they can only access interdental alveolar bone.

Computed Tomography became popular in dentistry after the development of CBCT that allowed the cost and radiation dose reduction of the technique. Thanks to this new technology, the measurement of the alveolar bone height, which was previously limited when performed through 2D radiographs or when done through periodontal probing, was finally achievable in an accurate manner (Sun et al., 2011; Swennen & Schutyser, 2006). The correct assessment of alveolar bone levels is of fundamental importance for treatment planning in a great variety of dental specialties (Fuhrmann, 2008). In orthodontics, for example, it is often necessary to make use of controlled projection of lower incisors to correct malocclusions, as this region presents greater frequency of dehiscence and thinner bone thickness.

Studies have been published on the assessment of the reproducibility and accuracy of the measurement of the height of the alveolar border through CBCT images with results demonstrating good reproducibility and good accuracy in measuring this distance (Leung, Palomo, Griffith, & Hans, 2010; Loubele et al., 2008; Sun, Zhang, Shen, Wang, & Fang, 2015; Walter et al., 2020). However, both cone beam and spiral tomography devices still have some limitations related to spatial resolution, impairing the visualization of the alveolar bone when it is thinner than 0.6 mm (Sun et al., 2011; Leung, Palomo, Griffith, & Hans, 2010). Some of the limitations were addressed by the advent of μCT, as it allows the measurement of structures at a

micro scale, going from millimetres to micrometers. Alveolar bone level in animals have been measured and distances from CEJ to alveolar bone crest as low as 100µm can be accurately assessed (Monasterio, Castillo et al. 2018, Lubcke, Ebbers et al. 2019, Catunda et al., 2021). This great advantage came also with the burden of increased doses of radiation and a machine that only fits small specimens (Marciano et al., 2012). Hence the need of further investigation on accurate methods of assessing the alveolar bone level that cause less harm to the patient and can be used clinically.

The use of US to evaluate periodontium has been studied in the attempt to evaluate its potential as a diagnostic tool. US is a painless imaging device that uses sound waves produced in a device called transducer, responsible for sending the ultrasonic waves to the tissue to be evaluated. In dentistry, it has been gaining more and more space in the analysis of the temporomandibular joint (TMJ) and in the field of oral and maxillofacial surgery, being also of great value in the diagnosis of salivary gland disorders. US can be used on any patient, such as children or pregnant women, as it is a safe tool, performed in real-time, non-invasive, and repeatable whenever necessary without producing deleterious effects to the patient. However, it is an operator-dependent device, meaning that the radiologist experience is considered of great value (Chandak et al., 2011, Ferreira et al., 2002). The present study found excellent reliability and good accuracy of US to evaluate the facial alveolar bone height compared to the µCT gold standard. Salmon et al. (2012) developed an ultrasound prototype (25 MHz) adapted for the periodontal evaluation of the oral cavity, similarly to our study. They assessed effectiveness of ultrasound in determining the bone level around implants, which is inaccessible by radiography. The authors suggested that the use of the US device is safe, and its dynamism makes it suitable for bone level assessment. Mahmoud et al. (2010) investigated the use of high-frequency ultrasound (30-60MHz) to obtain 3D images of bone defects present in cadavers' jawbone, as the present study. The authors concluded that the system is accurate in detecting bone defects, superior to conventional radiographs and demonstrating great potential for the diagnosis of periodontal defects. This reinforces our findings that point at this new device as a new modality for diagnosis.

The first step for the creation of a new method of assessment is defining what is being measured and how it can be measured. The answers for those questions can be obtained by

performing exploratory research with the objective of finding out the best way to acquire reliable measurements. Reliable measurements are replicable and consistent, meaning they can generate the same results. This leads us to the first challenge that had to be overcome in this research project: the difference between µCT and US imaging techniques and the principles on which they operate. US uses sound echoes that are decoded into a digital signal, through a computer coupled to the transducer. These are observed on the monitor as a grayscale with different shades of grey. Ultrasound waves are reflected by structures with different impedances acoustics - the biological tissues - thus obtaining the desired information (Chandak et al., 2011). In contrast, µCT uses ionizing radiation (Steiner, Synek, & Pahr, 2020) , and the result is a computer generated three-dimensional (3D) image that can be fully manipulated by the operator. The resulting computer images shown as the shades of grey that are used as a visual interpretation for CT and US are fundamentally different, therefore they require specific training for operators without previous US experience. In addition, µCT ionizing radiation fully penetrates the samples and we can save a digital representation in full of a particular sample, whereas the US echoes only penetrate the tissues superficially; if the alveolar bone plate is buried under a thick layer of gingiva, it might not be detected at all by the transducer. Therefore, the digital representation of an US scan only displays the superficial surface of a sample, only a few millimetres deep.

Another difference between µCT and US is that while the µCT scans an anatomical structure and exports data in 3D, the US scan of the same anatomical structure exports the data only in 2D but with an unknown degree of volumetric averaging and superimposition. As a result, a µCT data file can be viewed and measured in 3D (sagittal, axial, coronal) while a US data file can only be viewed and measured in 2D (equivalent of sagittal and coronal with no measurable transverse dimension). This is the main reason why the gold standard measurement on the µCT for each sample was considered and analyzed by the averaging of three measurements that span transversally across the diameter of a given notch (almost 1mm), and not just using a single measurement in the centre of the notch. In the µCT recorded and analyzed for each measured sample, the distance from the inferior border of the reference notch in the tooth, to the tip of the bone, was calculated as the average of 3 measurements: from the tip of the bone to the inferior border of the notch in the centre of the notch, from the tip of the bone to the inferior border of the notch towards the mesial edge of the notch and from the tip of the bone to the inferior border of the notch towards the distal edge of the notch.

These key physical and digital representation differences between μCT and US imaging made comparing the two imaging techniques quite challenging, and the methodology of this study had to have been conceived in such a way that it still allowed a reliable direct comparison between the two. In the current literature of periodontal assessment, we have values that can vary up to 1mm when probing methods are used (Badersten et al., 1984). For assessing the clinical attachment level by using a regular 2D x-ray, that value is very similar, up to 1mm of underestimation of true alveolar bone level of infra-bony defects, with the lowest variation for periodontal assessments was seen with digital calipers when used to measure gingival recession (0.7mm) (Fageeh et al., 2019). Regarding the clinical relevance, some literature points that errors for loss of attachment assessment should be maintained at 0.13 mm for whole-mouth average and 0.54 mm for individual sites (Kingman et al., 1991), while others say that the number for clinical attachment level variability should remain under 2 mm (Fageeh et al., 2019). Therefore, our results can also be considered clinically relevant as our average SD values, when comparing the US to the μCT (gold standard), ranged from 0.330 to 0.399 mm.

In a study from Fageeh et al (2019), they compared the precision of US and a digital caliper (calibration of 0.01mm) for measurements of gingival thickness. Their results showed that mean gingival thickness ranged from 0.56–1.02 mm and both techniques were considered comparable, since the study did not yield any difference that was statistically significant. Digital calipers are extremely accurate; however, they are invasive to use intra-orally to measure gingival thickness. Even though this study did not attempt to compare US to alveolar bone measurements and used a completely different device as gold standard (digital caliper), it showed good accuracy of this imaging modality to measure another anatomical structure of the periodontium coming to conclusions that are in agreement with our findings.

Studies that looked at utilizing CBCT for alveolar bone measurements such as CEJ-alveolar bone crest, showed high reliability, good accuracy with varying precision (Timock et al, 2011, Cook et al., 2015). These studies compared periodontal measurements of cadavers using a long scan (26.9 seconds; 619 projection images; 360^{o} rotation; 0.2 mm voxel size), a default scan (8.9 seconds; 309 projection images; 360^{o} rotation; 0.3 mm voxel size), a short scan (4.8 seconds; 169 projection images; 180^{o} rotation; 0.3 mm voxel size) and compared to a digital caliper. They concluded that short and long scans were accurate but short scan had less precision than long

scan. The SD varied from 0.12mm (long scan) to 0.32mm (short scan) (Timock et al, 2011, Cook et al., 2015). Although CBCT has shown good accuracy and reliability and has been suggested as a non-invasive method to precisely measure hard and soft tissues of the alveolar bone complex, the radiation dose is an important issue to prevent this image modality to be used as a routine in clinical practice for this purpose (Fu et al., 2010, Januario et al., 2008). The US accuracy and reliability were shown in our study and the great advantage of this new technique is the lack of radiation involved. According to the UNSCEAR 2000, diagnostic x-rays account for approximately 1.2 mSv individual yearly radiation exposure. As previously mentioned, dental x-rays vary from 0.005mSv to 0.024mSv whereas a CBCT can reach 0.1mSv. The maximum dose as per Canadian Radiation Protection Regulations (SOR/2000-203) varies from 15-50mSv per year (any individual), depending on the exposed area (i.e., eyes are more sensitive than skin). Therefore, the strict control of the necessity of assessments that utilize ionizing radiation needs to be carefully evaluated given their cumulative effect and the search for alternative methods of alveolar bone assessment such as US should be encouraged.

Our study attempted to measure alveolar bone crest in different groups of teeth in the cadavers. Those groups were: upper anterior (from canine to canine), lower anterior, upper premolars, lower premolars, upper molars and lower molars. This was an important addition to the literature since the previous clinical study by Nguyen et al. (2021) was only able to measure incisors and canines (given the intra-oral limitations as their study was a clinical trial) and Chifor et al (2012) looked at incisors, molars and premolars of a porcine mandible. Similar to our study, however, Nguyen et al. (2021) did not establish differences between groups of teeth.

Regarding the use of notches as landmarks when comparing the two imaging modalities, initially, the intent was to use the CEJ) since it is a landmark used in a clinical setting for measuring the alveolar bone height. However, for this ex-vivo study, using the CEJ was not the best landmark to use when comparing US to μCT for two reasons. Firstly, the CEJ as a landmark is rather difficult to precisely locate on the cadavers since a lot of the teeth samples have imperfections around the CEJ area; this in turn could have introduced an CEJ identification error in the US measurements. Also, discarding the teeth with defects around the CEJ was not an option either since it would have disqualified too many available samples from the study. In comparison, visually identifying the notches by the operator on the US images is more consistent

since the notches are round, placed in the superficial enamel and can be easily identifiable. Secondly, the CEJ as a landmark does not offer the opportunity to replicate the US transverse volumetric averaging on the μCT since the CEJ does not provide any transverse mesio-distal landmarks that can be used. Instead, by using a notch with a mesio-distal diameter of almost 1 mm, this study averaged three μCT measurements for each sample and this would be the equivalent of an US slice with the transverse thickness of almost 1 mm.

5.1 Limitations

The main limitation of this study was the number of viable samples available. Although initially there were 58 teeth that could have been used, only 38 samples satisfied the selection criteria for this project. Still, 38 samples represented a meaningful number of samples required that had enabled us to investigate the new US reliability and accuracy.

Another limitation of this study is the direct applicability of cadaver results to live humans. Although the results have shown the reliability and accuracy of the US on cadaver teeth by using μCT as a gold standard, the methodology devised in this study does not directly translate when attempting to measure on live humans. Notches can't be placed on live teeth and uCT can't be used on live humans due to its small size and high radiation dose. However, the methodology can be modified for it to be applicable on measuring on US on live humans. A possible such change could be to use of the CEJ as a reference landmark for the US and the use of an intra-oral measurement with calipers as a clinical reference standard.

5.2 Directions for Future Studies

Based on the challenges and the experience gained from this study comparing US to μCT, the following recommendations can be made for future studies in order to minimize or eliminate the effect of certain factors that had to be accepted as is in this study:

1. Investigate how to better replicate the Ultrasound volumetric averaging / superimposition in the way the samples are measured on the μCT – as previously explained, the main challenge of this study was the μCT and US differences on which they operate and the way the imaging data is presented to the operator. When

measuring a sample with the US transducer, some degree of volumetric averaging and superimposition occurs. As a result, when measuring the bone height with the US transducer, the highest bony peak will be visible on the 2D US image, however, there is no precise way to determine where this highest bony peak is mesio-distally. The μCT that was used as a reference gold standard imaging modality, had the resolution of 0.03 mm and the μCT software is very precise in selecting a certain frame mesio-distally, however, the μCT software lacks the ability to merge successive slices of a sample in order to create a thicker superimposed structure on which the highest bony peak will be measured. With the current devised methodology, the way to minimize the effect of this limitation was to use the notches as landmarks that were roughly 1 millimetre in diameter and measure the bony peak on the μCT in three different locations relative to the notch: in the centre of the notch, mesially and distally, followed by averaging the three measurements that was used in the statistical analysis. Therefore, a possible option worth exploring is if a bigger reference notch that is used as a landmark makes a difference in comparing the US images to μCT or if there is any commercial software available that would allow successive μCT slices to be superimposed in order to create a thicker superimposed structure that will approximate an US image that includes a certain degree of superimposition.

2. Minimize the biological constraint for US – For this project, the ex-vivo human samples were sourced from three different cadavers. Although this might not be of significance in case of imaging with μCT in which the radiation penetrates the samples regardless of tissue density, it could theoretically make a difference in the case of Ultrasound imaging since a certain degree of tissue density difference could be theoretically expected among the three cadavers. For future testing, the impact of tissue density on the Ultrasound measurements might be something worth investigating.

3. The results of the present study show an excellent reliability and good accuracy of the device; however, the study was performed on human cadavers in a controlled

environment as a preclinical study. The next step in the research phase would be a clinical trial.

References

Aldrich, J. E. (2007). Basic physics of ultrasound imaging. *Crit Care Med, 35*(5 Suppl), S131-137. doi:10.1097/01.CCM.0000260624.99430.22

Badersten, A., Nilveus, R., Egelberg, J. (1984). Reproducibility of probing attachment level measurements. *J Clin Periodontol* 11(7), 475–485, https://doi.org/10.1111/j.1600-051x.1984.tb01347.x

Chandak, R., Degwekar, S., Bhowte, R.R., Motwani, M., Banode, P., Chandak, M., Rawlani, S. (2011). An evaluation of efficacy of ultrasonography in the diagnosis of head and neck swellings. *Dentomaxillofac Radiol*, 40(4), 213-21. doi: 10.1259/dmfr/68658286

Chifor R, Li M, Nguyen KT, Arsenescu T, Chifor I, Badea AF, Badea ME, Hotoleanu M, Major PW, Le LH. (2021) Three-dimensional periodontal investigations using a prototype handheld ultrasound scanner with spatial positioning reading sensor. Med Ultrason, 23(3), 297-304. doi: 10.11152/mu-2837. Epub 2021 Mar 3. PMID: 33657191.

Cook, V.C., Timock, A.M., Crowe, J.J., Wang, M., Covell, D.A. Jr. (2015). Accuracy of alveolar bone measurements from cone beam computed tomography acquired using varying settings. *Orthod Craniofac Res*,18 Suppl 1, 127-36. doi: 10.1111/ocr.12072.

Demirtas, N., Mihmanli, A., Aytuğar, E., & Bayer, S. (2015). Limitations of Panoramic Radiographs: Report of Two Cases. Bezmialem Science, 2, 82-85. doi:10.14235/bs.2014.328

Fageeh, H., Meshni, A., Jamal, H., Preethanath, R., & Halboub, E. (2019). The accuracy and reliability of digital measurements of gingival recession versus conventional methods. *BMC Oral Health*, 19 (154). doi:10.1186/s12903-019-0851-0

Ferreira, R. I., de Almeida, S. M., Bóscolo, F. N., Santos, A. O., & Camargo, E. E. (2002). Bone scintigraphy as an adjunct for the diagnosis of oral diseases. J Dent Educ, 66(12), 1381-1387. PMID: 12521065

Fu, J.H., Yeh, C.Y., Chan, H.L., Tatarakis, N., Leong, D.J., Wang, H.L. (2010). Tissue bio-type and its relation to the underlyingbone morphology.*J Periodontol*, 81 (4),569–74. doi: 10.1902/jop.2009.090591

Fuhrmann, R. (2002). Three-dimensional evaluation of periodontal remodeling during orthodontic treatment. *Semin Orthod*, 8(1), 23-28. doi: 10.1053/sodo.2002.28168

Government of Canada. (2022, August), Radiation Protection Regulations SOR/2000-203. Justice Laws. Government of Canada. https://laws-lois.justice.gc.ca/eng/regulations/SOR-2000-203/FullText.html

Januario, A.L., Barriviera, M., Duarte, W.R. (2008) Soft tissue cone-beam computed tomography: a novel method for the measurement of gingival tissue andthe dimensions of the dentogingival unit. *J Esthet Restor Dent*, 20 (6),366–73. doi: 10.1111/j.1708-8240.2008.00210.x

Kingman, A., Löe, H., Anerud, A., Boysen, H. (1991). Errors in measuring parameters associated with periodontal health and disease. *J Periodontol*,62(8),477-86. doi: 10.1902/jop.1991.62.8.477.

Leung, C.C., Palomo, L., Griffith, R., Hans, M.G. (2010). Accuracy and reliability of cone-beam computed tomography for measuring alveolar bone height and detecting bony dehiscences and fenestrations. *Am J Orthod Dentofacial Orthop*, 140(5),S109-119. doi: 10.1016/j.ajodo.2009.07.013

Loubele, M., Van Assche, N., Carpentier, K., Maes, F., Jacobs, R., van Steenberghe, D., & Suetens, P. (2008). Comparative localized linear accuracy of small-field cone-beam CT and multislice CT for alveolar bone measurements. Oral Surg Oral Med Oral Pathol Oral Radiol Endod, 105(4), 512-518. doi:10.1016/j.tripleo.2007.05.004

Lubcke, P. M., M. N. B. Ebbers, J. Volzke, J. Bull, S. Kneitz, R. Engelmann, H. Lang, B. Kreikemeyer and B. Muller-Hilke (2019). Periodontal treatment prevents arthritis in mice and methotrexate ameliorates periodontal bone loss. *Sci Rep* 9(1): 8128. Doi: 10.1038/s41598-019-44512-9

Mahmoud, Am.M., Ngan, P., Crout, R., Mukdadi, O.M. (2010). High-resolution 3D ultrasound jawbone surface imaging for diagnosis of periodontal body defects: an in vitro study. Ann Biomed Eng, 38(1), 3409-3422. doi: 10.1007/s10439-010-0089-0

Monasterio, G., F. Castillo, J. P. Ibarra, J. Guevara, L. Rojas, C. Alvarez, B. Fernandez, A. Aguero, D. Betancur and R. Vernal (2018). Alveolar bone resorption and Th1/Th17-associated immune response triggered during Aggregatibacter actinomycetemcomitans-induced experimental periodontitis are serotype-dependent.J Periodontol 89(10): 1249-1261. doi: 10.1002/JPER.17-0563

Quintero, J. C., Trosien, A., Hatcher, D., & Kapila, S. (1999). Craniofacial imaging in orthodontics: historical perspective, current status, and future developments. Angle Orthod, 69(6), 491-506. doi:10.1043/0003-3219(1999)069<0491:Ciiohp>2.3.Co;2

Salmon, B., Le Denmat, D. (2012). Intraoral ultrasonography : development of a specific high-frequency probe and clinical pilot study. Clin Oral Investig, 16(2), 643-649. doi: 10.1007/s00784-011-0533-z

Steiner, L., Synek, A., & Pahr, D. H. (2020). Comparison of different µCT-based morphology assessment tools using human trabecular bone. *Bone Rep, 12*, 100261. doi:10.1016/j.bonr.2020.100261

Sun, L., Zhang, L., Shen, G., Wang, B., & Fang, B. (2015). Accuracy of cone-beam computed tomography in detecting alveolar bone dehiscences and fenestrations. Am J Orthod Dentofacial Orthop, 147(3), 313-323. doi:10.1016/j.ajodo.2014.10.032

Sun, Z., Smith, T. Kortam, S., Kim, D.G. Tee, B.C., Fields, H. (2011). Effect of bone thickness on alveolar bone height measurements from cone-beam computed tomography images. *Am J Orthod Dentofacial Orthop*, 139 (2), e117-127. doi: 10.1016/j.ajodo.2010.08.016

Swennen G.R., Schutyser, F. (2006). Three-dimensional cephalometry: spiral multi-slice vs cone-beam computed tomography. Am J Orthod Dentofacial Orthop, 130(3),410-416. doi: 10.1016/j.ajodo.2005.11.035

Timock, A.M., Cook, V., McDonald, T., Leo, M.C., Crowe, J., Benninger, B.L., Covell, D.A. Jr. (2011). Accuracy and reliability of buccal bone height and thickness measurements from cone-beam computed tomography imaging. *Am J Orthod Dentofacial Orthop*, 140(5),734-44. doi: 10.1016/j.ajodo.2011.06.021

Walter, C., Schmidt, J. C., Rinne, C. A., Mendes, S., Dula, K., & Sculean, A. (2020). Cone beam computed tomography (CBCT) for diagnosis and treatment planning in periodontology: systematic review update. Clin Oral Investig, 24(9), 2943-2958. doi:10.1007/s00784-020-03326-0

White, S. C., & Pharoah, M. J. (2009). Oral radiology: Principles and interpretation. St. Louis, Mo: Mosby/Elsevier.

CHAPTER 6 - CONCLUSIONS

6.1 Research Question 1

Based on the information presented in this study, the intra examiner measurements done by R1 for µCT have an ICC = 0.998 with a 95% confidence interval [0.997-0.999]. The US measurements have an ICC = 0.997 with a 95% confidence interval [0.995-0.999]. Therefore, the Research Question 1 null hypothesis was accepted as true.

Ho1: The µCT and US measurements done by R1 are reliable with an excellent degree of intra-rater reliability.

6.2 Research Question 2

Based on the information presented in this study, the inter examiner measurements done by R1 compared to R2 for µCT have an ICC = 0.996 with a 95% confidence interval [0.992-0.998]. The US measurements have an ICC = 0.947 – 0.950 with a 95% confidence interval [0.896-0.974]. Therefore, the Research Question 2 null hypothesis was accepted as true.

H_o2: The µCT and US measurements done by R1 are reliable compared to R2 with an excellent degree of inter-rater reliability.

6.3 Research Question 3

Based on the information presented in this study, the US measurements compared to the µCT gold standard have an ICC = 0.885 – 0.894 with a 95% confidence interval [0.789-0.944]. Therefore, the Research Question 3 null hypothesis was accepted as true.

H_o3: The US device is accurate to determine alveolar bone crest height on the buccal aspect of maxillary and mandibular human teeth with a good level of accuracy when compared to the µCT gold standard.

In conclusion, the intra examiner and inter examiner reliability for both the μCT and US alveolar bone crest measurements was found to be excellent, and the accuracy of the US was found to be good compared to μCT. Also, there aren't enough samples available in all the groups in order to compare the reliability and accuracy of the US across different regions of the mouth..

REFERENCES

Abdelkarim, A. (2019). Cone-Beam Computed Tomography in Orthodontics. *Dent J (Basel), 7*(3). doi:10.3390/dj7030089

Agrawal, P., Sanikop, S., & Patil, S. (2012). New developments in tools for periodontal diagnosis. *Int Dent J, 62*(2), 57-64. doi:10.1111/j.1875-595X.2011.00099.x

Ainamo, J., & Loe, H. (1966). Anatomical characteristics of gingiva. A clinical and microscopic study of the free and attached gingiva. *J Periodontol, 37*(1), 5-13. doi:10.1902/jop.1966.37.1.5

Aldrich, J. E. (2007). Basic physics of ultrasound imaging. *Crit Care Med, 35*(5 Suppl), S131-137. doi:10.1097/01.CCM.0000260624.99430.22

Alfuriji, S., Alhazmi, N., Alhamlan, N., Al-Ehaideb, A., Alruwaithi, M., Alkatheeri, N., & Geevarghese, A. (2014). The effect of orthodontic therapy on periodontal health: a review of the literature. *Int J Dent, 2014*, 585048. doi:10.1155/2014/585048

Applegate, K. E., & Cost, N. G. (2013). Image Gently: a campaign to reduce children's and adolescents' risk for cancer during adulthood. *J Adolesc Health, 52*(5 Suppl), S93-97. doi:10.1016/j.jadohealth.2013.03.006

Applegate, K. E., & Thomas, K. (2011). Pediatric CT--the challenge of dose records. *Pediatr Radiol, 41 Suppl 2*, 523-527. doi:10.1007/s00247-011-2161-9

Badersten, A., Nilveus, R., Egelberg, J. (1984). Reproducibility of probing attachment level measurements. *J Clin Periodontol* 11(7), 475–485, https://doi.org/10.1111/j.1600-051x.1984.tb01347.x

Baird, E., Taylor, G. (2017). X-ray micro computed-tomography. *Curr Biol*, 27(8), 289-291. doi: 10.1016/j.cub.2017.01.066.

Ballrick, J.W., Palomo, J.M., Ruch, E., Amberman, B.D., Hans, M.G. (2008). Image distortion and spatial resolution of a commercially available cone-beam computed tomography machine. Am *J Orthod Dentofacial Orthop*, 134(4), 573-82. doi: 10.1016/j.ajodo.2007.11.025

Bin Bahar, B. S. K., Alkhalidy, S. R., Kaklamanos, E. G., & Athanasiou, A. E. (2020). Do orthodontic patients develop more gingival recession in anterior teeth compared to untreated individuals? A systematic review of controlled studies. *Int Orthod, 18*(1), 1-9. doi:10.1016/j.ortho.2019.08.025

Boerckel, J. D., Mason, D. E., Mcdermott, A. M., Alsberg, E. (2014). Microcomputed tomography: approaches and applications in bioengineering. *Stem Cell Res Ther*, 5(6),144. doi: 10.1186/scrt534.

Bohner, L., Habor, D., Tortamano, P., Radermacher, K., Wolfart, S., & Marotti, J. (2019). Assessment of Buccal Bone Surrounding Dental Implants Using a High-Frequency

Ultrasound Scanner. *Ultrasound Med Biol, 45*(6), 1427-1434. doi:10.1016/j.ultrasmedbio.2019.02.002

Bouxsein, M.L., Boyd, S.K., Christiansen, B.A., Guldberg, R.E., Jepsen, K.J., Müller, R. (2010). Guidelines for assessment of bone microstructure in rodents using micro-computed tomography. *J Bone Miner Res*, 25,1468–1486. Doi: 10.1002/jbmr.141

Castro Rodríguez, Y., & Grados Pomarino, S. (2017). Orthodontic dental movement and its association with the presence of gingival recession. *Revista Odontológica Mexicana, 21*(1), e8-e11. doi:https://doi.org/10.1016/j.rodmex.2017.02.005

Catunda, R. Q., Ho, K. K.-Y., Patel, S., & Febbraio, M. (2021). A 2-plane micro-computed tomographic alveolar bone measurement approach in mice. *Imaging Sci Dent*, 51(4), 389-398. doi: 10.5624/isd.20210058

Chałas, R., Szlązak, K., Wójcik-Chęcińska, I., Jaroszewicz, J., Molak, R. (2017). Observations of mineralised tissues of teeth in X-ray micro-computed tomography. *Folia Morphologica*, 76(2), 143-148. doi: 10.5603/FM.a2016.0070

Chan, H. L., & Kripfgans, O. D. (2020). Ultrasonography for diagnosis of peri-implant diseases and conditions: a detailed scanning protocol and case demonstration. *Dentomaxillofac Radiol, 49*(7), 20190445. doi:10.1259/dmfr.20190445

Chan, H. L., Sinjab, K., Chung, M. P., Chiang, Y. C., Wang, H. L., Giannobile, W. V., & Kripfgans, O. D. (2017). Non-invasive evaluation of facial crestal bone with ultrasonography. *PLoS One, 12*(2), e0171237. doi:10.1371/journal.pone.0171237

Chandak, R., Degwekar, S., Bhowte, R.R., Motwani, M., Banode, P., Chandak, M., Rawlani, S. (2011). An evaluation of efficacy of ultrasonography in the diagnosis of head and neck swellings. *Dentomaxillofac Radiol*, 40(4), 213-21. doi: 10.1259/dmfr/68658286

Chen, J. X., Kachniarz, B., Gilani, S., & Shin, J. J. (2014). Risk of malignancy associated with head and neck CT in children: a systematic review. *Otolaryngol Head Neck Surg, 151*(4), 554-566. doi:10.1177/0194599814542588

Chifor R, Li M, Nguyen KT, Arsenescu T, Chifor I, Badea AF, Badea ME, Hotoleanu M, Major PW, Le LH. (2021) Three-dimensional periodontal investigations using a prototype handheld ultrasound scanner with spatial positioning reading sensor. *Med Ultrason*, 23(3), 297-304. doi: 10.11152/mu-2837. Epub 2021 Mar 3.

Clark, D. P., Badea, C. T. (2014). Micro-CT of rodents: state-of-the-art and future perspectives. *Physica medica*, 30(6), 619-634. doi: 10.1016%2Fj.ejmp.2014.05.011

Coatney, R. W. (2001). Ultrasound imaging: principles and applications in rodent research. *ILAR J, 42*(3), 233-247. doi:10.1093/ilar.42.3.233

Cook, V.C., Timock, A.M., Crowe, J.J., Wang, M., Covell, D.A. Jr. (2015). Accuracy of alveolar bone measurements from cone beam computed tomography acquired using varying settings. *Orthod Craniofac Res*,18 Suppl 1, 127-36. doi: 10.1111/ocr.12072.

Cotti, E., Campisi, G., Garau, V., & Puddu, G. (2002). A new technique for the study of periapical bone lesions: ultrasound real time imaging. *Int Endod J, 35*(2), 148-152. doi:10.1046/j.1365-2591.2002.00458.x

Czochrowska, E., & Rosa, M. (2014). The Orthodontic / Periodontal Interface. *Semin Orthod, 21*. doi:10.1053/j.sodo.2014.12.001

Dalstra, M., Cattaneo, P. M., Laursen, M. G., Beckmann, F., Melsen, B. (2015). Multi-level synchrotron radiation-based microtomography of the dental alveolus and its consequences for orthodontics. *J Biomech*, 48 (5), 801-806. doi: 10.1016/j.jbiomech.2014.12.014

Demirtas, N., Mihmanli, A., Aytuğar, E., & Bayer, S. (2015). Limitations of Panoramic Radiographs: Report of Two Cases. Bezmialem Science, 2, 82-85. doi:10.14235/bs.2014.328

Du Plessis, A., Boshoff, W. P. (2019). A review of X-ray computed tomography of concrete and asphalt construction materials. *Construction and Building Materials*, 199, 637-651. doi.org/10.1016/j.conbuildmat.2018.12.049.

Evirgen, S., & Kamburoglu, K. (2016). Review on the applications of ultrasonography in dentomaxillofacial region. *World J Radiol, 8*(1), 50-58. doi:10.4329/wjr.v8.i1.50

Fageeh, H., Meshni, A., Jamal, H., Preethanath, R., & Halboub, E. (2019). The accuracy and reliability of digital measurements of gingival recession versus conventional methods. *BMC Oral Health*, 19 (154). doi:10.1186/s12903-019-0851-0

Feldkamp, L.A., Goldstein, S.A., Parfitt, A.M., Jesion, G. (1989). The direct examination of three-dimensional bone architecture in vitro by computed tomography. J Bone Miner Res, 4,3-11. doi: 10.1002/jbmr.5650040103

Ferrare, N, Leite, A.F., Caracas, H.C.P.M., Azevedo, R.B., Melo, N.S., Figueiredo, P.T. (2013). Cone-beam computed tomography and microtomography for alveolar bone measurements. *Surg Radiol Anat*, 35, 495-502. doi: 10.1007/s00276-013-1080-x

Ferreira, R. I., de Almeida, S. M., Bóscolo, F. N., Santos, A. O., & Camargo, E. E. (2002). Bone scintigraphy as an adjunct for the diagnosis of oral diseases. *J Dent Educ*, 66(12), 1381-1387. PMID: 12521065

Foster, B. L. (2017). On the discovery of cementum. *J Periodontal Res, 52*(4), 666-685. doi:10.1111/jre.12444

Fu, J.H., Yeh, C.Y., Chan, H.L., Tatarakis, N., Leong, D.J., Wang, H.L. (2010). Tissue bio-type and its relation to the underlyingbone morphology.*J Periodontol*, 81 (4),569–74. doi: 10.1902/jop.2009.090591

Fuhrmann, R., Bücker, A., & Diedrich, P. (1997). Radiological assessment of artificial bone defects in the floor of the maxillary sinus. *Dentomaxillofac Radiol, 26*(2), 112-116. doi:10.1038/sj.dmfr.4600223

Fuhrmann, R. A., Bücker, A., & Diedrich, P. R. (1995). Assessment of alveolar bone loss with high resolution computed tomography. *J Periodontal Res, 30*(4), 258-263. doi:10.1111/j.1600-0765.1995.tb02131.x

Fuhrmann, R. (2002). Three-dimensional evaluation of periodontal remodeling during orthodontic treatment. *Semin Orthod*, 8(1), 23-28. doi: 10.1053/sodo.2002.28168

Gargiulo, A. W., Wentz, F. M., & Orban, B. (1961). Dimensions and Relations of the Dentogingival Junction in Humans. *The Journal of Periodontology, 32*(3), 261-267. doi:https://doi.org/10.1902/jop.1961.32.3.261

Garib, D. G., Henriques, J. F., Janson, G., de Freitas, M. R., & Fernandes, A. Y. (2006). Periodontal effects of rapid maxillary expansion with tooth-tissue-borne and tooth-borne expanders: a computed tomography evaluation. *Am J Orthod Dentofacial Orthop, 129*(6), 749-758. doi:10.1016/j.ajodo.2006.02.021

Gonzalez, S. M. (2013). *Interpretation Basics of Cone Beam Computed Tomography*. Ames, Iowa: Wiley-Blackwell.

Gorbunkova, A., Pagni, G., Brizhak, A., Farronato, G., & Rasperini, G. (2016). Impact of Orthodontic Treatment on Periodontal Tissues: A Narrative Review of Multidisciplinary Literature. *Int J Dent, 2016*, 4723589. doi:10.1155/2016/4723589

Government of Canada. (2022, August), Radiation Protection Regulations SOR/2000-203. Justice Laws. Government of Canada. https://laws-lois.justice.gc.ca/eng/regulations/SOR-2000-203/FullText.html

Gracco, A., Lombardo, L., Mancuso, G., Gravina, V., & Siciliani, G. (2009). Upper incisor position and bony support in untreated patients as seen on CBCT. *Angle Orthod, 79*(4), 692-702. doi:10.2319/081908-437.1

Gyawali, R., & Bhattarai, B. (2017). Orthodontic Management in Aggressive Periodontitis. *Int Sch Res Notices, 2017*, 8098154. doi:10.1155/2017/8098154

Hall, E. J., & Giaccia, A. J. (2006). *Radiobiology for the radiologist* (6th ed., pp. ix, 546 p.). Retrieved from https://ovidsp.ovid.com/ovidweb.cgi?T=JS&PAGE=booktext&NEWS=N&DF=bookdb&AN=01382670/6th_Edition&XPATH=/PG(0)

Hanke, R., Fuchs, T., Salamon, M., & Zabler, S. (2016). 3 - X-ray microtomography for materials characterization. In G. Hübschen, I. Altpeter, R. Tschuncky, & H.-G. Herrmann (Eds.), Materials Characterization Using Nondestructive Evaluation (NDE) Methods (pp. 45-79): Woodhead Publishing.

Holdsworth, D. W., Thornton, M. M. (2002). Micro-CT in small animal and specimen imaging. *Trends in Biotechnology*, 20 (8), 34-39. doi: 10.1016/S0167- 7799(02)02004-8

Hughes, D. A., Girkin, J. M., Poland, S., Longbottom, C., Button, T. W., Elgoyhen, J., Hughes, H., Meggs, C., Cochran, S. (2009). Investigation of dental samples using a 35MHz

focussed ultrasound piezocomposite transducer. *Ultrasonics, 49*(2), 212-218. doi:10.1016/j.ultras.2008.08.007

Hughes, F. J. (2013). *Clinical problem solving in periodontology & implantology* (1st ed.). Edinburgh ; New York: Churchill Livingstone Elsevier.

Hutchinson, J.C., Shelmerdine, S.C., Simcock, I.C., Sebire, N.J., Arthurs, O.J. (2017). Early clinical applications for imaging at microscopic detail: microfocus computed tomography (micro-CT). *Br J Radiol*, 90(1075), 20170113. doi: 10.1259/bjr.20170113.

Jacques, P. D., Nummer, A. R., Heck, R. J., Machado, R. (2014). The use of microtomography in structural geology: A new methodology to analyse fault faces. *Journal of Structural Geology*, 66, 347-355. doi: 10.1016/j.jsg.2014.06.004

Jain, S. (2020). What is the periodontium. In. Prestige Dental Care Raipur.

Januario, A.L., Barriviera, M., Duarte, W.R. (2008) Soft tissue cone-beam computed tomography: a novel method for the measurement of gingival tissue andthe dimensions of the dentogingival unit. *J Esthet Restor Dent*, 20 (6),366–73. doi: 10.1111/j.1708-8240.2008.00210.x

Johal, A., Katsaros, C., Kiliaridis, S., Leitao, P., Rosa, M., Sculean, A., . . . Zachrisson, B. (2013). State of the science on controversial topics: orthodontic therapy and gingival recession (a report of the Angle Society of Europe 2013 meeting). *Prog Orthod, 14*, 16. doi:10.1186/2196-1042-14-16

Jones, J. K., & Frost, D. E. (1984). Ultrasound as a diagnostic aid in maxillofacial surgery. Report of a case. *Oral Surg Oral Med Oral Pathol, 57*(6), 589-594. doi:10.1016/0030-4220(84)90277-9

Kim, I., Paik, K.S., Lee, S.P. (2007). Quantitative evaluation of the accuracy of micro- computed tomography in tooth measurement. *Clinical Anatomy*, 20(1), 27- 34. doi: 10.1002/ca.20265

Kim, J., Shin, T. J., Kong, H. J., Hwang, J. Y., & Hyun, H. K. (2019). High-Frequency Ultrasound Imaging for Examination of Early Dental Caries. *J Dent Res, 98*(3), 363-367. doi:10.1177/0022034518811642

Kingman, A., Löe, H., Anerud, A., Boysen, H. (1991). Errors in measuring parameters associated with periodontal health and disease. *J Periodontol*,62(8),477-86. doi: 10.1902/jop.1991.62.8.477.

Kleinerman, R. A. (2006). Cancer risks following diagnostic and therapeutic radiation exposure in children. *Pediatr Radiol, 36 Suppl 2*, 121-125. doi:10.1007/s00247-006-0191-5

Koo, T.K., Li, M.Y. A Guideline of Selecting and Reporting Intraclass Correlation Coefficients for Reliability Research (2016). *J Chiropr Med*, 15 (2), 155-63. doi: 10.1016/j.jcm.2016.02.012

Lee, S., Crean, M. (2013). The story of radiology contents. Vienna, Austria (101p): European Society of Radiology.

Leung, C. C., Palomo, L., Griffith, R., & Hans, M. G. (2010). Accuracy and reliability of cone-beam computed tomography for measuring alveolar bone height and detecting bony dehiscences and fenestrations. *Am J Orthod Dentofacial Orthop, 137*(4 Suppl), S109-119. doi:10.1016/j.ajodo.2009.07.013

Li, H., Zhang, H., Tang, Z., Hu, G. (2008) Micro-computed tomography for small animal imaging: Technological details. *Progress in Natural Science*, 18(5), 513- 521. doi: 10.1016/j.pnsc.2008.01.002.

Li, Y., Zhan, Q., Bao, M., Yi, J., & Li, Y. (2021). Biomechanical and biological responses of periodontium in orthodontic tooth movement: up-date in a new decade. *Int J Oral Sci, 13*(1), 20. doi:10.1038/s41368-021-00125-5

Liedke G.S., da Silveira H.E., da Silveira H.L., Dutra V., de Figueiredo J.A. (2009). Influence of voxel size in the diagnostic ability of cone beam tomography to evaluate simulated external root resorption. *J Endod*, 35(2), 233-5. doi: 10.1016/j.joen.2008.11.005

Lindhe, J., Lang, N. P., & Karring, T. (2008). *Clinical periodontology and implant dentistry* (5th ed.). Oxford ; Ames, Iowa: Blackwell Munksgaard.

Lopes, A. P.; Fiori A. P.; Reis Neto, J. M.; Marchese, C.; Vasconcellos, E. M. G. et al. (2002). Three-dimensional analysis of rocks through X-ray computerized microtomography Integrated to petrography. *Geociencias*, 31(1), 129-142. Retrieved from http://www.ppegeo.igc.usp.br/index.php/GEOSP/article/view/7248.

Loubele, M., Van Assche, N., Carpentier, K., Maes, F., Jacobs, R., van Steenberghe, D., & Suetens, P. (2008). Comparative localized linear accuracy of small-field cone-beam CT and multislice CT for alveolar bone measurements. *Oral Surg Oral Med Oral Pathol Oral Radiol Endod, 105*(4), 512-518. doi:10.1016/j.tripleo.2007.05.004

Lubcke, P. M., M. N. B. Ebbers, J. Volzke, J. Bull, S. Kneitz, R. Engelmann, H. Lang, B. Kreikemeyer and B. Muller-Hilke (2019). Periodontal treatment prevents arthritis in mice and methotrexate ameliorates periodontal bone loss. *Sci Rep* 9(1): 8128. Doi: 10.1038/s41598-019-44512-9

Lurie, A. G., & Kantor, M. L. (2020). Contemporary radiation protection in dentistry: Recommendations of National Council on Radiation Protection and Measurements Report No. 177. *J Am Dent Assoc, 151*(10), 716-719 e713. doi:10.1016/j.adaj.2020.05.007

Machado, A. C., Lima, I., Lopes, R. T. (2014). Effect of 3D computed microtomography resolution on reservoir rocks. *Radiation Physics and Chemistry*, 95, 405-407. doi: 10.1016/j.radphyschem.2012.12.029.

Mahesh, M. (2013). The Essential Physics of Medical Imaging, Third Edition. *Med Phys, 40*(7). doi:10.1118/1.4811156

Mahmoud, Am.M., Ngan, P., Crout, R., Mukdadi, O.M. (2010). High-resolution 3D ultrasound jawbone surface imaging for diagnosis of periodontal body defects: an in vitro study. *Ann Biomed Eng*, 38(1), 3409-3422. doi: 10.1007/s10439-010-0089-0

Marciano, M.A., Duarte, M.A.H., Ordinola-Zapata, R., Del Carpio-Perochena, A., Cavenago, B.C., Villas-Bôas, M.H., Minotti, P.G., Bramante, C.M., Moraes, I.G. (2012). Applications of micro-computed tomography in endodontic research. In: Méndez-Vilas A, editor. Current microscopy contributions to advances in science and technology. Badajoz, Spain (p782-788): Formatex research center.

Maret, D., Telmon, N., Peters, O.A., Lepage, B., Treil, J., Inglese, J.M., et al. (2012). Effect of voxel size on the accuracy of 3D reconstructions with cone beam CT. *Dentomaxillofac Radiol*, 41(8), 649-55. doi: 10.1259/dmf/81804525

Marotti, J., Heger, S., Tinschert, J., Tortamano, P., Chuembou, F., Radermacher, K., & Wolfart, S. (2013). Recent advances of ultrasound imaging in dentistry--a review of the literature. *Oral Surg Oral Med Oral Pathol Oral Radiol, 115*(6), 819-832. doi:10.1016/j.oooo.2013.03.012

Menditto, A., Patriarca, M., Magnusson, B. Understanding the meaning of accuracy, trueness and precision (2007). *Accred Qual Assur* 12, 45–47. doi: 10.1007/s00769-006-0191-z

MiLabs (2022). Adaptive diagnostic CT. Retrieved August 16, 2022, from https://www.milabs.com/u-ct/

Mol, A., & Balasundaram, A. (2008). In vitro cone beam computed tomography imaging of periodontal bone. *Dentomaxillofac Radiol, 37*(6), 319-324. doi:10.1259/dmfr/26475758

Monasterio, G., F. Castillo, J. P. Ibarra, J. Guevara, L. Rojas, C. Alvarez, B. Fernandez, A. Aguero, D. Betancur and R. Vernal (2018). Alveolar bone resorption and Th1/Th17-associated immune response triggered during Aggregatibacter actinomycetemcomitans-induced experimental periodontitis are serotype-dependent. *J Periodontol* 89(10): 1249-1261. doi: 10.1002/JPER.17-0563

Mulie, R. M., & Hoeve, A. T. (1976). The limitations of tooth movement within the symphysis, studied with laminagraphy and standardized occlusal films. *J Clin Orthod, 10*(12), 882-893, 886-889. Retrieved from https://www.ncbi.nlm.nih.gov/pubmed/1074868

Nanci, A., & Bosshardt, D. D. (2006). Structure of periodontal tissues in health and disease. *Periodontol 2000, 40*, 11-28. doi:10.1111/j.1600-0757.2005.00141.x

Neves, A. A., Jaecques, S., Van Ende, A., Cardoso, M. V., Coutinho, E. et al. (2014). 3D-microleakage assessment of adhesive interfaces: exploratory findings by µct. *Dent Mater*, 30(8), 799-807. doi: 10.1016/j.dental.2014.05.003

Newman, M. G., Takei, H. H., Klokkevold, P. R., & Carranza, F. A. (2012). *Carranza's clinical periodontology* (11th ed., pp. 1 online resource (xlv, 824 p.)). Retrieved from https://search.ebscohost.com/login.aspx?direct=true&scope=site&db=nlebk&db=nlabk&AN=448414

Nguyen, K. T., Le, B. M., Li, M., Almeida, F. T., Major, P. W., Kaipatur, N. R., . . . Le, L. H. (2021). Localization of cementoenamel junction in intraoral ultrasonographs with machine learning. *J Dent*, 112, 103752. doi:10.1016/j.jdent.2021.103752

Nguyen, K. T., Pacheco-Pereira, C., Kaipatur, N. R., Cheung, J., Major, P. W., & Le, L. H. (2018). Comparison of ultrasound imaging and cone-beam computed tomography for examination of the alveolar bone level: A systematic review. *PLoS One, 13*(10), e0200596. doi:10.1371/journal.pone.0200596

Olejniczak, A. J., Grine, F. E. (2006). Assessment of the accuracy of dental enamel thickness measurements using microfocal X-ray computed tomography. *The Anatomical Record*, 288 (3), 263-275. doi: 10.1002/ar.a.20307

Palou, M. E., McQuade, M. J., & Rossmann, J. A. (1987). The use of ultrasound for the determination of periodontal bone morphology. *J Periodontol, 58*(4), 262-265. doi:10.1902/jop.1987.58.4.262

Papapanou, P. N., Sanz, M., Buduneli, N., Dietrich, T., Feres, M., Fine, D. H., . . . Tonetti, M. S. (2018). Periodontitis: Consensus report of workgroup 2 of the 2017 World Workshop on the Classification of Periodontal and Peri-Implant Diseases and Conditions. *J Periodontol, 89 Suppl 1*, S173-S182. doi:10.1002/JPER.17-0721

Park, C. H., Abramson, Z. R., Taba, M., Jr., Jin, Q., Chang, J., Kreider, J. M. Giannobile, W. V. (2007). Three-dimensional micro-computed tomographic imaging of alveolar bone in experimental bone loss or repair. *J Periodontol*, 78(2), 273-281. doi:10.1902/jop.2007.060252

Particelli, F., Mecozzi, L., Beraudi, A., Montesi, M., Baruffaldi, F., Viceconti, M. (2012). A comparison between micro-CT and histology for the evaluation of cortical bone: effect of polymethylmethacrylate embedding on structural parameters. *J Microsc*, 245(3),302-10. doi: 10.1111/j.1365-2818.2011.03573

Pauwels R, Araki K, Siewerdsen JH, Thongvigitmanee SS. Technical aspects of dental CBCT: state of the art. *Dentomaxillofac Radiol*. 2015;44(1):20140224. doi: 10.1259/dmfr.20140224. PMID: 25263643; PMCID: PMC4277439.

Persson, R. E., Hollender, L. G., Laurell, L., & Persson, G. R. (1998). Horizontal alveolar bone loss and vertical bone defects in an adult patient population. J Periodontol, 69(3), 348-356. doi:10.1902/jop.1998.69.3.348

Pradeep, K., Rajababu, P., Satyanarayana, D., & Sagar, V. (2012). Gingival recession: review and strategies in treatment of recession. *Case Rep Dent, 2012*, 563421. doi:10.1155/2012/563421

Preshaw, P. M., Kupp, L., Hefti, A. F., & Mariotti, A. (1999). Measurement of clinical attachment levels using a constant-force periodontal probe modified to detect the cemento-enamel junction. *J Clin Periodontol, 26*(7), 434-440. doi:10.1034/j.1600-051x.1999.260704.x

Pye, G., & Pye, A. (2017). Orthodontic and periodontal multidisciplinary care. *Dental Update, 44*(6), 558-562. doi:10.12968/denu.2017.44.6.558

Quintero, J. C., Trosien, A., Hatcher, D., & Kapila, S. (1999). Craniofacial imaging in orthodontics: historical perspective, current status, and future developments. *Angle Orthod*, 69(6), 491-506. doi:10.1043/0003-3219(1999)069<0491:Ciiohp>2.3.Co;2

Reda, R., Zanza, A., Cicconetti, A., Bhandi, S., Miccoli, G., Gambarini, G., & Di Nardo, D. (2021). Ultrasound Imaging in Dentistry: A Literature Overview. *J Imaging, 7*(11). doi:10.3390/jimaging7110238

Reichert, C., Hagner, M., Jepsen, S., & Jäger, A. (2011). Interfaces between orthodontic and periodontal treatment: their current status. *J Orofac Orthop, 72*(3), 165-186. doi:10.1007/s00056-011-0023-6

Roberto-Rodrigues, M., Fernandes, R. M., Senos, R., Scoralick, A. C., Bastos, A. A. et al. (2015). Novel rat model of nonunion fracture with vascular deficit. *Injury*, 46(4), 649-654. doi: 10.1016/j.injury.2015.01.033

Rungcharassaeng, K., Caruso, J. M., Kan, J. Y., Kim, J., & Taylor, G. (2007). Factors affecting buccal bone changes of maxillary posterior teeth after rapid maxillary expansion. *Am J Orthod Dentofacial Orthop, 132*(4), 428 e421-428. doi:10.1016/j.ajodo.2007.02.052

Salmon, B., & Le Denmat, D. (2012). Intraoral ultrasonography: development of a specific high-frequency probe and clinical pilot study. *Clin Oral Investig, 16*(2), 643-649. doi:10.1007/s00784-011-0533-z

Sarikaya, S., Haydar, B., Ciger, S., & Ariyurek, M. (2002). Changes in alveolar bone thickness due to retraction of anterior teeth. *Am J Orthod Dentofacial Orthop, 122*(1), 15-26. doi:10.1067/mod.2002.119804

Scarfe WC, Farman AG, Sukovic P. (2006). Clinical applications of cone-beam computed tomography in dental practice. *J Can Dent Assoc*, 72(1), 75-80. PMID: 16480609

Schambach, S. J., Bag, S., Groden, C., Schiling, L., Brockmann, M. A. (2009). Vascular imaging in small rodents using micro-CT. *Methods*, 50(1), 26-35. doi: 10.1016/j.ymeth.2009.09.003

Schon, R., Duker, J., & Schmelzeisen, R. (2002). Ultrasonographic imaging of head and neck pathology. *Atlas Oral Maxillofac Surg Clin North Am, 10*(2), 213-241. doi:10.1016/s1061-3315(02)00009-4

Shah, N., Bansal, N., & Logani, A. (2014). Recent advances in imaging technologies in dentistry. *World J Radiol, 6*(10), 794-807. doi:10.4329/wjr.v6.i10.794

Shatskiy, I . (2021) Effective doses and radiation risks from common dental radiographic, panoramic and cbct examinations. Radiation Protection Dosimetry, 195 (3-4), 296–305. Doi: 10.1093/rpd/ncab069

Shirmohammadi, A., Faramarzie, M., & Lafzi, A. (2008). A clinical evaluation of anatomic features of gingiva in dental students in tabriz, iran. *J Dent Res Dent Clin Dent Prospects, 2*(3), 90-94. doi:10.5681/joddd.2008.019

Sim, H. Y., Kim, H. S., Jung, D. U., Lee, H., Lee, J. W., Han, K., & Yun, K. I. (2017). Association between orthodontic treatment and periodontal diseases: Results from a national survey. *Angle Orthod, 87*(5), 651-657. doi:10.2319/030317-162.1

Spin-Neto R, Gotfredsen E, Wenzel A. (2013). Impact of voxel size variation on CBCT based diagnostic outcome in dentistry: a systematic review. *J Digit Imaging*, 26(4), 813-20. doi: 10.1007/s10278-012-9562-7

Spranger, H. (1971). Ultra-sonic diagnosis of marginal periodontal diseases. *Int Dent J, 21*(4), 442-455. Retrieved from https://www.ncbi.nlm.nih.gov/pubmed/5292204

Steiner, G. G., Pearson, J. K., & Ainamo, J. (1981). Changes of the marginal periodontium as a result of labial tooth movement in monkeys. *J Periodontol, 52*(6), 314-320. doi:10.1902/jop.1981.52.6.314

Steiner, L., Synek, A., & Pahr, D. H. (2020). Comparison of different uct-based morphology assessment tools using human trabecular bone. *Bone Rep*, 12, 100261. doi:10.1016/j.bonr.2020.100261

Stock, S. R. (1999). X-ray microtomography of materials. *International Materials Reviews*, 44 (4), 141-164. doi: 10.1179/095066099101528261

Sun, L., Zhang, L., Shen, G., Wang, B., & Fang, B. (2015). Accuracy of cone-beam computed tomography in detecting alveolar bone dehiscences and fenestrations. *Am J Orthod Dentofacial Orthop, 147*(3), 313-323. doi:10.1016/j.ajodo.2014.10.032

Sun, Z., Smith, T. Kortam, S., Kim, D.G. Tee, B.C., Fields, H. (2011). Effect of bone thicknesson alveolar bone height measurements from cone-beam computed tomography images. *Am J Orthod Dentofacial Orthop*, 139 (2), e117-127. doi: 10.1016/j.ajodo.2010.08.016

Swain, M.V., Xue, J. (2009). State of the art of Micro-CT applications in dental research. *Int J Oral Sci*, 1(4), 177-88. doi: 10.4248/IJOS09031.

Swasty, D., Lee, J. S., Huang, J. C., Maki, K., Gansky, S. A., Hatcher, D., & Miller, A. J. (2009). Anthropometric analysis of the human mandibular cortical bone as assessed by cone-beam computed tomography. *J Oral Maxillofac Surg,* 67(3), 491-500. doi:10.1016/j.joms.2008.06.089

Swennen G.R., Schutyser, F. (2006). Three-dimensional cephalometry: spiral multi-slice vs cone-beam computed tomography. *Am J Orthod Dentofacial Orthop*, 130(3),410-416. doi: 10.1016/j.ajodo.2005.11.035

Timock, A.M., Cook, V., McDonald, T., Leo, M.C., Crowe, J., Benninger, B.L., Covell, D.A. Jr. (2011). Accuracy and reliability of buccal bone height and thickness measurements from

cone-beam computed tomography imaging. *Am J Orthod Dentofacial Orthop*, 140(5),734-44. doi: 10.1016/j.ajodo.2011.06.021

Tsiolis, F. I., Needleman, I. G., & Griffiths, G. S. (2003). Periodontal ultrasonography. *J Clin Periodontol, 30*(10), 849-854. doi:10.1034/j.1600-051x.2003.00380.x

Tubiana, M. (1996). [Wilhelm Conrad Rontgen and the discovery of X-rays]. *Bull Acad Natl Med, 180*(1), 97-108. Retrieved from https://www.ncbi.nlm.nih.gov/pubmed/8696882

Vizzotto, M.B., Silveira, P.F., Arus, N.A., Montagner, F., Gomes, B.P., da Silveira, H.E. (2013). CBCT for the assessment of second mesiobuccal (MB2) canals in maxillary molar teeth: effect of voxel size and presence of root filling. *Int Endod J*, 46(9),870-6. doi: 10.1111/iej.12075

Walter, C., Schmidt, J. C., Rinne, C. A., Mendes, S., Dula, K., & Sculean, A. (2020). Cone beam computed tomography (CBCT) for diagnosis and treatment planning in periodontology: systematic review update. *Clin Oral Investig, 24*(9), 2943-2958. doi:10.1007/s00784-020-03326-0

Wennstrom, J. L., Lindhe, J., Sinclair, F., & Thilander, B. (1987). Some periodontal tissue reactions to orthodontic tooth movement in monkeys. *J Clin Periodontol, 14*(3), 121-129. doi:10.1111/j.1600-051x.1987.tb00954.x

White, S. C., & Pharoah, M. J. (2009). Oral radiology: Principles and interpretation. St. Louis, Mo: Mosby/Elsevier.

Wilensky, A., Gabet, Y., Yumoto, H., Houri-Haddad, Y., & Shapira, L. (2005). Three-dimensional quantification of alveolar bone loss in Porphyromonas gingivalis-infected mice using micro-computed tomography. *J Periodontol*, 76(8), 1282-1286. doi:10.1902/jop.2005.76.8.1282

Xiang, X., Sowa, M. G., Iacopino, A. M., Maev, R. G., Hewko, M. D., Man, A., & Liu, K. Z. (2010). An update on novel non-invasive approaches for periodontal diagnosis. *J Periodontol, 81*(2), 186-198. doi:10.1902/jop.2009.090419

Yamada, C., Kitai, N., Kakimoto, N., Murakami, S., Furukawa, S., & Takada, K. (2007). Spatial relationships between the mandibular central incisor and associated alveolar bone in adults with mandibular prognathism. *Angle Orthod, 77*(5), 766-772. doi:10.2319/072906-309

Zanolli, C., Schillinger B., Beaudet, A., Kullmer, O., Macchiarelli, R. et al. (2017). Exploring hominin and non-hominin primate dental fossil remains with neutron microtomography. *Physics Procedia*, 88, 109-115. doi: 10.1016/j.phpro.2017.06.014